Human Use of Flexible Tools for Dynamic Teleoperation

Aiple, M.

DOI
10.4233/uuid:1dd97312-bb7b-43c5-a931-303bd8649883

Publication date
2021

Document Version
Final published version

Citation (APA)
Aiple, M. (2021). *Human Use of Flexible Tools for Dynamic Teleoperation*. [Dissertation (TU Delft), Delft University of Technology]. https://doi.org/10.4233/uuid:1dd97312-bb7b-43c5-a931-303bd8649883

Important note
To cite this publication, please use the final published version (if applicable).
Please check the document version above.

Human Use of Flexible Tools for Dynamic Teleoperation

Human Use of Flexible Tools for Dynamic Teleoperation

Dissertation

for the purpose of obtaining the degree of doctor
at Delft University of Technology
by the authority of the Rector Magnificus Prof. dr. ir. T. H.J.J. van der Hagen,
chair of the Board for Doctorates
to be defended publicly on Friday, 26 February 2021

by

Manuel AIPLE

Diplom-Ingenieur, Karlsruher Institut für Technologie, Karlsruhe, Germany,
Ingénieur de l'École nationale supérieure d'arts et métiers, Paris, France,
born in Breisach am Rhein, Germany.

This dissertation has been approved by the

promotor:	Prof. dr. F. C.T. van der Helm
copromotor:	Dr. ir. A. Schiele

Composition of the doctoral committee:

Rector Magnificus,	chairperson
Prof. dr. F. C.T. van der Helm,	Technische Universiteit Delft, promotor
Dr. ir. A. Schiele,	Technische Universiteit Delft, copromotor
Independent members:	
Prof. dr. ir. D. A. Abbink	Technische Universiteit Delft
Prof. dr. A. Bicchi	Università di Pisa
Prof. dr. ir. B. Vanderborght	Vrije Universiteit Brussel
Prof. dr. ir. S. Stramigioli	Universiteit Twente
Prof. dr. J. B.J. Smeets	Vrije Universiteit Amsterdam
Reserve member:	
Prof. dr. ing. H. Vallery	Technische Universiteit Delft

This research was supported by the Dutch Technology Foundation STW (H-Haptics research project 12161), which is part of the Netherlands Organization for Scientific Research (NWO), and which is partly funded by the Ministry of Economic Affairs, supported by and conceptualized jointly with the Telerobotics and Haptics Lab of the European Space Agency, and supported by the Science Center Delft.

Keywords: Dynamic Teleoperation, Variable Impedance Actuator, Elastic Tool Use

Printed by: Gildeprint

Front & Back: CAD rendering of the Dyrac variable impedance actuator prototype

ISBN 978-94-6419-130-1

An electronic version of this dissertation is available at
http://repository.tudelft.nl/.

Contents

Summary

This thesis explores possibilities and constraints in performing dynamic tasks through teleoperated robots. Teleoperation is commonly used to execute tasks by a human operator guiding a robot remotely through means of a teleoperation system. The teleoperation system bidirectionally mirrors the motions and forces between a handle device held by the operator and a robotic tool device interacting with the environment. While the use of teleoperation to execute slow motions precisely and with appropriate forces has been researched intensively, teleoperation for dynamic motions occurring in explosive movement tasks like throwing, hammering, shaking, and jolting is not yet sufficiently understood. Nevertheless, these motions also belong to the portfolio of motions that non-disabled humans routinely carry out. A deeper understanding of teleoperation for explosive movement tasks could be especially helpful for applications of field robotics, like disaster recovery scenarios, future planetary exploration missions, and other teleoperation applications in unknown environments where some degree of improvisation is useful.

Classical mechanically stiff robots suffer from high wear through dynamic loads as occur during high-velocity impacts. Series elastic actuators (SEAs) and variable impedance actuators (VIAs) undergo significantly less wear from dynamic loads due to their intrinsic compliance, making them exciting technologies for performing dynamic tasks with robots. Additionally, it has been shown for automated applications that the actuator elasticity can be used to increase the output velocity in explosive movement tasks. SEAs and VIAs are, therefore, promising candidate technologies for robots performing dynamic tasks.

Still, it is so far not sufficiently understood how elastic tools can be exploited in teleoperated applications, where the trajectory to be followed is defined by the human operator. For making elastic tool devices useful in teleoperation, the human capabilities in the use of elastic tools need to be determined, and a teleoperation system is required that matches these capabilities. Furthermore, typical teleoperation scenarios comprise not only explosive movement tasks but also precise positioning tasks, arguably even to a larger degree. Hence, the teleoperation system should allow performing both types of tasks, requiring the system to adapt to the task at hand.

This thesis aims to research how human operators can use SEAs and VIAs optimally through teleoperation to efficiently and intuitively perform explosive movement tasks like hammering, without relying on a task-specific tool but still preserving the full versatility also to perform precision tasks with the same system.

The research consisted of user studies on the one side, and teleoperation system design and realization on the other. Two experiments provided the basis for the system design. The first examined whether the human operator can at all interact efficiently with an elastic tool device for explosive movement tasks. The second analyzed the requirements

in terms of dynamic range and teleoperator transparency. The teleoperation system design consisted of the design and realization of a VIA suitable for explosive movement tasks and developing a self-adapting impedance variation algorithm to offload from the human operator the responsibility to change the tool impedance depending on the type of task to be performed for precision or dynamic tasks. The self-adapting impedance variation algorithm does not require any additional sensors to measure the operator's limb stiffness, but changes the tool device impedance based on the handle device velocity following a principle that can be described as "slow and stiff/fast and soft," *i.e.*, low velocities are mapped to high impedances and high velocities to low impedances.

The results of this dissertation show that untrained human operators can exploit tool elasticity after a few dozen trials to achieve a peak end-effector speed of double the peak joint speed with a teleoperated SEA tool device. They achieve similar performance even without perfect transparency of the teleoperation system, in either the absence of visual feedback, the absence of force feedback, or the presence of significant time delays. They adapt to the elastic tool device characteristics by matching their motions to the device resonance frequency.

This thesis also shows that VIAs can be adapted for telemanipulation of precision as well as dynamic tasks. A new actuator was presented covering the dynamic range from human precision motions to human hammering motions. A final user study confirmed that the implemented teleoperation system allows human operators to perform precision and dynamic tasks intuitively and flexibly without requiring extensive training and without the user needing to be aware of the tool device impedance.

The main conclusions of this dissertation are that humans can appreciate VIA tool devices to perform teleoperated precision and dynamic tasks efficiently with the same actuator and that a self-adapting impedance variation algorithm based on the "slow and stiff/fast and soft" principle can help humans to interact with the system, without explicit mode changes between precision and dynamic tasks and without additional sensors to measure the operator's limb stiffness.

Preface

I discovered the world of haptic teleoperation late, during my traineeship in 2011 at André Schiele's Telerobotics and Haptics Lab at the European Space Research and Technology Centre (ESTEC) of the European Space Agency (ESA) in Noordwijk. I had asked for a transfer from ESA's European Space Operations Centre (ESOC) in Darmstadt to ESTEC after getting to know about the plans to conduct experiments where astronauts onboard the International Space Station (ISS) would remotely control a robot in the lab in Noordwijk as a test for future Mars missions.

Fascinated by this new environment at the forefront of research and technology, full of robotic arms and exoskeletons, I briefly touched the domain of haptic feedback with a project on the CyperGrasp, a commercial force-feedback glove, but then my tasks, now as a junior engineer, were soon fully focused on electronics and software engineering within the Haptics-1 project.[1] Still, with three PhD students in the lab working on different aspects of haptics and teleoperation, I could not but get pulled more and more into the field. I also followed with big interest the research around variable stiffness actuators at the German Aerospace Center (DLR) and other institutes. Then, in autumn 2014, on a long car drive back from testing the Haptics-1 hardware in the European Astronaut Centre (EAC) in Cologne, we discussed with André Schiele the possibility to start a PhD project on combining variable stiffness actuators with teleoperation from February 2015 on. That was the first step towards this dissertation.

This thesis was conducted as part of the H-Haptics project, a large research project involving 16 PhD students and 3 postdocs under Frans C.T. van der Helm (principal investigator and dissertation promotor) and David Abbink (co-principal investigator) funded by NWO (Nederlandse Organisatie for Wetenschappelijk Onderzoek, formerly STW) from 2011 to 2016. The goal of the H-Haptics project was "to understand the benefits and limitations of using haptic shared control, which can guide users and make task requirements and spatio-temporal constraints tangible."[2] Within the H-Haptics project, this dissertation was embedded in the project "Multimodal Space Robotics Teleoperation for Uncertainty Robustness in Human-Robot and Robot-Environment Variations" under the lead of André Schiele (co-promotor). This dissertation would not have been possible without the facilities provided by the Telerobotics and Haptics Lab, the TU Delft Haptics Lab, the Science Centre Delft, and without all the people supporting me and sharing their knowledge with me.

Manuel Aiple
Delft, February 2021

[1] https://www.nasa.gov/mission_pages/station/research/experiments/explorer/Investigation.html?#id=1530
[2] https://delfthapticslab.nl/programme/human-centered-haptics/

1

Introduction

1

1.1. Background

1.1.1. Motivation

Telerobotics [1] is a set of technologies allowing a human operator to control a robot at one place while possibly being located at another, distant, place. The reasons to apply telerobotic technology can be varied. Some environments are hazardous for humans to operate in (*e.g.*, environments contaminated with nuclear radiation [2], coal mines [3], or dangerous disaster sites [4]). Other environments are not reachable for humans at all (*e.g.*, deep-sea [5]), or it would be too expensive or too slow to bring a qualified person on-site (*e.g.*, space [6] or specialized surgery in rural areas [7]). Sometimes robotic assistance can enhance human motion accuracy while still leaving the operator in full control (*e.g.*, in laparoscopic robotic surgery [7]). In other cases, telerobotics allows one person to be present and act at multiple sites quickly after another without physically moving from one place to another (*e.g.*, care applications in people's homes [8]). In such scenarios, specialized robots can be useful as they can be designed to resist harsh environments, execute very accurate motions, have a large workspace, or be very strong. They also can be duplicated to be deployed at multiple sites. This way, a synergy is formed, combining the human operator's intelligence and versatility with the precision, strength, and robustness of the robot, even its disposability in extreme cases (*e.g.*, military applications [9]).

Currently, there is also a trend for robots to be deployed in environments initially built for humans [10] that also affects teleoperation, *e.g.*, when inspecting a collapsed building or assisting people in their homes. Therefore, it can be desirable that teleoperated robots be able to manipulate physical objects in the same way as humans. This way, the robot can work efficiently, and controlling the robot is intuitive for the human operator. In telerobotics, transparency [11] is often defined as the desirable property of the teleoperated robot to reproduce the motion of the operator smoothly, while rendering the interaction of the robot with its environment accurately to the operator, ideally such that "the human operator cannot distinguish between operating in a local or a distant environment" [12]. In simpler words, from a user's point of view, one could say that the robot should "just work" and be operated as expected so that it can be deployed quickly in a new human-centered environment without requiring extensive training of the operator with a particular robot. This entails that the robot can move the same as humans do in terms of workspace, force, and, notably, the same dynamics.

The motion dynamics strongly influence the requirements on the actuators (motors or muscles) and the control system (motor drivers or central nervous system). The more dynamic a motion is, the stronger the actuators and the faster the control systems need to be [13, 14]. In dynamic tasks involving possible collisions, stiffness also becomes an important factor to take into account. While high stiffness is desirable during movement in free air to avoid oscillations and achieve precise motion, lower stiffness is often desirable in contact to avoid damage from excessive forces and allow fine force control under the limitations of comparatively slow control systems [15].

Consequently, one can observe that humans manipulate objects differently in terms of speed/dynamics and stiffness, depending on the task to be performed. The wide range of the speed-stiffness spectrum that humans can cover to perform different tasks is shown in figure 1.1 and compared to the range covered by different kinds of robots:

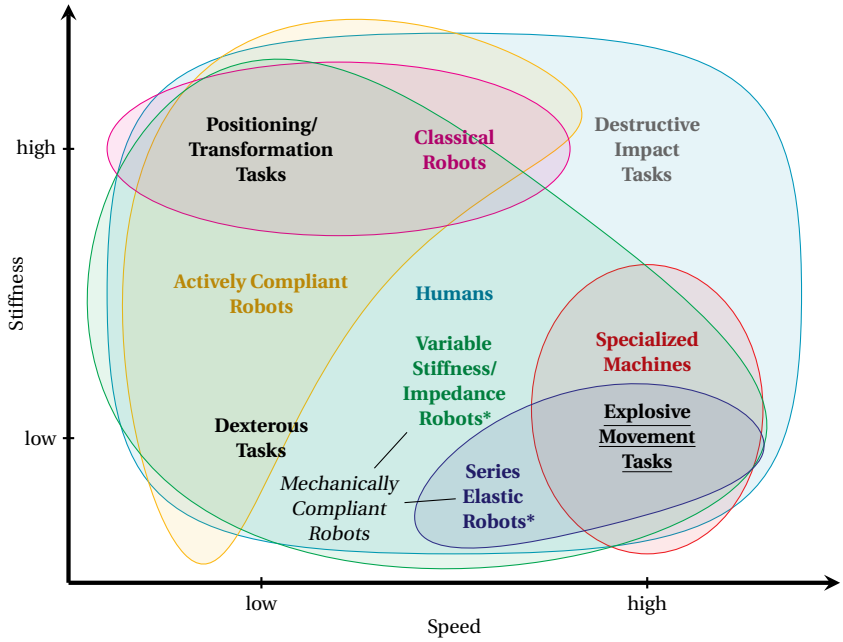

Figure 1.1: Tasks arranged in the stiffness-speed-spectrum and their coverage by humans and different robots and tool machines. This thesis explores how series elastic robots and variable stiffness/impedance robots (marked with an asterisk) can be used efficiently for explosive movement tasks (underlined) in teleoperation. Positioning/Transformation tasks require high forces at high positional accuracy / low speed when operating under external disturbing forces, *e.g.*, to move the end-effector to a precise position in free air or to remove material from the workpiece only where needed and without slipping. Dexterous tasks such as exploration or insertion tasks, or interaction with fragile objects, require as low as possible forces at high positional accuracy, which comes at the cost of lower speed. Destructive impact tasks aim at transferring as much energy as possible on impact to an object, so the stiffness is very high at the moment of impact to increase the contact forces (grayed out as not relevant for robots). Explosive movement tasks as throwing a ball or performing a strike with a hammer aim to accelerate an object and require high speed but reduced stiffness to protect from the impact forces. This is the sort of tasks that will be treated in this thesis. Humans can cover this range of tasks to a large extent and adapt their muscular stiffness specifically to the task at hand. Classical robots are designed to be very stiff and are thereby well adapted to execute transformation tasks, such as machine tools for milling. Actively compliant robots have similar designs as classical robots but are equipped with force sensors to regulate the forces they apply through a control loop. Specialized machines have been built for scenarios where high speeds at low stiffness are needed by only loosely coupling the part that interacts with the environment to the mechanism that accelerates it. Mechanically compliant robots are series elastic robots, variable stiffness robots, and variable impedance robots built with a physical elastic element. Series elastic robots are mechanically different from classical robots as they are designed with some elastic element integrated into their actuators, making them mechanically compliant. Variable stiffness robots also incorporate an elastic element in their actuators in a similar way to series elastic robots. However, in this case, a mechanism allows for changing the mechanical stiffness dynamically. Variable impedance robots additionally allow for varying the damping of the actuator.

- *Positioning/Transformation tasks* require high forces at high positional accuracy and low speed when operating under external disturbing forces, *e.g.*, to move a heavy part to a precise position in free air or to remove material from the workpiece only where needed and without slipping. Examples of transformation tasks performed by humans are planing, scraping, whittling, carving, etc.

- *Dexterous tasks* such as exploration or insertion tasks, or interaction with fragile objects, require low forces at high positional accuracy, which comes at the cost of lower speed. For example, in a peg-in-hole task, speed and stiffness should be low to avoid skewing and friction that might lead to a lock-down between the peg and the hole. In exploration tasks as finding the way in a dark room, stiffness and speed are typically low, not to get hurt or make objects tumble that are in the way. Likewise, in a surgery task, stiffness and speed are low to avoid damaging tissues.

- *Destructive impact tasks* like boxing aim at transferring as much kinetic energy as possible to an object on impact, so velocity and stiffness are maximized at the moment of impact to achieve a high momentum as the product of velocity and so-called "effective mass" [16, 17]. Injuries are accepted as a risk by the boxer. However, these tasks are barely relevant for robots as machines that do work, and will not further be discussed.

- *Explosive movement tasks*, *e.g.*, throwing a ball or performing a strike with a hammer, aim to accelerate an object and require high speed. Once the object is accelerated, the arm's stiffness is reduced to protect the arm from injuries or the robot from excessive wear.

Humans can cover such a wide range of tasks by their capability to adapt their muscular stiffness according to the task at hand by co-contraction of the agonist and antagonist muscles [18] or by adjusting their proprioceptive reflexes [19]. They can even accept injuries to some degree to execute destructive impact tasks as they have the ability to heal, which machines do not yet, although there is research towards self-healing robots [20].

The stiffness of *classical robots*, on the other side, typically depends on their mechanical design, is fixed, and was designed for high positioning accuracy with maximum stiffness [15], orders of magnitude higher than the joint stiffness that humans can maintain in their limbs. Their high stiffness and optimization for position control make them well adapted to execute positioning tasks and transformation tasks, for example, as pick-and-place or milling machines. The higher the robot's stiffness, the higher the working speed can be in these tasks [15].

Actively compliant robots have similar designs as classical robots but are equipped with force sensors to regulate the applied force through a force control loop. Their mechanical joint stiffness is also typically lower than of classical robots to facilitate precise force control, but the joints are not designed for large mechanical deflection. The force control enables them to be very compliant at low speeds. However, at higher speeds, the minimum virtual stiffness that can be rendered is limited by the bandwidth of the control loop [21]. Therefore, the maximum speed of actively compliant robots is bound by the desired softness in contacts.

Specialized machines have been built for scenarios where a high speed at a low stiffness is needed, such as pile drivers [22], jackhammers [23], or hammer drills [24]. The common property of these devices is that the part that interacts with the environment (*e.g.*, the chisel of a jackhammer) is only loosely coupled to the mechanism that accelerates it (*e.g.*, in the case of a jackhammer, it is pneumatically accelerated). Thus, only a small replaceable part suffers the wear of the repeated shock loads, while the complex mechanism that drives it is only exposed to relatively small loads. Nevertheless, these are single-task tools that are not suitable for teleoperation requiring human-like motion.

Mechanically compliant robots, such as series elastic robots [25], variable stiffness robots [26], and variable impedance robots [27], are mechanically different from classical position-controlled robots and actively compliant robots, as they are built with a physical elastic element (*e.g.*, a spring) that gives them considerable mechanical compliance.

Series elastic robots are the simplest type with a constant spring stiffness, yet have some strong advantages compared with actively compliant robots. The spring allows for stable and simple torque control in contact with rigid objects, even at higher speed. The spring acts as a low-pass filter, reducing the controller bandwidth required for stability during contacts significantly. The large deflections make it possible to measure the torque simply by measuring the position difference between the joint and the end-effector. The spring stiffness of SEAs is independent of the working speed, contrarily to actively compliant robots, where the stiffness increases with the working speed due to the fixed controller bandwidth. SEAs are, therefore, suitable to reduce collision forces in high-speed motions. Furthermore, the elastic element can be used as temporary energy storage, which is beneficial in explosive movement tasks [28].

Variable stiffness robots also have an elastic element similarly incorporated in their actuators as series elastic robots do. Thus, they also provide a temporary energy tank. However, in this case, a mechanism allows to change the mechanical stiffness dynamically, thereby not only allowing to execute tasks where low stiffness is advantageous but also tasks for which high stiffness is important (*e.g.*, the AwAS-II actuator has a range "from very soft to completely rigid" [29]).

Variable impedance robots allow for varying the damping of the actuator in addition to the stiffness, with impedance being the combination of stiffness and damping.[1] Variable damping capability is especially useful in rapid movement tasks to reduce undesired oscillations through high damping after a fast motion performed with low damping [30].

These are promising properties for series elastic robots, variable stiffness robots, and variable impedance robots to perform "fast and soft" tasks [31] through teleoperation, a gap so-far left open by classical and actively compliant robots. This thesis focuses on explosive movement tasks as they open intriguing possibilities, especially for disaster recovery and teleoperated exploration applications. The idea is to extend the range of tasks that humans can perform through teleoperation by designing a teleoperation system that can efficiently execute human-like explosive movements and is easy for untrained operators to control.

[1] More generally, the complex impedance Z links force F and velocity v such that $F = Z\,v$.

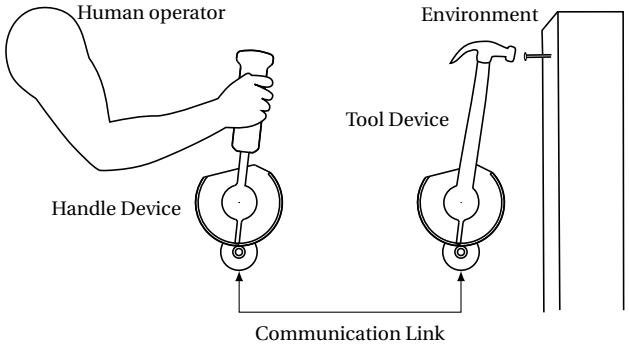

Figure 1.2: In a teleoperation scenario, the human operator interacts with the teleoperation system through the handle device, and the handle device interacts with the environment through the tool device. Velocity and force information is transmitted between handle and tool device through the communication link, such that velocities and forces are mirrored as closely as possible between the two.

1.1.2. State of the Art

While the research to make robots fully autonomous has made remarkable progress (*e.g.*, on object manipulation [32, 33], humanoid robots [34], and social robots [35]), teleoperation is still often more practical in complex scenarios through its combination of the intelligence and versatility of humans with the ruggedness and precision of robotic manipulators. In teleoperation such as illustrated in Figure 1.2, human operators located at one site interact with the handle device of the teleoperation system, performing the motions to be copied by the robotic tool device, possibly at another site, and feeling the interaction forces of the tool device with its environment through the handle device that recreates them [1]. In bilateral teleoperation, velocity and force information is exchanged in both directions to achieve very accurate mirroring between handle and tool device. Especially in unstructured environments, such as in exploration missions with little prior knowledge about the situation on-site, teleoperation allows for reacting quickly to unexpected situations, *e.g.*, blocked paths, wrongly assembled parts, the unsuccessful opening of doors, etc.

Fully transparent teleoperation systems should allow human operators to execute motions remotely as if they were on-site [12]. Thus, one can postulate that they should also cover the full speed-stiffness spectrum of human tasks in the field. However, this is not the case with state-of-the-art teleoperated robots. Classical robots are designed to achieve maximum mechanical stiffness at the end-effector [15]. This is to ensure that its position is affected the least possible by external loads. For example, the robot end-effector could be a gripper placing an object precisely or a power tool drilling a hole. In these cases, the end-effector position should not be influenced by the object's weight or any forces acting on the drill. A lot of knowledge and experience has been acquired on how to achieve high mechanical stiffness in robots. That was justified as robots have been mostly used in mass production for precise positioning tasks in structured environments. In these applications, contact forces are either intentionally high or are within an acceptable range

in a predetermined task.[2] Also, robots with high stiffness pose fewer control problems than soft robots, which deform less predictably and can have mechanical resonance at unsuitable frequencies [37, 38]. However, for the dynamic type of tasks considered in this thesis, very stiff robots might not be the most suitable technology.

1.2. Problem description

Teleoperation systems with traditionally designed tool devices being typically stiff results in the following limitations:

1. The range of tasks that human operators can perform through a stiff teleoperator system is limited to positioning/transformation tasks and dexterous tasks.
2. Stiff robots can harm humans because the shock loads are high on collision with humans.
3. Stiff robots get damaged by shock loads, making them less suitable for harsh unstructured environments.

SEAs and variable stiffness actuators (VSAs) have been developed to make robots less stiff but more passively compliant. Various VSA designs have been proposed that allow to continuously vary the actuator stiffness, and vast research has been done to control SEAs and VSAs efficiently [27, 39]. The execution of explosive movements with VSAs optimized according to optimal control theory has been studied thoroughly [40–42]. In particular, it has been shown that VSAs can reach up to four times higher speed than rigid actuators in automated explosive movements, by intelligently using the spring to store and release energy in a backward-forward motion [43].

This thesis focuses on human upper-limb explosive movements performed through a teleoperation system with a variable impedance actuators (VIAs) tool device, which still lacks research. As humans are not machines that can perform motions with mathematical precision, the solutions mentioned above from optimal control theory cannot simply be transferred to teleoperation applications, as they require the exact knowledge of the system's dynamics and being able to time the motion precisely. Both are difficult for human operators to estimate and perform, even more so in teleoperation, due to imperfections in the teleoperation system.

Hardly any teleoperation system can achieve perfect transparency. As a result, the forces rendered through the handle device do not match the external forces acting on the tool device perfectly [44], which makes it more difficult for the human to estimate the system dynamics. Also, some communication delay typically exists between the handle device and the tool device [44], making precise timing even more difficult for humans than it is already. Therefore, it is likely impractical to teach a human operator how to perform explosive movements optimally.

Instead, the approach in this thesis is to design the teleoperation system such that it allows the human operators to perform explosive movement tasks in the way that they

[2] Remote center of compliance devices [36] allowing for small deformations at the end-effector of a robot are also elastic elements for robots, commonly used to make stiff robot manipulators more tolerant to alignment errors in placement tasks, but are very different to SEAs in their practical usage and will not be considered in this thesis.

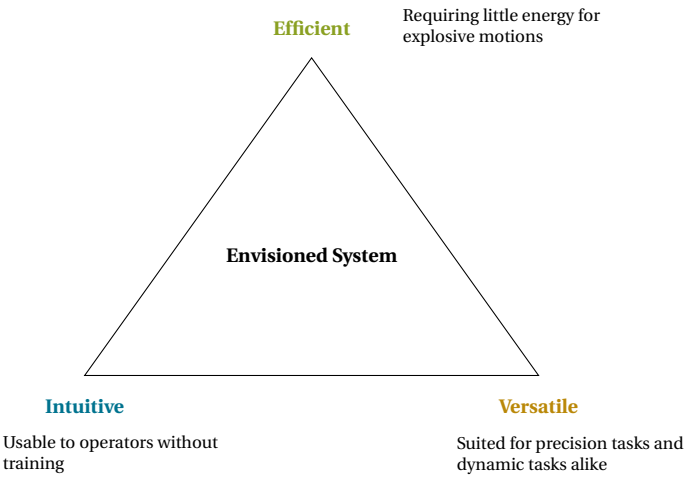

Figure 1.3: The vision of this thesis is to design a teleoperation system that is energy efficient, intuitive to use, and versatile to allow to perform a wide range of tasks.

are used to from motions they know (*e.g.*, from throwing and hammering). This means strategies have to be found to make the human operator and the variable stiffness tool actuator interact efficiently and intuitively on the hardware level and the control level.

1.3. Aim and Scope

This thesis aims to allow human operators to perform explosive movement tasks through teleoperation, which is new in the field. This includes designing a teleoperation system with a variable impedance tool device and a method for impedance variation. The system should allow human operators to use a variable stiffness robot efficiently and intuitively for explosive movements and precision tasks alike without requiring the operator to explicitly change the mode (cf. Figure 1.3). From these considerations, the following high-level requirements emerge for the teleoperation system envisioned in this thesis:

1. Efficiency: The system should allow human operators to achieve a high velocity gain and, consequently, a significantly higher output velocity than a rigid actuator in explosive movements.

2. Intuitiveness: The operators should be enabled to interact with the system without requiring long training, ideally being able to use the system in the first session.

3. Versatility: The system should not be a specialized tool for one task as, for example, hammering, but a wide-range teleoperation system, suitable for precision tasks and dynamic tasks alike.

As these requirements are impractical to be fully satisfied all three at the same time (*e.g.*, the most efficient system would follow a hammering trajectory given by optimal control theory, but this is very difficult to follow for a human operator as it requires very precise

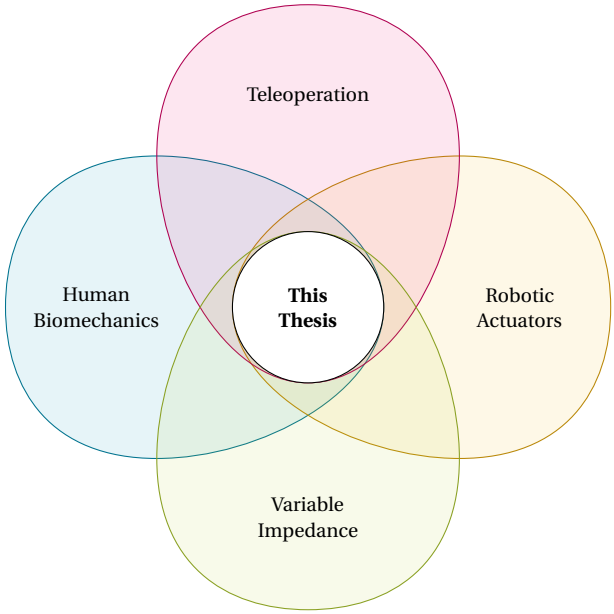

Figure 1.4: This thesis combines aspects from human biomechanics, telerobotics, robotic actuators, and variable impedance.

timing and this trajectory is optimized for exactly one motion), the challenge of this thesis is to find a good trade-off between the three requirements.

1.4. Approach

Aspects from human biomechanics, telerobotics, robotic actuators, and variable impedance affect this thesis (cf. Figure 1.4).

First, for the idea of dynamic teleoperation to have any prospects of success, the human operators need to be understood, and their capabilities and limitations to interact with an elastic actuator need to be evaluated. This is done in chapter 2 through two experiments, the first in direct manipulation and the second in teleoperation.

A VIA is then required for validating impedance adaptation strategies experimentally. It needs to be fast enough to reproduce the human motion, and to independently and dynamically modify the stiffness and damping. Such an actuator is presented in chapter 3.

Finally, a suitable method for impedance variation is needed that gives a human operator fine control of the position for precision tasks while allowing to reach high gain and output velocity in dynamic tasks. Chapter 4 describes an algorithm meeting these criteria and its experimental validation.

For the experiments, hammering was selected as an exemplar for explosive movement tasks as it is a simple task that most people are familiar with. While hammering might be mistaken as a destructive impact task, hammering, unlike boxing, is done with a heavy tool that will transfer its kinetic energy on impact. Injuries to the operator's arm should be avoided during hammering. Consequently, hammering is done by accelerating the

hammer head and then decoupling the arm from it before impact, making it an explosive movement task. The decoupling is achieved by reducing grip strength and arm stiffness. The hammering was reduced to one-degree-of-freedom to keep the experimental setups simple and the motion well-defined. In chapter 5, this thesis' findings are summarized, discussed, and put into perspective for future research.

2

Increasing Impact by Mechanical Resonance for Teleoperated Hammering

Series elastic actuators (SEAs) are attractive for usage in harsh environments as they are more robust than rigid actuators. This paper shows how SEAs can be used in teleoperation to increase output velocity in dynamic tasks. A first experiment is presented that tested human ability to achieve higher hammerhead velocities with a flexible hammer than with a rigid hammer and to evaluate the influence of the resonance frequency. In this experiment, 13 participants executed a hammering task in direct manipulation using flexible hammers in four conditions with resonance frequencies of 3.0 Hz to 9.9 Hz and one condition with a rigid hammer. A second experiment is then presented that tested the ability of 32 participants to reproduce the findings of the first experiment in teleoperated manipulation with different feedback conditions: with visual and force feedback, without visual feedback, without force feedback, and with a communication delay of 40 ms. The results indicate that humans can exploit a flexible system's mechanical resonance to at least double the output velocity without combined force and vision feedback. This is an unexpected result, allowing the design of simpler and more robust teleoperators for dynamic tasks.

This chapter is based on the following publications:

- M. Aiple and A. Schiele, "Towards teleoperation with human-like dynamics: Human use of elastic tools", *2017 IEEE World Haptics Conference (WHC)*, Munich, 2017, pp. 171-176
- M. Aiple, J. Smisek, and A. Schiele, "Increasing Impact by Mechanical Resonance for Teleoperated Hammering", in *IEEE Transactions on Haptics*, vol. 12, no. 2, pp. 154-165, 1 April-June 2019

2.1. Introduction

Teleoperation is classically desired to be performed with a transparent system [1]. This is often realized by using mechanically stiff devices. While this is advantageous for precision, it is an issue for dynamic tasks, where high impacts can be experienced during contact, such as in harsh environments in search and rescue missions [45], explosive ordnance disposal [45], nuclear research maintenance [46], teleoperated forestry [47], or underwater robotics [5]. A stiff robot experiences high shock loads on impact, which can damage the robot's gears [25]. Series elastic actuators (SEAs) promise higher mechanical robustness [25], but their usage for precision [48] and high-impact tasks in teleoperation still requires research.

One appealing feature of SEAs is the possibility to maximize power transfer from an operator controlling a handle device to a tool device if the mechanical resonance intrinsic to SEAs is well exploited during the movement. By "exploiting," we mean sense and utilize the system's resonance frequency and excite it to achieve maximum power transfer and maximum output velocity. Until now, there have been only a few studies on maximum power transfer in SEAs, with the focus on designing fully automatic control laws [43, 49, 50].

However, to the authors' knowledge, the following three questions have received little attention in previous research.

1. Can humans sense and identify the resonance frequency of SEAs?
2. Within which resonance frequency/stiffness range can humans sense the resonance frequency and tune their motor actions to the timing required to exploit SEAs for maximum power transfer?
3. What type and quality of feedback should be given to humans to exploit SEAs for maximum power transfer?

Answering these open questions will enable the design of new teleoperation systems with variable stiffness tool actuators with the objective of allowing not only for precise positioning but also the performance of high-impact tasks.

The present study aimed to explore these questions experimentally by having human operators execute a hammering task with a haptic teleoperated single degree of freedom hammering apparatus (cf. Figure 2.1). To this end, two experiments were conceived. The first was designed to investigate the first two questions above and to determine:

a) the influence of frequency/stiffness on human performance in exploiting SEAs for maximum power transfer,
b) the degree to which humans can achieve the optimal excitation timing (see section 2.2 for a definition of the optimal timing), and
c) the practically achievable output velocity to input velocity amplification.

In the following section, we will explain how a flexible system can achieve a higher power transfer than a rigid system. The second experiment was designed to approach the third question by quantifying the dependence of the human manipulation of flexible tools concerning the availability of visual and force feedback, as well as their sensitivity to the presence of time delay.

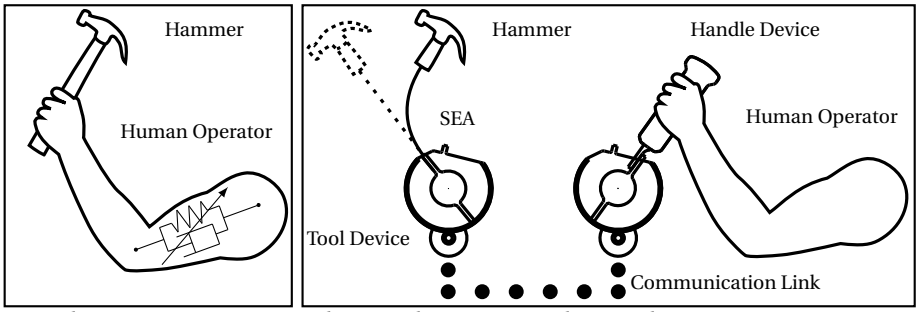

Figure 2.1: Visualization of the conceptual transfer from human manual hammering (left) to human teleoperated hammering with an elastic tool device (right). Mechanical compliance, which is inherent to human muscles, is substituted through a spring in the robotic tool in the experiments presented in this chapter.

In both experiments, hammering was selected as the experimental task, as the principles are generally known, and the task itself can be simplified to one degree of freedom. It might seem paradoxical to use an elastic hammer, which can less effectively transmit forces through the handle to the hammerhead. However, the primary objective of hammering is to transform kinetic energy into mechanical work by the impact. The effect of the force transmitted through the handle during the impact is negligible in comparison. Consequently, typical hammers have longer handles to obtain high hammerhead velocities (while keeping the same hand velocity). Furthermore, hammers in practice are held loosely at the moment of impact to reduce the shock load to the hands and arms. The same principle is applied in power machines, such as pile drivers, jackhammers, and hammer drills. In these machines, the hammer head either runs free during the impact or is only loosely coupled to the actuator.

We advocate that hammering with an elastic hammer could have a double benefit for teleoperated hammering:

1. an elastic hammer could achieve a higher impact velocity than a rigid hammer with the same velocity of the tool actuator, and
2. the shock loads to the tool actuator could be reduced.

Such a system could provide a better performance and have a longer lifetime without requiring more powerful actuators or stronger mechanical structures.

2.2. Increasing Impact with a Flexible Hammer by Mechanical Resonance

2.2.1. Modeling of the Rigid and the Flexible Hammer

The following explanations are illustrated with a linear mass-spring-damper model instead of a rotational mass-spring-damper model. The equations are the same for linear variables and their rotational equivalents. The transfer function $H_{rigid}(s)$ of a mass $m > 0$, exposed to viscous damping $b > 0$, as illustrated in Fig. 2.2a, is trivially described in the

Laplace domain by

$$H_{rigid}(s) = \frac{V_{rig}(s)}{V_{in}(s)} = 1\,, \tag{2.1}$$

with $V_{in}(s)$ and $V_{rig}(s)$ the Laplace-transformation of $v_{in}(t)$ and $v_{rig}(t)$, which are the input velocity and the velocity of the rigid hammer.

The transfer function of a mass-spring-damper system with stiffness $k > 0$ as modeled in Fig. 2.2b is obtained from the equality of forces acting on the mass m as

$$(s\,m + b)\;\; V_{flx}(s) = -\frac{1}{s}\,k\;\left(V_{flx}(s) - V_{in}(s)\right), \tag{2.2}$$

with $V_{flx}(s)$ the Laplace-transformation of $v_{flx}(t)$, which is the velocity of the flexible hammer, resulting in

$$H_{flexible}(s) = \frac{V_{flx}(s)}{V_{in}(s)} = \frac{k}{s^2\,m + s\,b + k}\,. \tag{2.3}$$

The resonance frequency f_0 is the frequency f for which the magnitude of $H_{flexible}(s)$ is maximized. This is obtained by solving the minimization problem of the denominator:

$$\min_s \left\| s^2\,m + s\,b + k \right\|, \tag{2.4}$$

with the Laplace variable $s = j\,\omega$, and the angular frequency $\omega = 2\,\pi\,f > 0$. Equation 2.4 is solved for the resonance frequency

$$f_0 = \frac{1}{2\,\pi}\,\sqrt{\frac{k}{m} - \frac{b^2}{2\,m^2}}\,. \tag{2.5}$$

Because the term under the square-root has to be positive for f_0 to have a real value, the criterion for resonance to occur is

$$b < \sqrt{2\,k\,m}\,. \tag{2.6}$$

In the following, we assume that this condition is satisfied and that $b \ll \sqrt{2\,k\,m}$. The equation for the resonance frequency can then be simplified to

$$f_0 \approx \frac{1}{2\,\pi}\,\sqrt{\frac{k}{m}}\,. \tag{2.7}$$

2.2.2. Exploiting Mechanical Resonance for Increased Output Velocity

The frequency-domain responses and time domain responses of rigid and flexible hammers can be analyzed in detail using equations 2.1, 2.3, and 2.7: Fig. 2.2c shows the velocity transfer function magnitudes of the rigid hammer $\left\| H_{rigid}(s) \right\|$ and the flexible hammer $\left\| H_{flexible}(s) \right\|$ over the frequency f. $\left\| H_{rigid}(s) \right\|$ equals 1 for all frequencies, meaning that the amplitude of the output velocity $v_{rig}(t)$ of the rigid tool always equals the amplitude of the input velocity $v_{in}(t)$. However, $\left\| H_{flexible}(s) \right\|$ is considerably greater than 1 for frequencies around the resonance frequency, meaning that the amplitude of the output velocity $v_{flx}(t)$ is much higher than that of the input velocity $v_{in}(t)$ at these

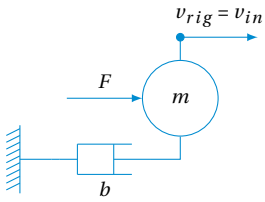

(a) Rigid Hammer Model

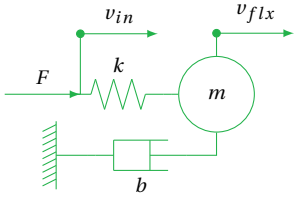

(b) Flexible Hammer Model

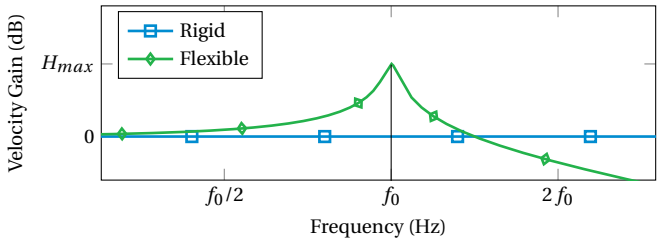

(c) Velocity Transfer Function Magnitude

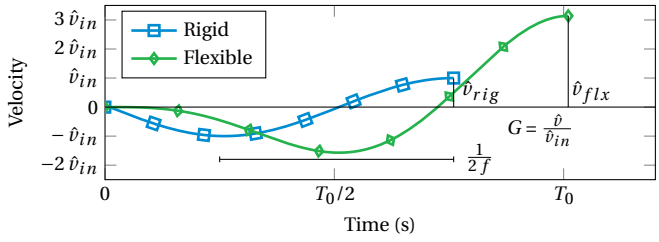

(d) Velocity Time Domain Response

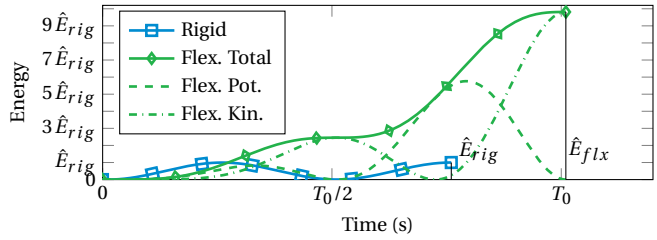

(e) Energy Time Domain Response

Figure 2.2: Comparison of a rigid hammer and a flexible hammer driven by an ideal velocity source: (a) rigid hammer model, (b) flexible hammer model, (c) velocity transfer function magnitude plot, (d) velocity response to a hammering motion in the time domain until impact (vertical black line), (e) energy response to a hammering motion in the time domain until impact (vertical black line). m is the mass of the hammerhead; b is the damping factor; k is the spring stiffness; v_{in} is the source velocity; v_{rig} and v_{flx} are the velocities of the rigid and the flexible hammer, respectively; f_0 is the resonance frequency; $H_{max} = \max\left|H_{flexible}(s)\right|$ is the maximum gain of the flexible hammer; $T_0 = 1/f_0$ is the resonance period; $\hat{v}_{rig}$ and $\hat{v}_{flx}$ are the peak velocities of the rigid and the flexible hammer; $G = \frac{\hat{v}}{\hat{v}_{in}}$ is the velocity gain, with $\hat{v} = \hat{v}_{rig}$ for the rigid hammer and $\hat{v} = \hat{v}_{flx}$ for the flexible hammer; f is the excitation frequency; $\hat{E}_{rig}$ and $\hat{E}_{flx}$ are the peak energy of the rigid and the flexible hammer, respectively.

frequencies. Only for excitation frequencies considerably higher than the resonance frequency (for frequencies greater than approximately 1.5 f_0), is the output velocity of the flexible tool lower than the input velocity.

Fig. 2.2c shows that the excitation frequency should be as close as possible to the resonance frequency f_0 in order to achieve the highest velocity with a flexible hammer. This holds for a periodic motion, as well as for a motion with only one reversal of motion, such as a single hammer strike, as will be analyzed next.

2.2.3. Implications of Mechanical Resonance for Hammering with a Flexible Hammer

The principle of hammering is to impact a hammerhead on a target with maximal kinetic energy E_k. E_k depends on the mass of the hammerhead m and its velocity v (equal to v_{rig} for the rigid hammer or v_{flx} for the flexible hammer), as

$$E_k = \frac{1}{2} m v^2 . \tag{2.8}$$

Fig. 2.2d shows the velocity response in the time domain to a hammering motion at the resonance frequency of the flexible hammer compared to the response of the rigid hammer driven by the same velocity source (the input velocity is equal to the velocity of the rigid tool and therefore not displayed in the plot).

In the following, we will refer to the motion profile depicted in Fig. 2.2d as one *strike*. The strike starts with a backward motion (negative velocity) followed by a forward motion (positive velocity) until the peak, marked by the vertical line. The peak should coincide with the impact when hammering on a target. The reversal of motion direction has to occur after half the resonance period T_0 for the excitation frequency f to match the resonance frequency f_0. We refer to this as the optimal timing:

$$T^* = \frac{T_0}{2} = \frac{1}{2 f_0} = \pi \sqrt{\frac{m}{k}} . \tag{2.9}$$

Hence, the ability to accurately time the reversal is critical to achieving maximum impact with a flexible hammer.

Fig. 2.2e shows the energy increase in the flexible hammer compared to the rigid hammer during one strike. While the energy of the rigid hammer consists only of the kinetic energy E_k, the energy of the flexible hammer equals to the sum of the kinetic energy and the potential energy in the spring E_p:

$$E_p = \frac{1}{2} k \Delta x^2 , \tag{2.10}$$

with Δx being the spring deflection. If the excitation frequency equals the resonance frequency, the kinetic energy of the hammerhead is fully transferred into potential energy of the spring during the reversal of motion and back into kinetic energy during the forward swing motion, thereby achieving the highest kinetic energy on impact. Thus, exciting the mechanical resonance of a flexible hammer increases the power transferred to the hammerhead, which results in a significantly increased peak velocity and peak energy compared to a rigid hammer driven by the same velocity source.

2.3. Experiment 1: Direct Manipulation

The first experiment of this study examined how humans interact with elastic tools for maximum output velocity tasks. Maximum output velocity tasks are tasks as throwing and hammering, aimed at giving the most kinetic energy to an object with as little input energy as possible. We picked this class of tasks for this experiment as it makes use of SEAs' advantage compared to rigid actuators, their capacity to store energy in their spring when switching from a backward motion to forward motion, and then releasing it as kinetic energy. Optimal control strategies have been proposed for SEAs and variable stiffness actuators (VSAs) executing maximum output velocity tasks [50]. Output velocities of 272% of the maximum motor speed have been measured with VSAs [42].

We took one step back from the teleoperation scenario to exclude effects coming from the teleoperator system (*e.g.*, time-delay, missing fidelity in force-feedback rendering, dynamic constraints of the slave) and performed an experiment with direct use of an elastic tool, asking participants to hit a target as hard as possible with an elastic hammer. We analyzed the task performance as a function of the stiffness of the elastic hammer, the number of trials, and the motion profile.

2.3.1. Hypothesis

The following hypothesis was formulated for the direct manipulation experiment:

Hypothesis H1: Humans can exploit a flexible hammer's elasticity in direct manipulation to maximize power transfer in a strike and achieve higher output velocity than with a rigid hammer.

2.3.2. Conditions

Five hammer stiffness conditions were used (with corresponding resonance frequencies): 0.62 N m/rad (3 Hz), 2.3 N m/rad (4.8 Hz), 4.1 N m/rad (6.9 Hz), 11 N m/rad (9.9 Hz), and rigid (stiffness higher than 10 000 N m/rad and resonance frequency higher than 300 Hz). The conditions are denoted in the text using the resonance frequency (determined through system identification measurements [51]). The stiffness settings were chosen based on a pilot study. For stiffness settings below 0.62 N m/rad, pilot participants reported that they did not get the impression that they were creating any impact. For stiffness settings higher than 11 N m/rad, pilot participants reported not being able to distinguish between flexible and rigid hammer extension.

2.3.3. Participants

The experiment was performed by 13 participants (8 male, 5 female, 12 righthanded, 1 ambidextrous, age 21-41). The participants were researchers and project engineers with a higher education background. None of the participants had prior experience with the experiment. The experiment had been approved by the human research ethics committee of TU Delft, and all participants gave written informed consent before participation.

2.3.4. Experiment Procedure

Fig. 2.3 visualizes the experiment procedure. The participants received verbal task instructions and then conducted 100 training trials followed by 20 performance trials per

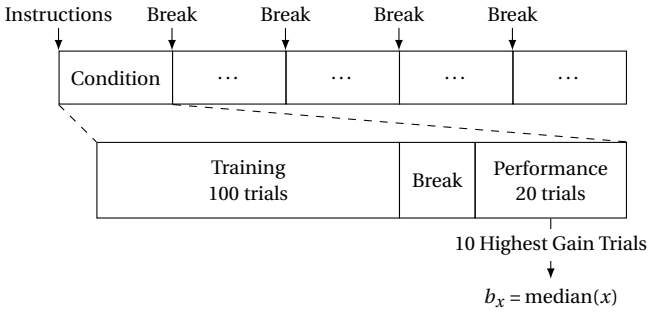

Figure 2.3: Experimental procedure of Experiment 1.

condition. The order of conditions was randomly selected for each participant. There was a short break (approximately 1 min) to download the data between training trials and performance trials. Between two conditions, there was a break to download the data and change the spring of the flexible hammer extension (approximately 5 min). Only the trials conducted in the performance phase were used for the analysis.

2.3.5. Experiment Apparatus

An apparatus was designed for this study to enable the performance of a one degree of freedom flexible hammering task in either direct or teleoperated manipulation with identical handle and tool devices (see photos in Fig. 2.4 as well as the illustration in Fig. 2.5). We mounted the hammer hanging down so that the spring was stable in the neutral position with the handle in the vertical position. Participants could execute hammering motions by moving the handle with their right hand. The setup constrained the motion to one degree of freedom. Therefore, the motion was quite different from the hammering participants might have been accustomed to. Besides, the backswing was a pushing motion for the participants, and the forward swing was a pulling motion. Although one might consider this as making the experimental setup unrealistic, we thought this was beneficial as it reduced possible effects from participants' previously acquired skills. We assumed that participants had a general understanding of elastic tools, but no knowledge about this particular setup.

Although the required motion of the operator is different from hammering with a conventional hammer, the authors believe that the setup provides good insights into how humans interact with flexible tools in general. The teleoperation system used in Experiment 2 is explained in more detail in Section 2.4.

The handle device and the tool device had a one degree of freedom rotational actuator with a torque sensor, driven by a 70 W brushless DC Maxon EC-max 40 motor with gear and capstan drive (total gear ratio 35:1). It was a modified version of the setup described by Rebelo *et al.* [52]. We used only one unit and decoupled the motor from the output axis by removing the wire from the capstan gear. We replaced the original end-effector with a handle and a hammer. The hammer consisted of a 115 g hammerhead (similar to light commercial hammers) attached to the output shaft of the tool device through an exchangeable extension in such a way that the distance between the rotation axis and

(a) Direct manipulation

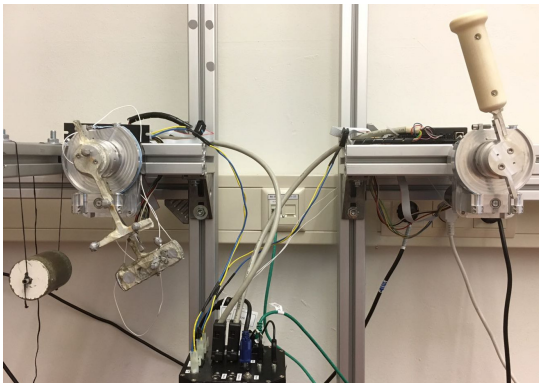

(b) Teleoperated manipulation

Figure 2.4: Experimental apparatus used for the two experiments.

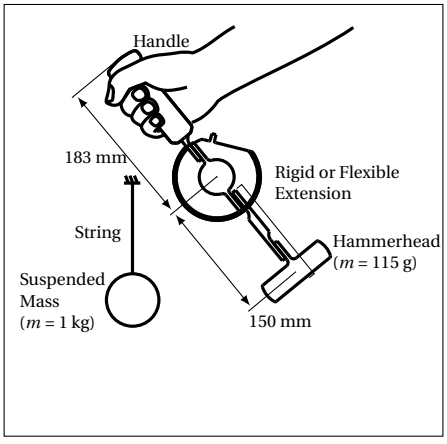

Experiment 1: Direct Manipulation Setup

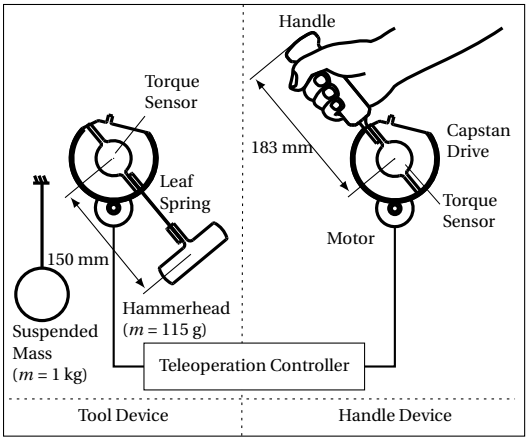

Experiment 2: Teleoperated Setup

Figure 2.5: Schematic view of the setups for Experiment 1 and Experiment 2. In Experiment 1, the handle is mounted on the same rotating axis as the hammer. In Experiment 2, the handle is mounted to the handle device, whereas the hammer is mounted to the tool device. The handle device and the tool device are coupled by a four-channel teleoperator. They are fixed to separate frames to isolate the vibrations between the tool device and the handle device.

the hammer head center of mass was 150 mm. The extension consisted of either a leaf spring or a rigid extension of the same length. For simplification, linear behavior of the leaf spring was assumed in general. However, the methods used for data processing and analysis did not require linearity of the spring. The handle device and the tool device were mounted on separate mechanical structures to prevent any vibrations from being propagated from the tool device to the handle device.

A handle for the operator was mounted on the output shaft of the tool device or the handle device with a distance of 183 mm between rotation axis and handle tip. In the direct manipulation configuration, the handle was mounted to the tool device, and there was a mechanical coupling between the handle held by the operator and the hammer. In this configuration, the motor of the tool device was decoupled from the capstan drive to reduce friction.

In the teleoperated manipulation configuration, the handle was mounted on the handle device, and the tool device was driven by the motor controlled by the four-channel bilateral teleoperation controller running at 1 kHz (see section 2.4.5). At the same time, force feedback was provided to the operator through the motor on the handle device side, which was also controlled by the teleoperation controller.

A mass of 1 kg served as the target to be struck by the flexible hammer. It was suspended so that it could be struck by the hammer and provide the participants with a simple visual impression of the impact energy: The greater the impact energy, the higher the target swung after the impact.

2.3.6. Experiment Task

The task for both experiments was identical: a one degree of freedom flexible hammering task. The motion should consist of one hammer strike per trial consisting of one backward swing followed by one forward swing. The goal of the task for the participants was to find the best timing for achieving maximum impact with least effort, while using a similar effort in every trial and focusing primarily on the timing of the change of direction of motion. It was communicated to the participants that what was important was the velocity gain, not the absolute energy in the impact. In other words, the task instructions were explicitly formulated with the emphasis on the velocity gain and timing for resonance, because during pilot studies, participants had tended to put all their effort into achieving maximum impact, thereby quickly suffering fatigue without utilizing the resonance (which was not in accordance with the goal of the experiment).

2.3.7. Data Acquisition

The tool device joint and hammer head positions were tracked simultaneously using one Vicon motion capture system at a sampling rate of 1 kHz. To this end, reflective markers were attached rigidly to the actuator joint and the hammer head. This way, all relevant data was acquired by the same system, and inaccuracies through the measurement method were reduced. In the post-processing, these positions were transformed into polar coordinates, the angular velocities of joint and hammer were derived, and the individual trials were segmented and synchronized as following.

The markers fixed to the handle and the hammer head defined two positions in the motion capture system: position E, coupled to the handle, and position H, coupled

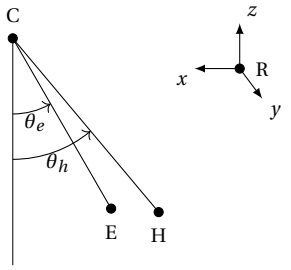

Figure 2.6: Mapping from motion capture system coordinates x,y,z in the reference frame R to rotation angles of the handle θ_e and the hammer head θ_h around the rotation axis center C. The points E and H are the positions of the objects defined by the markers on the handle extension and the hammer head, respectively.

to the hammer head. We converted the Cartesian coordinates x, y, z measured by the motion capture system into polar coordinates θ_e and θ_h by mapping them to two circles around a common center C and lying in the same plane (cf. Fig. 2.6). This produced two one-dimensional signals for analysis. We segmented the time sequences to isolate the individual hammer strikes and synchronized the segments to have the impact with the suspended mass at time 0 s. For the following calculations, we cropped the segments to the time -425 ms up to 0 s. For every segment, we calculated the gain G defined by the peak hammer head velocity $\dot{\theta}_{h,max}$ divided by the peak handle velocity $\dot{\theta}_{e,max}$, and estimated the input frequency f from the half period between the minimum and the maximum handle velocity (cf. Fig. 2.2d).

2.3.8. Dependent Measures

Three dependent measures, listed in Table 2.1, were used to compare the hammering task performance. As illustrated in Fig. 2.2d, the measures were extracted from the time domain data as following for each segment (cf. [51]). The peak joint velocity $\hat{v}_{in}$ and peak hammerhead velocity $\hat{v}$ were obtained by calculating the maximum of the joint velocity v_{in} and of the hammer velocity v before the impact. The gain $G = \hat{v}/\hat{v}_{in}$ was calculated as the ratio of peak joint velocity to peak hammerhead velocity. The excitation frequency $f = 1/(2 \cdot T/2)$ was calculated from half the period $T/2$, calculated from the time between the minimum and the maximum of the joint velocity v_{in}.

It was decided to use the peak velocity as measure instead of the impact velocity, which might be different, as the primary research question of this study was how to exploit mechanical resonance. Therefore, the peak velocity is more relevant than the impact velocity. In practice, the peak velocity of a given velocity profile can be made to occur at the impact position by adapting the start position.

The peak hammer velocity $\hat{v}$ measured the achieved result and gave an indication of the effectiveness of the task execution. The dimensionless gain G gave an indication of the energy efficiency of the task execution and was the primary measure to be maximized. The excitation frequency f was used to assess whether the participants tried to sense and excite the flexible hammer's mechanical resonance to achieve better performance. The closer the excitation frequency to the resonance frequency, the better they had adapted

Measure	Symbol	Description
Output	$\hat{v}$	Peak hammer velocity (rad/s)
Efficiency	G	Gain (-)
Adaptation	f	Excitation frequency (Hz)

Table 2.1: Dependent Measures

to the system. Therefore, the excitation frequency indicated whether the participants tried to influence the experiment's outcome by changing their strategy (hammering faster or slower), or whether they kept the same strategy throughout the experiment and the outcome was influenced only by the properties of the system.

2.3.9. Data Analysis

A single value per trial of each dependent measure was obtained through the described procedure. Trials were discarded if no values could be extracted for the dependent measures, *e.g.*, if the motion did not consist of a backward and forward swing. For the remaining trials, the 10 best trials were selected based on the highest gain G, and the median of each measure $\hat{v}$, G, f was calculated from these 10 trials and notated $b_{\hat{v}}$, b_G, and b_f, respectively. This was done to ensure that learning or fatigue effects did not affect the results. In a preceding analysis, the data were analyzed for patterns in the learning or fatigue, correlating with the order or the type of conditions, but none were observed.

2.3.10. Statistical Evaluation

Friedman's test [53] was used to check for column effects in the dependent measures ($b_{\hat{v}}$, b_G, and b_f) after adjusting for possible row effects ($\alpha = 5\,\%$, row effects: participant-dependent variations, column effects: condition-dependent variations). For Experiment 1, where Friedman's test indicated an effect, Wilcoxon's signed-rank test [54] was applied for pairwise testing of the conditions ($\alpha = 1\,\%$ to compensate for multiple comparisons). The effect sizes, reported as $\Delta b_{\hat{v}}$, Δb_G, and Δb_f, were calculated as the median of the pair differences, with corresponding 95% confidence intervals. The 4.8 Hz condition of Experiment 1 was included as a reference condition in the box plots of Experiment 2 for visual comparison of the performance differences between teleoperated manipulation (Experiment 2) and direct manipulation (Experiment 1). It was not used for the statistical analysis of Experiment 2.

Finally, an estimate of the minimum effect size [55] was provided for each measure. It was calculated through statistical power analysis as the minimum required difference between medians to reject the null hypothesis with $1 - \beta = 80\,\%$, given the number of participants and the estimated variation [56]. Because the data were not normally distributed, the calculation was based on an equivalent standard deviation estimation $\overline{\sigma}$ using the median absolute deviation MAD: $\overline{\sigma} = 1.48\,\mathrm{MAD}$ [57]. Thus, the estimates give an indication of the required effect sizes, but an exact comparison with the results of Friedman's test and Wilcoxon's signed-rank test would be difficult to make.

Condition	$f_0 = \frac{\omega_0}{2\pi}$	ζ
0.4 mm	2.98 Hz	$23 \cdot 10^{-3}$
0.6 mm	4.82 Hz	$32 \cdot 10^{-3}$
0.8 mm	6.93 Hz	$40 \cdot 10^{-3}$
1.0 mm	9.89 Hz	$17 \cdot 10^{-3}$

Table 2.2: System identification results for the transfer function $H(s) = \frac{\dot{\theta}_h}{\dot{\theta}_e} = \frac{1}{1+\frac{2\zeta}{\omega_0}s+\frac{1}{{\omega_0}^2}s^2}$.

2.3.11. Results

System Identification

As explained above, we modeled the elastic hammer as a mass-spring system with the handle velocity as input and the hammer head velocity as output. We extracted the second-order transfer function for the different extensions through system identification to determine the resonance frequency f_0 and damping ratio ζ (table 2.2). For the system identification, we used a separate measurement with manual input at different frequencies, with the hammer head able to move freely (suspended mass removed). Based on this transfer function, we calculated the reference gain G_{ref} with a theoretical reference velocity profile input, which was a bang-bang type profile with half a period of back swing followed by half a period of forward swing according to Haddadin *et al.* [50].

Figs. 2.7 to 2.9 show the qualitative difference between the velocity profiles and system responses. Fig. 2.7 shows the measured input (handle) and output (hammer head) velocity profiles after normalization and taking the median of all participant performance phase trials. The median velocity profile is suitable for representing a typical velocity profile as the participants adopted very similar profiles at the end of the learning phase. Fig. 2.8 visualizes the simulated system response to the human input velocity profile, showing a good match between simulation and measurement data compared to Fig. 2.7. Fig. 2.9 shows the results of the simulated system response to the reference input velocity profiles. We can see that the difference in timing is more prominent for the reference profiles than for the human input profiles. The reference profiles have much shorter back swing and forward swing phases for stiffer springs than for softer springs, whereas the human input profiles lie closer to each other.

Human Performance

The raw measurement data are available in the archives of the 4TU Centre for Research Data [58]. Fig. 2.10 shows the gain over the cumulative trial count, independent of the condition, combining learning and performance trials. We normalized the gains so that a value of 1 corresponds to the median over all trials of the same condition, and we grouped per ten trials, calculating the medians per participant and the medians of the medians of all participants. No significant learning effect can be seen for most learning phases. In some cases, a small learning effect can be observed over the first 20 to 30 trials of the learning phase, and in others, the performance decreases after 60 to 70 trials, perhaps due to participants getting bored or tired.

Fig. 2.11 shows the box plots of the dependent measures for the five conditions of

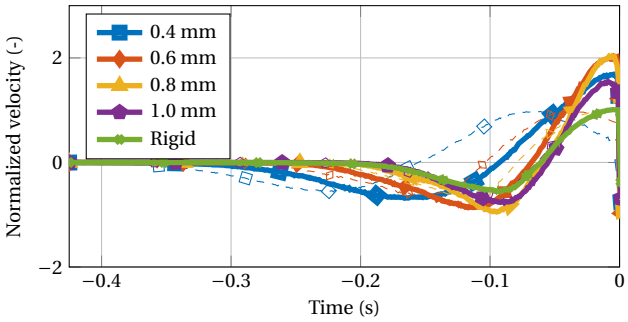

Figure 2.7: Median normalized velocity profiles of input (handle) and output (hammer head) for the performance phase trials of the different conditions (1 = peak input velocity of the respective trial). Thin lines represent the respective input velocity, and thick lines the output velocity. For the rigid condition, input and output velocity are identical. The input velocity profile is similar for the different conditions but executed slower for softer springs and faster for stiffer springs.

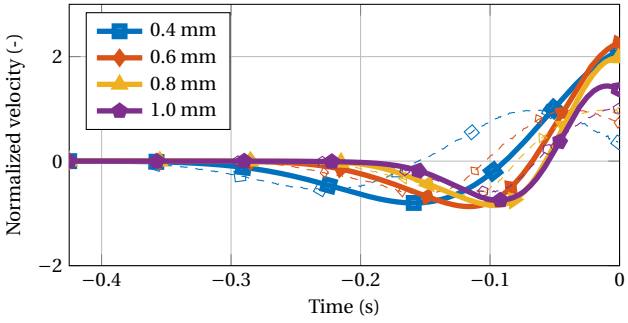

Figure 2.8: Simulated system response to a human input profile. Thin lines are used for the input and thick lines for the output velocity (1 = peak input velocity of the respective trial).

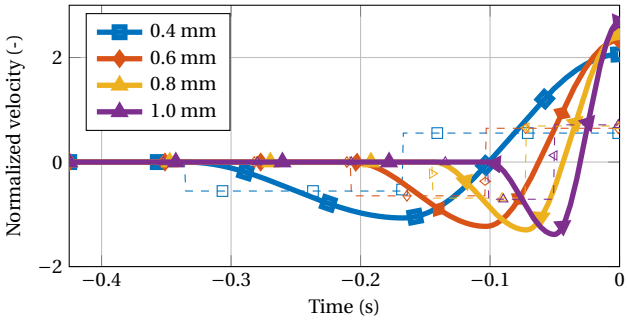

Figure 2.9: Simulated system response to a square input profile of an ideal velocity source for reference gain calculation. Thin lines are used for the input and thick lines for the output velocity.

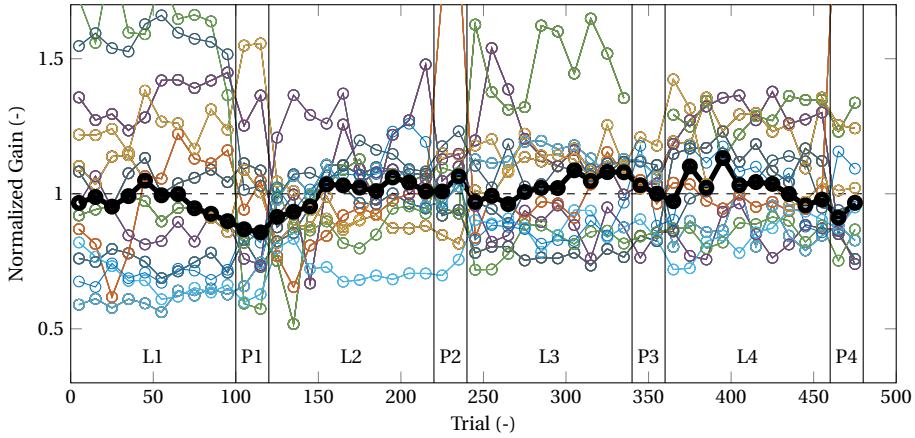

Figure 2.10: Normalized gain over cumulated trial count for all flexible condition trials. A value of 1 corresponds to the median over all trials of the same condition. Thin lines connect the median gains over ten trials per participant. The thick line connects the median of the medians over ten trials of all participants. Learning phases, labeled L1 to L4, consist of 100 trials, and performance phases, labeled P1 to P4, consist of 20 trials. Vertical bars show the limits of the phases. After every learning phase (L1, L2, L3, L4) there was a short interruption to download the measurement data; after every performance phase (P1, P2, P3, P4) there was a short break to change the hammer extension.

Experiment 1: peak hammer velocity $b_{\hat{v}}$, gain b_G, and excitation frequency b_f. Two participants could not finish all conditions because of technical problems with the setup (participant 3 did not finish the 9.9 Hz condition or the rigid condition, and participant 6 did not finish the 3.0 Hz condition or the 4.8 Hz condition). Therefore, the number of samples is 11 for the Friedman's tests and 11 or 12 for the Wilcoxon's signed-rank tests depending on which conditions are compared.

Peak Hammer Velocity

The resonance frequency had a significant effect on the peak hammer velocity $\hat{v}$, as shown in Fig. 2.11a ($b_{\hat{v}}$: $\chi^2 = 27.20$, $p < 0.001$, $n = 11$).

The peak hammer velocity $b_{\hat{v}}$ was higher for the flexible conditions with 4.8 Hz, 6.9 Hz, and 9.9 Hz resonance frequency than for the rigid condition, and higher for a 4.8 Hz resonance frequency than for 3.0 Hz (4.8 Hz and rigid condition: $\Delta b_{\hat{v}} = 14.34$ rad/s, $\mathrm{CI}_{95\%} = [11.30, 15.43]$ rad/s, $p = 0.001$, $n = 11$; 6.9 Hz and rigid condition: $\Delta b_{\hat{v}} = 9.88$ rad/s, $\mathrm{CI}_{95\%} = [8.00, 16.72]$ rad/s, $p = 0.001$, $n = 11$; 9.9 Hz and rigid condition: $\Delta b_{\hat{v}} = 7.95$ rad/s, $\mathrm{CI}_{95\%} = [6.14, 12.39]$ rad/s, $p = 0.001$, $n = 11$; 4.8 Hz and 3.0 Hz condition: $\Delta b_{\hat{v}} = 9.54$ rad/s, $\mathrm{CI}_{95\%} = [5.09, 12.67]$ rad/s, $p = 0.001$, $n = 12$).

The estimated minimum effect size for $b_{\hat{v}}$ is 7.8 rad/s ($\overline{\sigma} = 10$ rad/s, $n = 11$).

Gain

The resonance frequency had a significant effect on the gain, as shown in Fig. 2.11b (b_G: $\chi^2 = 30.25$, $p < 0.001$, $n = 11$).

The gain b_G was higher for all flexible conditions than for the rigid condition and higher for the 4.8 Hz condition than for the 3.0 Hz and 9.9 Hz conditions (3.0 Hz and rigid

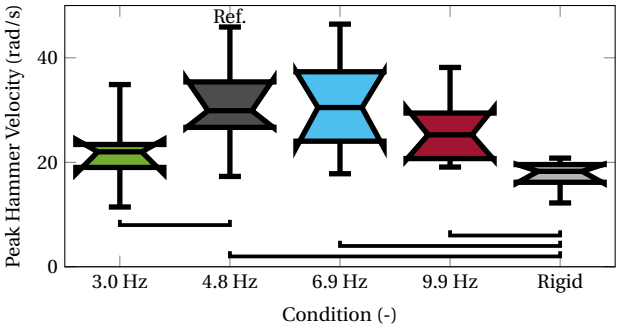

(a) Peak Hammer Velocity

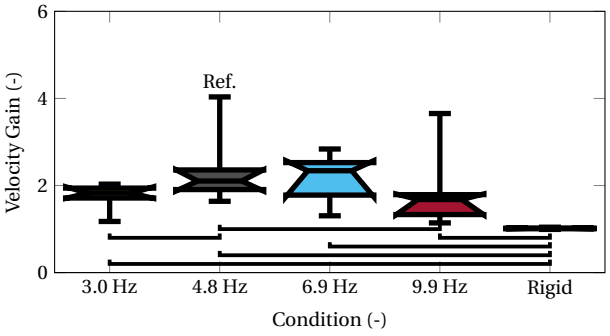

(b) Gain

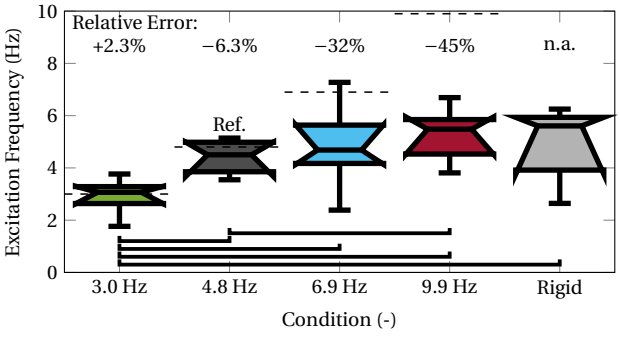

(c) Input Frequency

Figure 2.11: Box plots comparing the conditions of Experiment 1 through the dependent measures: peak hammer velocity $b_{\hat{v}}$, gain b_G, and excitation frequency b_f. The lower and upper limits of the boxes represent the first and third quartiles, respectively. The notches represent the 95 % confidence interval of the median, and the whiskers show the minimum and maximum values. Brackets show relevant statistically significant differences between conditions. The condition marked "Ref." was used as a reference for Experiment 2. The dashed lines in Fig. 2.11c show the resonance frequencies of the conditions. The numbers on top show the relative error in percent per condition of the median excitation frequency compared to the resonance frequency. It was calculated as the dimensionless ratio between the difference of excitation frequency and resonance frequency divided by the resonance frequency.

condition: $\Delta b_G = 0.84$, $CI_{95\%} = [0.70, 0.98]$, $p = 0.001$, $n = 11$; 4.8 Hz and rigid condition: $\Delta b_G = 1.16$, $CI_{95\%} = [0.93, 1.36]$, $p = 0.001$, $n = 11$; 6.9 Hz and rigid condition: $\Delta b_G = 1.31$, $CI_{95\%} = [0.73, 1.51]$, $p = 0.001$, $n = 11$; 9.9 Hz and rigid condition: $\Delta b_G = 0.66$, $CI_{95\%} = [0.35, 0.79]$, $p = 0.001$, $n = 11$; 4.8 Hz and 3.0 Hz condition: $\Delta b_G = 0.35$, $CI_{95\%} = [0.03, 0.66]$, $p < 0.001$, $n = 12$; 4.8 Hz and 9.9 Hz condition: $\Delta b_G = 0.43$, $CI_{95\%} = [0.08, 0.83]$, $p = 0.007$, $n = 11$).

The estimated minimum effect size for b_G is 0.51 ($\overline{\sigma} = 0.65$, $n = 11$).

Input Frequency

The resonance frequency had a significant effect on the excitation frequency, as shown in Fig. 2.11c (b_f: $\chi^2 = 26.84$, $p < 0.001$, $n = 11$).

The excitation frequency b_f was higher for the conditions with 4.8 Hz, 6.9 Hz, and 9.9 Hz resonance frequency and the rigid condition than for the condition with 3.0 Hz resonance frequency, and higher for the 9.9 Hz condition than for the 4.8 Hz condition (4.8 Hz and 3.0 Hz conditions: $\Delta b_f = 1.58$ Hz, $CI_{95\%} = [0.91, 1.84]$ Hz, $p < 0.001$, $n = 12$; 6.9 Hz and 3.0 Hz conditions: $\Delta b_f = 1.58$ Hz, $CI_{95\%} = [1.02, 2.69]$ Hz, $p = 0.001$, $n = 12$; 9.9 Hz and 3.0 Hz conditions: $\Delta b_f = 2.73$ Hz, $CI_{95\%} = [1.79, 2.77]$ Hz, $p = 0.001$, $n = 11$; rigid and 3.0 Hz condition: $\Delta b_f = 2.37$ Hz, $CI_{95\%} = [1.13, 2.67]$ Hz, $p = 0.001$, $n = 11$; 9.9 Hz and 4.8 Hz condition: $\Delta b_f = 0.88$ Hz, $CI_{95\%} = [0.50, 1.11]$ Hz, $p = 0.003$, $n = 11$).

The estimated minimum effect size for b_f is 0.74 Hz ($\overline{\sigma} = 0.95$ Hz, $n = 11$).

2.4. Experiment 2: Teleoperated Manipulation

2.4.1. Hypotheses

Experiment 2 (the teleoperated manipulation experiment) used the optimum stiffness configuration with a resonance frequency of 4.8 Hz found during Experiment 1 (the direct manipulation experiment). The following hypotheses were formulated for this experiment, based on Experiment 1 and pilot studies for Experiment 2:

Hypothesis H2: Humans can exploit a flexible hammer's elasticity in teleoperated manipulation to maximize the power transfer in a strike and achieve a higher output velocity than they can with a rigid hammer.

Hypothesis H2.1: The absence of visual feedback does not influence the hammering task performance.

Hypothesis H2.2: The absence of force feedback decreases the hammering task performance.

Hypothesis H2.3: Communication delay decreases the hammering task performance.

2.4.2. Conditions

Four conditions with different feedback were compared:

FF Visual and force feedback without communication delay.

NV No visual feedback (the participants were blindfolded).

NF No force feedback; only visual feedback without communication delay.

DL Visual and force feedback with 40 ms round-trip communication delay (the participants could see the setup, but the communication delay was asymmetric to achieve the same delay for visual and for force feedback (see Section 2.4.5)). The time delay corresponded approximately to round-trip delays encountered on long-distance Internet connections, *e.g.*, Amsterdam–Barcelona or Los Angeles–Chicago [59].

The order of conditions was balanced using Latin squares to block possible learning and carryover effects.

The participants were verbally informed about the ongoing condition, and the conditions were clearly distinguishable: The participants were blindfolded for the NV condition, they did not feel the impact in the NF condition, and they felt a delay-induced damping in the DL condition.

2.4.3. Participants

The experiment was performed by 32 participants (26 male, 6 female, all right-handed, age 21-34). The participants were university students and employees with a higher education background. None of the participants had participated in Experiment 1 or had previous experience with the experiment apparatus. The experiment had been approved by the human research ethics committee of TU Delft, and all participants gave written informed consent before participation.

2.4.4. Experiment Procedure

In Experiment 2, the participants were given less training time than in Experiment 1 to explore the resonance mechanism themselves to decrease the experiment time per participant. To compensate for it, the participants were shown a four-minute video (accessible at [60]) before the start of the experiment, describing the goal of the experiment, giving detailed task instructions, and explaining the basics of mechanical resonance. As there were (arguably small) differences that make the two experiments difficult to compare directly, the data obtained in Experiment 1 only serve as an indicative reference for Experiment 2, and no statistical comparisons are made between the experiments.

Before starting the actual hammering task, the participants had a familiarization phase, which lasted approximately two to three minutes until they decided to stop. The familiarization phase was different from the hammering task, as during this time, the suspended mass was removed, and the participants were asked to "wobble" the handle to get an impression of the movement required to excite the mechanical resonance of the flexible hammer. The teleoperation system settings used for this familiarization phase corresponded to the settings of the first experimental condition to ensure that the performance during the first block of hammering trials was based only on the feedback available with the first condition.

After the familiarization phase, the suspended mass was put in place, and the participants conducted 40 hammering trials with each condition. After each trial, verbal feedback was given to the participants about their performance in terms of gain. For the verbal feedback, the words "Okay," "Good," "Very good," and "Excellent" were used from the worst to the best performance, with the rating adapted according to the participants' individual performance trend. To this end, the experiment conductor had a display that

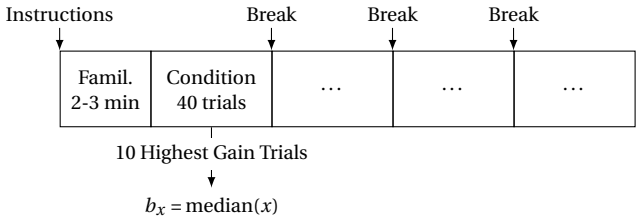

Figure 2.12: Experiment procedure Experiment 2

Contr.	Cond.	Parameter				
		C_m = - C_4	C_s = C_1	C_2	C_3	T_d
1	FF, NV	$0.8 + \frac{10}{s}$	$0.8 + \frac{10}{s}$	1	1	0 s
2	DL	$0.8 + \frac{10}{s}$	$0.8 + \frac{10}{s}$	1	1	40 ms
3	NF	0	$0.8 + \frac{10}{s}$	0	1	0 s

Table 2.3: Controller gains of the system shown in Fig. 2.13

was not visible to the participants, showing the measured gain G immediately after every trial, allowing him to give the participant feedback. Between two conditions, there was a break to download the data (approx. 2 min). Fig. 2.12 visualizes the experiment procedure. For the analysis, the familiarization phase was not taken into account; only the hammering trials were.

2.4.5. Teleoperation System Tuning and Identification

Different controllers were programmed in the teleoperator control system to provide force feedback without communication delay, force feedback with communication delay, or no force feedback. The controllers' structure was based on the Lawrence architecture [11] (see Fig. 2.13), using different tuning gains C_m, C_s, C_1, C_2, C_3, C_4. These three controllers covered the four experiment conditions (see Table 2.3).

Controller 1 was tuned for optimal transparency according to the rules of Hashtrudi-Zaad and Salcudean [61]. Controller 2 was derived from Controller 1 by adding a communication delay of T_d = 40 ms only in the tool device to handle device direction. This way, a visual communication delay identical to the force feedback communication delay could be simulated without requiring the installation of a sophisticated video transmission system. Controller 3 was derived from Controller 1 by disabling the force feedback.

A system identification was carried out to assess the performance of the teleoperator. A sine sweep identification input signal (0.1 Hz to 20 Hz over 100 s) was used to analyze the teleoperator transparency by comparing the transmitted impedance Z_{to} for the three controllers with the environment impedance Z_e. The environment impedance is the impedance of the flexible hammer in free air. The transmitted impedance Z_{to} should be close to the environment impedance Z_e to make the teleoperated hammer behave like

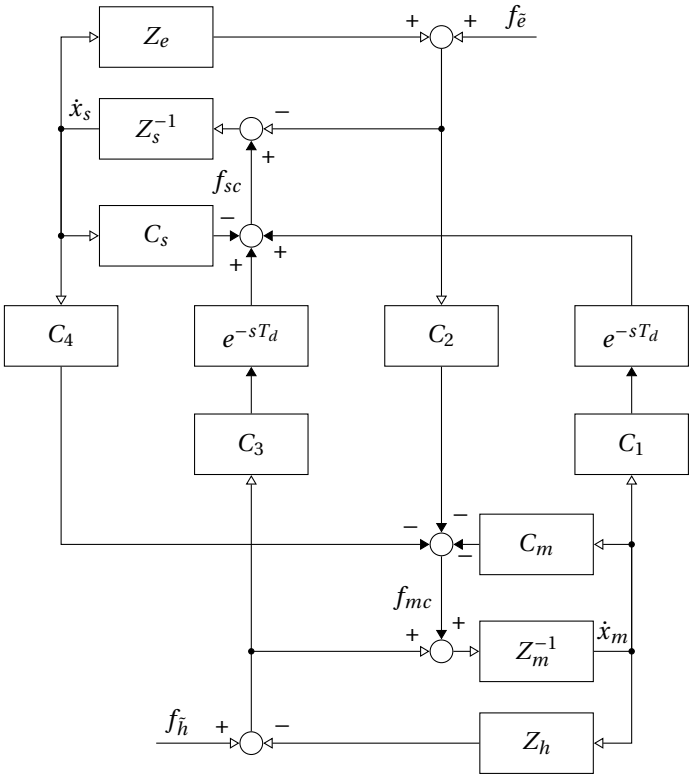

Figure 2.13: Controller architecture of the teleoperator. Three different settings were used for the controller gains C_m, C_s, C_1, C_2, C_3, C_4, and the delay T_d for the conditions of Experiment 2. Note that communication delay was implemented only on the forward channels (handle device to tool device) and not on the feedback channels (tool device to handle device) to achieve communication delay for the visual feedback. Therefore, T_d represents the round-trip time and not the one-way delay time. Z_e is the environment impedance; Z_h is the impedance of the human operator; Z_m is the impedance of the handle device; Z_s is the impedance of the tool device; $f_{\tilde{e}}$ is the sum of external forces on the hammer; $f_{\tilde{h}}$ is the force intentionally exerted by the human operator on the handle device; f_{mc} and f_{sc} are the forces commanded by the controller to the handle device and tool device; $\dot{x}_m$ and $\dot{x}_s$ are the velocities of the handle device and the tool device. (Adapted from [61])

the directly manipulated hammer in Experiment 1. Only the free air behavior of the setup was measured as this was the relevant mode of operation for this experiment.

Fig. 2.14 shows the Bode plots of the impedance Z_{to} transmitted through the teleoperator compared to the environment impedance Z_e for the three controllers.

The black dashed line shows the modeled curve of Z_e:

$$Z_e = K \frac{k\ (m\,s + b)}{m\,s^2 + b\,s + k}, \tag{2.11}$$

with the numeric values obtained from the system identification measurement ($K = 0.5$, $m = 2.59\,\mathrm{g\,m^2}$, $k = 2.23\,\mathrm{N\,m/rad}$, $b = 3 \times 10^{-3}\,\mathrm{N\,m\,s/rad}$).

The other dashed lines show the modeled curves of Z_{to} for the three controllers with the parameters in Table 2.3. They were derived from the Z_e model using the Haptic Analysis Toolbox [48].

Controller 1, with optimal transparency gains, has a good fidelity of the transmitted impedance. The frequency of the maximum impedance magnitude of the transmitted impedance closely matches the environment impedance, and the magnitude profiles of both curves are generally close within the boxed region. The maximum impedance is at least 16 dB higher than at the frequencies 1 Hz higher or lower in both curves. This can be compared to a signal-to-noise ratio for the sensing of the mechanical resonance. The higher the signal-to-noise ratio, the easier it should be for the operator to sense and excite the mechanical resonance with only impedance information as feedback.

The impedance maximum is slightly shifted for Controller 2 and is at approximately 4.6 Hz instead of 4.8 Hz. Also, the ratio between the minimum magnitude and the magnitude 1 Hz higher or lower is only about 5.5 dB. Thus, with Controller 2, it should be more difficult for the operator to sense and excite the mechanical resonance with only impedance information as feedback than is the case with Controller 1.

For Controller 3, no impedance minimum can be distinguished, and therefore the mechanical resonance cannot be identified based on impedance feedback.

2.4.6. Results

The raw measurement data are available in the archives of the 4TU Centre for Research Data [62]. Fig. 2.15 shows the box plots of the dependent measures for the reference condition of Experiment 1 and the four conditions of Experiment 2: peak hammer velocity $b_{\hat{v}}$, gain b_G, and excitation frequency b_f.

There are no effects significant at the 5 % level for $b_{\hat{v}}$ and b_G ($b_{\hat{v}}$: $\chi^2 = 0.56$, $p = 0.91$, $n = 32$; b_G: $\chi^2 = 6.86$, $p = 0.076$, $n = 32$). Friedman's test showed a significant effect at the 5 % level for b_f ($\chi^2 = 8.59$, $p = 0.035$, $n = 32$), but Wilcoxon's test indicated no effect at the 1 % level for the pairwise comparisons. Therefore, the possible effects are weak and not consistent over the three measures. There were also no significant effects of the order of conditions that the subjects have performed.

The estimated minimum effect sizes are 4.86 rad/s for $b_{\hat{v}}$ ($\overline{\sigma} = 9.81$ rad/s, $n = 32$), 0.31 for b_G ($\overline{\sigma} = 0.62$, $n = 32$), and 0.53 Hz for b_f ($\overline{\sigma} = 1.06$ Hz, $n = 32$).

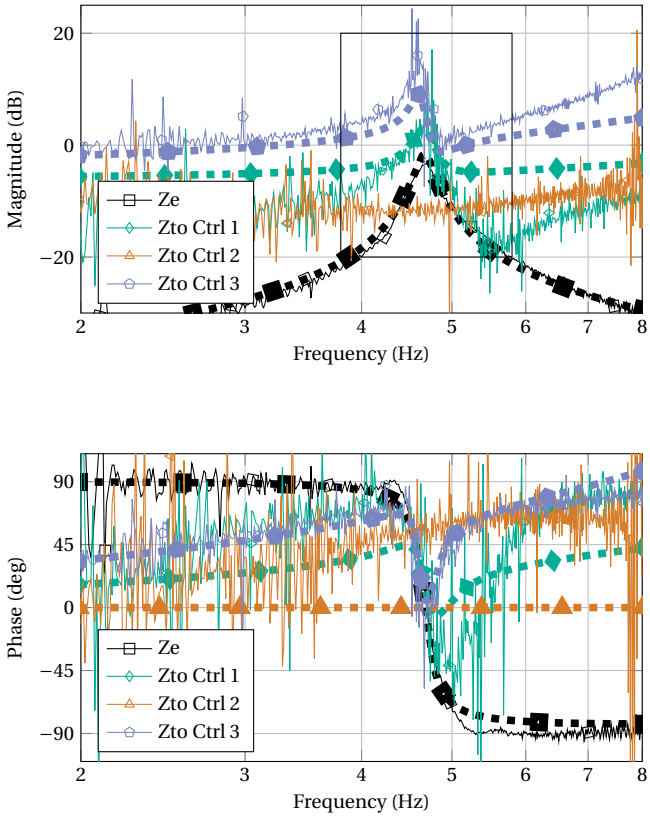

Figure 2.14: Bode plots of the modeled and measured environment impedance Z_e and modeled and measured transmitted impedance Z_{to} for the three controllers. The box in the magnitude plots from 3.8 Hz to 5.8 Hz frequency and 0 dB to 20 dB magnitude highlights the critical region around the resonance frequency of 4.8 Hz.

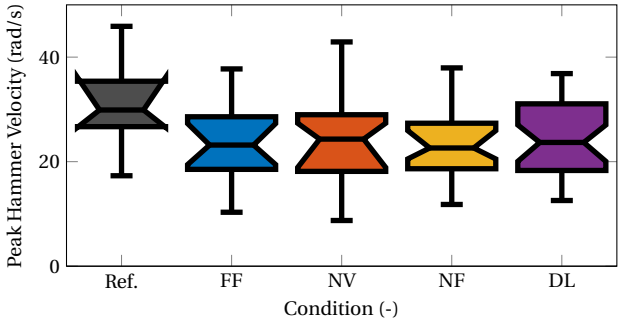

(a) Peak Hammer Velocity

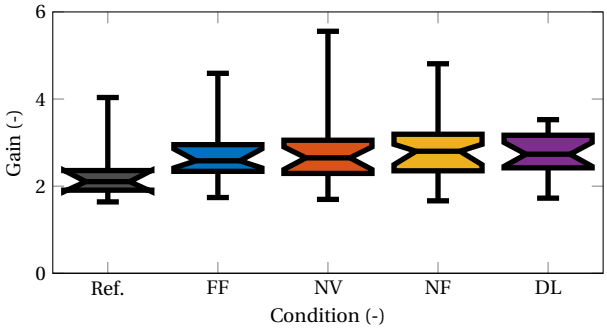

(b) Gain

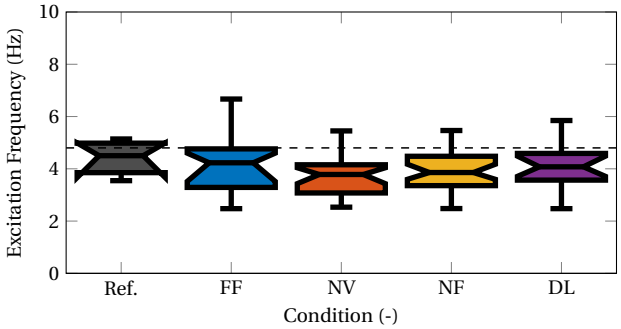

(c) Input Frequency

Figure 2.15: Box plots comparing the conditions of Experiment 2 through the dependent measures: peak hammer velocity $b_{\hat{v}}$, gain b_G, and excitation frequency b_f. The lower and upper limits of the boxes represent the first and third quartiles, respectively. The notches represent the 95 % confidence interval of the median, and the whiskers show the minimum and maximum values. There is no significant effect of the condition on the performance as the 95 % confidence intervals of the medians overlap. The condition marked "Ref." is the 4.8 Hz condition from Experiment 1 used as a reference for Experiment 2. The dashed line shows the resonance frequency.

2.5. Discussion

This study shows that human operators can exploit a flexible hammer to achieve higher peak velocities in a hammering task than with a rigid hammer. A gain of over 200 % was measured, defined as peak hammer velocity divided by peak handle velocity (*e.g.*, Experiment 1 4.8 Hz condition: 208 % median gain). This is comparable to the results reported by Wolf *et al.* [42] for automated motion with SEAs (272 %), but significantly lower than the results reported by Garabini *et al.* [43] for an analytical solution with SEAs (400 %). The achieved velocity and gains are comparable between direct manipulation and teleoperation. In the following, we will discuss the observed effects in more detail.

2.5.1. Humans can exploit the mechanical resonance of a flexible hammer

The results of flexible hammering in direct manipulation (Experiment 1) indicate that humans can sense and excite a flexible hammer's mechanical resonance to achieve a higher peak velocity than with a rigid hammer (supporting hypothesis H1). They achieved this performance after a short learning phase of less than 20 to 30 trials for new stiffness conditions, not showing significant improvements over the longer learning phase of 100 trials. Therefore, the participants seem to have an intuitive understanding of the dynamic system properties. These results are coherent with research showing that humans can tune their limbs to a specific resonance frequency [63, 64]. An optimum working point was found for a flexible hammer with a resonance frequency of 4.8 Hz in terms of velocity gain and matching the resonance frequency. Participants achieved a similar performance in terms of peak velocity and velocity gain for the condition with 6.9 Hz resonance frequency. However, the excitation frequency was closer to the resonance frequency in the 4.8 Hz condition.

2.5.2. Teleoperation and direct manipulation with flexible hammers offer similar task performance

The results of hammering in teleoperated manipulation (Experiment 2) indicate that humans can sense and excite a flexible hammer's mechanical resonance to achieve a higher peak velocity than they can with a rigid hammer also through a teleoperation system (supporting hypothesis H2).

They also suggest that the absence of visual feedback (condition NV) does not affect the peak velocity or the velocity gain. This confirms sub-hypothesis H2.1. Contrary to sub-hypothesis H2.2, the results do not show an effect of the absence of force feedback (condition NF) in the teleoperated flexible hammering task. Sub-hypothesis H2.3 was also not confirmed by the results of Experiment 2: No effect of a communication delay of 40 ms round-trip time was observed (condition DL), although this represents a considerable communication delay compared to the execution time of one hammer strike (approximately 20 % for a resonance frequency of 4.8 Hz). In Experiment 2, only one resonance frequency was studied experimentally in order to limit the parameter space. However, based on the experience with the experiment apparatus, we believe that the results can be generalized to the full range of frequencies that were tested in Experiment 1.

2.5.3. Sensitivity of the gain to the excitation frequency

It was unexpected that no effect of visual feedback, force feedback, or communication delay could be measured. This raises the question of whether the same results could be achieved without any feedback. As shown in Fig. 2.2c, the velocity gain is greater than 1 for all frequencies lower than approximately 1.5 times the resonance frequency. In essence, the excitation frequency does not have to match the resonance frequency exactly to obtain a higher output velocity with a flexible hammer. Nevertheless, as we saw in Experiment 1 (Fig. 2.11c), the participants changed their excitation frequency for different resonance frequencies, indicating that they tried to achieve the highest possible gain.

The participants achieved the best results with the 0.6 mm leaf-spring, obtaining a median gain of 2.08 (Experiment 1). Although some participants performed better with the 0.8 mm leaf-spring, others had more difficulties with the faster motion, resulting in a bigger spread of results between participants. Therefore, we observed no statistically significant improvement in the gain for the 0.8 mm leaf-spring compared to the other flexible conditions. The 0.6 mm leaf-spring with a resonance frequency of 4.82 Hz seems to be the one the participants could best adjust to.

For higher resonance frequencies, it is difficult for a human operator to execute the motion fast enough. As shown by the results of Experiment 1, the excitation frequency was consistently below 8 Hz (which corresponds to the upper frequency limit of coordinated hand movements [65]), even though the resonance frequency of the stiffest condition was approximately 10 Hz. Therefore, the highest gain can be expected for resonance frequencies between 4 Hz and 8 Hz.

2.5.4. Influence of the task motion profile

The results of Experiment 2 do not indicate an effect of the absence of force feedback on the flexible hammering task. However, for dexterous manipulation at much lower frequencies (*e.g.*, lower than 1 Hz), it has been shown that force feedback has a significant effect, resulting in reduced task execution time, contact forces, and task load [66–68].

The difference in results between dexterous manipulation experiments and our experiments might be due to a difference in the arm/hand movements executed by subjects in our hammering experiments. Kunesch *et al.* differentiate between slow type I motions at frequencies up to 2 Hz involving focal sensory control (*e.g.*, tactile exploration), and fast type II motions at frequencies between 4 Hz and 8 Hz monitored by pre-attentive sensory processes (*e.g.*, writing, tapping, shading) [65]. The excitation frequencies observed in this study are in the frequency range of type II motions. Therefore, it is coherent that the feedback channel has little influence on the task performance.

Research on human motor control also indicates that joint stiffness control for particular tasks is largely controlled by muscle activation patterns triggered by the cerebellum in a feedforward manner [69]. As the system dynamics did not change in Experiment 2, it might have been easy for the participants to build an internal model for feedforward control, independently of the type of feedback.

2.5.5. Implications for the use of SEAs

In this study, we found that it can be expected that human operators can do the flexible hammering task in teleoperated manipulation as well as they can in direct manipulation. This is an encouraging result for the use of SEAs in future dynamic teleoperation systems, as similar tasks, such as shaking, jolting, and throwing, could also benefit from SEAs. This study is trailblazing a path toward the performance of real-life human dynamic tasks through teleoperation.

We see two immediate recommendations for the design of teleoperator systems with flexible tool device actuators:

1. If the quality of the force feedback in teleoperation is less critical for high-speed tasks than for slow dexterous manipulation, the force fed back to the operator could be scaled down for faster tasks without performance penalties. Scaling down the force on the handle device side of the teleoperation system reduces the power delivered by the handle device, as it is the product of force times velocity. This could lead to a method to increase the stability of teleoperation systems without introducing high damping, unlike what is done in passivity observer and controller approaches [52].

2. If the precise matching of excitation frequency and the resonance frequency is not critical to obtain a velocity gain, the stiffness of the flexible hammer can be driven by design requirements other than the resulting resonance frequency. Even for flexible hammers, it is often desirable that the stiffness is sufficiently high to avoid excessive deflection. The results of Experiment 1 show that the flexible hammer could be designed with a resonance frequency 40 % higher than reachable by a human operator and still achieve a velocity gain of more than 200 %. Consequently, if a higher tool stiffness is desired while still allowing human operators to achieve a good velocity gain, stiffnesses resulting in resonance frequencies up to about 11 Hz can be chosen (corresponding to a stiffness of up to approximately 95 N m/rad for a hammer head of 500 g on a handle of 20 cm length).

2.5.6. Teleoperation with variable stiffness actuators

The presented findings support the notion of using SEAs as tool devices in teleoperation. However, a teleoperation system with large oscillations as used in this study is not practical for positioning tasks. It is, therefore, preferable to be able to change the mode of operation between soft and rigid according to the task at hand, as can be done with variable stiffness actuators [70]. Furthermore, Garabini *et al.* have shown that an additional velocity increase of 30 % can be achieved by varying the stiffness during the motion [43]. Therefore, it appears worthwhile to the authors to try to improve further the gain measured in the experiments presented in this paper by using a variable stiffness tool device actuator instead of a constant stiffness elastic actuator.

2.6. Conclusion

This paper shows that teleoperators can achieve peak velocities in a hammering task with a flexible (SEA-based) hammer of more than 200 % of the peak velocities achieved with a rigid hammer. Based on the performed experiments, we conclude that:

1. Humans can sense and excite the mechanical resonance of a flexible hammer to achieve a higher peak velocity than they do with a rigid hammer in direct manipulation;
2. Humans can quickly adapt to the resonance frequency for different stiffnesses;
3. a similar level of performance is achieved in teleoperated manipulation;
4. the absence of visual feedback or force feedback, or a communication delay of 40 ms has no significant effect on the performance in terms of peak hammer velocity, gain, and excitation frequency.

3

A Dynamic Robotic Actuator with Variable Physical Stiffness and Damping

This study is part of research aiming to increase the range of dynamic tasks for teleoperated field robotics to allow operators to use the full range of human motions without being limited by the robotic manipulator's dynamics. A new variable impedance actuator (VIA) was designed, capable to reproduce motions through teleoperation from precise positioning tasks to highly dynamic tasks. Based on previous human user studies, the design requirements were a stiffness changing time under load of 50 ms, a peak output velocity of 20 rad/s, and variable damping. This is a unique combination of features that is not met by other VIAs. The new design has three motors in a parallel configuration. Two are responsible for changing the VIA's neutral position and effective stiffness through a sliding pivot point lever mechanism. The third acts as a variable damper. A prototype was built. Performance measurements on the prototype showed an effective stiffness changing time of 50 ms to 120 ms for small to large stiffness steps, nominal output velocity of 16 rad/s, and a variable damper with a damping torque of 0 N m to 3 N m. Its effective stiffness range is 0.2 N m/rad to 313 N m/rad. This concludes that the new actuator is particularly suitable for highly dynamic tasks. The new actuator is also very versatile, i.e., suited for different applications (e.g., precision tasks and dynamic tasks), making it especially interesting for teleoperation and human-robot collaboration.

This chapter is based on the following article submitted for publication:

- M. Aiple, W. Gregoor and A. Schiele, *A Dynamic Robotic Actuator with Variable Physical Stiffness and Damping*, submitted to Elsevier Mechanism and Machine Theory, preprint available under arXiv:1906.07669

3.1. Introduction

Today, teleoperation is mostly used for performing slow motions for precision tasks like picking and placing objects or guiding tools. Therefore, teleoperated robots are typically optimized for precision instead of dynamics. However, in field robotics, as future space exploration or inspection of disaster sites, flexibility and improvisation can be very advantageous, *e.g.*, to clear the path for a robot deployed in the Fukushima Daiichi nuclear disaster [45]. Humans can perform a wide range of motions, including very dynamic ones like throwing and hammering, allowing them to cope with unexpected situations. Still, the current teleoperation systems are not capable of reproducing these, which can be a limiting factor for telerobotics in unstructured environments.

In a previous study, we could show with a simple teleoperated series elastic actuator (SEA) that humans can exploit a flexible tool device's resonance to reach a higher velocity at the hammer head than the actuator's motor velocity when hammering [71]. Nevertheless, the SEA used in that study was not suitable for performing precise positioning tasks as the high compliance made it hard to position in the presence of external forces. Also, its lack of damping meant that it oscillated for a long time after moving. However, an actuator needs to allow for performing positioning tasks and dynamic tasks alike for being truly useful for teleoperation in the field, suggesting the use of variable impedance actuators (VIAs). VIAs are currently the best candidate technology for building a telemanipulated robot appropriate for wide scope teleoperation as their compliance can be mechanically adapted to the task's needs. They can be used as rigid actuators for positioning tasks or as soft actuators for highly dynamic tasks, as shown for various applications [26–28, 31, 49, 72–76].

A suitable VIA to continue our research should match our previous findings concerning the frequency and velocity of teleoperated hammering [71] and provide variable stiffness and damping to increase precision and reduce oscillations compared to an SEA. Furthermore, Garabini *et al.* concluded that the peak output velocity achieved when hammering with a VIA could be increased by 30 % if the stiffness is adapted during the hammering motion compared to keeping the stiffness constant [43]. Thus, the stiffness changing mechanism of the VIAs should be fast enough to allow stiffness changes during the hammering motion. No existing design was found that could match all requirements. This paper aims to present the dynamic robotic actuator (Dyrac) design meeting the mentioned requirements, resulting in a unique actuator prototype for dynamic teleoperation research. While Dyrac is primarily designed for this research, it should also be useful as a generic VIA. Hence, it was designed to have an output torque and stiffness range comparable to other VIAs.

3.2. Design

3.2.1. Considerations

In the following, a subset of VIA design options is summarized that were considered in the Dyrac design, disregarding options that rely on modifying the material stiffness of the elastic element itself. A broader and more systematic classification of VIA designs has been done by Vanderborght *et al.* [27] and Wolf *et al.* [26], which is reflected in the following as far as relevant for the Dyrac design.

The joint position of VIAs depends on the *neutral position*, which is the joint position in the absence of external forces, the *effective stiffness* of the VIA, which is the stiffness of the elastic element multiplied by the stiffness variation factor, and the external forces acting on the joint output that cause a deflection of the joint. All VIAs need at least two motors to change the effective stiffness and the actuator's neutral position independently. These can be configured in parallel, with both motors mounted to the chassis or in series, with the second motor attached to the first motor's output axis. Typically, both motors are equally strong for actuators in a parallel configuration. In contrast, the second motor is typically smaller in a series configuration to reduce the mass that needs to be moved by the first motor. In a parallel configuration, the two motors typically work in opposite directions for changing the stiffness (as antagonists) and in the same direction for changing the neutral position, *e.g.*, the DLR BAVS [77]. In a series configuration, only the first motor influences the neutral position, whereas the second motor only influences the stiffness, *e.g.*, the IIT AwAS-II [29]. Designs using a parallel configuration typically have quicker stiffness changing times. Designs using a series configuration typically are more compact and lighter as only one powerful motor is required, while the second one can be relatively small.

Besides the motor configuration choice, a VIA's performance is strongly influenced by the stiffness changing mechanism. Cam-roller mechanisms couple the joint deflection to the spring deflection through a roller moving on a non-linearly shaped cam profile, *e.g.*, the DLR FSJ [78]. The cam profile is shaped so that as the deflection increases, the slope of the cam-profile increases as well, and thereby the effective stiffness increases. The stiffness at zero deflection can be varied by changing the roller's initial position on the cam profile, *e.g.*, by having two cam profiles that can move relative to each other. Cam-roller mechanisms can be made very compact, as the slope of the cam profile is relevant, but not the absolute height of the profile. Cam-roller mechanisms always have a non-linear torque-over-deflection curve, as this is required to change the stiffness, which might be desirable or not, depending on the application. Also, the typical stiffness range obtained is relatively small, as they are limited by the cam profile dimensions.

Lever mechanisms use a lever arm to reduce or increase the spring deflection compared to the joint deflection, *e.g.*, the vsaUT-II [79]. For varying the stiffness, the lever arm length can be modified, or the application point of the force on the lever arm can be moved, or the pivot point of the lever. Lever mechanisms can have a linear torque-over-deflection curve, as the deflection does not influence the stiffness variation factor. When changing the stiffness by moving the lever pivot point, the stiffness can be varied from zero to infinity (in practice, this is limited by the material stiffness). Furthermore, the stiffness can be changed while keeping the potential energy stored in the spring constant. Often lever-mechanism-based designs take more space to accommodate for the lever.

Different physical principles can be and have been used to implement variable physical damping for robotic actuators, *e.g.*, using friction brakes [80], Eddy currents [81], magnetorheological fluids [82], or an electric motor in direct drive configuration. Friction brakes are compact and can be disengaged fully to present zero damping torque. However, the torque is difficult to control precisely due to the complex friction processes. Eddy current based dampers require powerful electromagnets to induce the braking current into the rotor. Their behavior is very similar to the desired viscous damping behavior as

Design	Require-ments (Prototype Character-istics)	BAVS [77]	FSJ [78]	MACCEPA [83]	AwAS-II [29]	vsaUT-II [79]	VSA-Cube with Damper Module [84, 85]
Motor Con-figuration	— (Parallel)	Parallel	Serial	Serial	Serial	Parallel	Parallel
Stiffness Variation Mechanism	— (Lever pivot point)	Cam-roller	Cam-roller	Lever arm length	Lever pivot point	Lever pivot point	Agonistic-antagonistic
Nominal velocity	20 rad/s (16 rad/s)	12.6 rad/s	8.5 rad/s	5.8 rad/s	10.2 rad/s	2.2 rad/s	3 rad/s
Maximum torque	— (7 N m)	8 N m	67 N m	70 N m	80 N m	60 N m	3 N m
Stiffness changing time	50 ms (50 ms to 120 ms)	14 ms	330 ms	2600 ms	800 ms	500 ms	180 ms to 320 ms
Minimum stiffness	— (0.2 N m/rad)	3.9 N m/rad	52.4 N m/rad	5 N m/rad	0 N m/rad	0 N m/rad	3 N m/rad
Maximum stiffness	— (313 N m/rad)	146.6 N m/rad	826 N m/rad	110 N m/rad	∞	∞	14 N m/rad
Variable Damping	Yes (damping torque 3 N m)	No	No	No	No	No	Yes
Maximum Energy Stored	— (0.7 J)	0.9 J	5.3 J	27.9 J	5.8 J	1.6 J	0.047 J

Table 3.1: Comparison of selected existing VSA designs to the Dyrac requirements. The numbers in parentheses in the requirements column show the characteristics measured on the prototype.

their exerted torque's velocity-dependency is part of the physical principle they are based on. Dampers based on magnetorheological fluids allow for rendering viscous damping very accurately. However, they are complex to design and implement, requiring complex multiphysics finite element method (FEM) analysis and a mechanical design preventing leaking of the fluid. Electric motors are easy to integrate into an actuator and to control in torque mode to render viscous damping behavior. However, they are relatively big, and the damping torque is limited, meaning that the maximum viscous damping coefficient that can be rendered decreases with increasing speed.[1] They can also lead to unstable behavior of the actuator, thus requiring fine-tuning of the torque controller.

3.2.2. Requirements

Our previous research showed that humans execute hammering motions at a frequency of around 5 Hz and a peak velocity of 20 rad/s [71]. Furthermore, a stiffness changing time under 50 ms is required to perform the hard-soft-hard-soft cycle described in [43] within the measured typical hammering period of 200 ms. We considered it highly advisable to add variable physical damping as a requirement to the actuator. The importance of

[1] As the viscous damping coefficient $b = \frac{F}{v}$, the maximum value of b decreases with increasing values of the velocity v if the force F is limited.

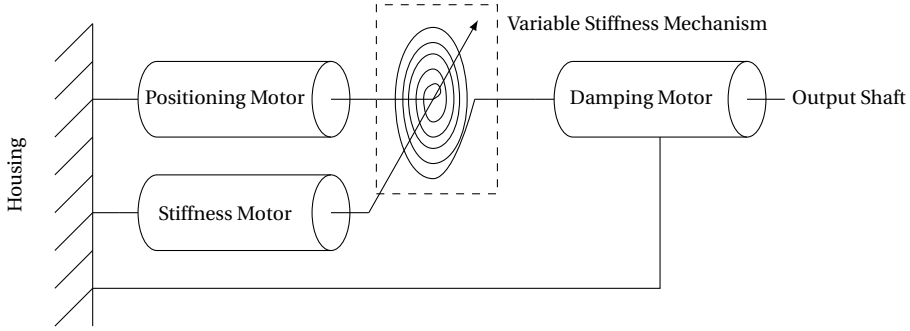

Figure 3.1: High-level configuration of the actuator. The actuator has three motors: the positioning motor changes the neutral position of the compliant joint, the stiffness motor changes the stiffness, and the damping motor serves to implement variable damping. The positioning motor and the stiffness motor are mounted in parallel to the housing. Thus, the stiffness motor has to move with the positioning motor to change the neutral position without changing the stiffness.

variable physical damping for oscillation suppression has been highlighted in previous research, *e.g.*, by Laffranchi *et al.* [86]. Table 3.1 summarizes the design requirements and compares them to the performance of selected existing VIA designs.

This study's primary design goal was to match the requirements of table 3.1, and the secondary design goal was to develop a very versatile actuator, allowing for exploring the parameter space velocity – stiffness – damping extensively. Existing actuator designs with similar performance as the requirements are among others: the Bidirectional Antagonistic Variable Stiffness joint (BAVS) [77], the Floating Spring Joint (FSJ) [78], the Mechanically Adjustable Compliance and Controllable Equilibrium Position Actuator (MACCEPA) [83], the Actuator with Adjustable Stiffness II (AwAS-II) [29], and the Variable Stiffness Actuator University Twente II (vsaUT-II) [79]. The BAVS [77] and the FAS [87] from DLR allow for a stiffness change within the required time. However, BAVS only reaches an angular velocity of 12.6 rad/s, and FAS is too small as it was designed to actuate a finger tendon, and neither has variable damping. Catalano *et al.* have implemented a variable damping module [85] to be combined with the VSA-Cube [84] to form a VIA with variable physical stiffness and damping similar to the requirements of this study, but too slow with a maximum velocity of 4.7 rad/s.

3.2.3. Actuator Principle

Based on the requirements of section 3.2.2 and the considerations of section 3.2.1, the architecture chosen for Dyrac is a parallel motor configuration design with a sliding pivot point lever stiffness variation mechanism, similar to the vsaUT-II, with a variable damper based on an electric motor in direct drive configuration. This architecture was chosen as the parallel motor configuration adds less inertia on the motor changing the neutral position, helping to achieve a fast end-effector acceleration. For the stiffness variation mechanism, a lever arm architecture with a changing pivot point was chosen. It enables changing the stiffness over the full stiffness scale, making the actuator useful for a wide range of studies to explore the velocity – stiffness – damping parameter space. An electric

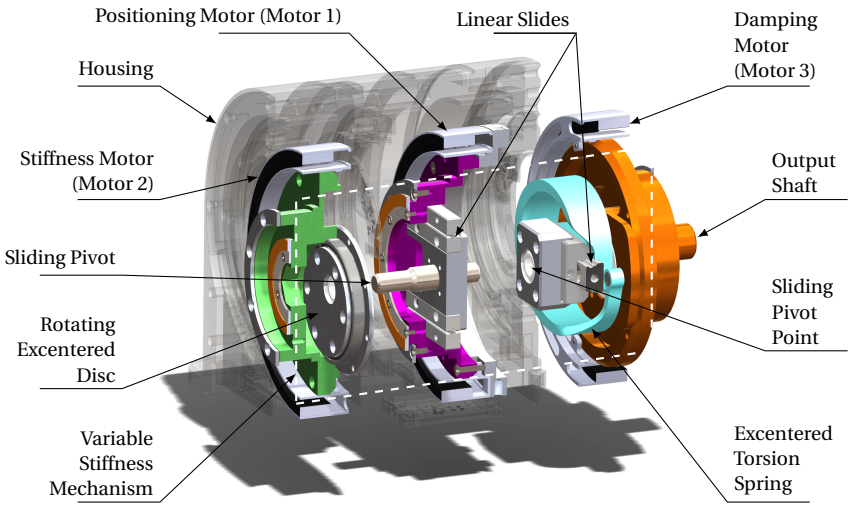

Figure 3.2: Exploded view of the Dyrac prototype CAD model. The stators of the motors are fixed to the housing (greyed out). The rotors of the motors all rotate around a common axis with the output shaft. The positioning motor turns the linear slide holding the sliding pivot, which carries the pivot point on the spring along when the pivot is out of the center. Depending on the pivot's position on the linear guide, the lever ratio for a force acting on the excentered torsion spring changes, thus changing the effective stiffness at the output shaft. The pivot position on the linear guide can be changed by rotating the stiffness motor relative to the positioning motor through the crankshaft mechanism formed by the rotating excentered disc. The damping motor sits on the output shaft implementing variable damping.

motor was chosen to implement the damper as it is not only much simpler to realize with commercially available components but also allows for actively influencing the output torque for precise torque servoing, making the actuator even more versatile. Again, the design was made such that the damping motor acts in parallel with the other motors, with the damping motor also mounted to the chassis. This design choice makes the overall architecture similar to the DM^2 approach in [88], which was shown to allow a recovery of performance lost by compliant actuators up to a certain extent [31]. However, here, the damping capability was the primary objective of this third motor.

Figure 3.1 shows the high level configuration of Dyrac and figure 3.2 shows an exploded view of the prototype CAD model. The actuator has three motors, a positioning motor for changing the neutral position, a stiffness motor for changing the effective stiffness, and a damping motor for variable damping. All motors and the output shaft are arranged on a common center axis in three stages.

The positioning motor is in the center, rotating a sliding table on which the pivot is fixed. When the pivot is excentered, it can exert a force in the tangential direction to induce torque on the output shaft. This happens through the pivot point mounted to the torsion spring, connected to the output shaft. The actuator's effective stiffness, *i.e.*, the stiffness as measured on the output shaft, depends on the distance of the pivot to the center axis because the spring is not located at the center axis but is excentered. Thus, the lever arm of the pivot relative to the output shaft changes in the opposite way to the lever arm of the pivot relative to the excentered torsion spring, when the pivot position changes (cf. Figure 3.3). Therefore, the force exerted by the spring on the pivot is different for the same torque on the output shaft, depending on the pivot's position because of the lever effect between force and torque. This way, the effective stiffness can be changed by changing the pivot position.

The stiffness motor on the left in figure 3.2 is used to change the pivot distance from the center axis through a crankshaft mechanism formed by an excentered disc. The pivot is connected to the excentered disc through a bearing, whose rotation axis is also excentered relative to the excentered disc. As a result, the pivot slides along the linear slide to a new distance from the center axis when the stiffness motor rotates relative to the positioning motor. The damping motor on the right in figure 3.2 is controlled in torque control mode and directly coupled to the output shaft, thereby allowing to implement variable damping.

3.2.4. Kinematics

Figure 3.3 shows the actuator kinematics with the center axis from left to right. Figure 3.4 shows the name conventions and geometric relations as seen from the left compared to figure 3.3 with the center axis pointing out of the paper. The angular polar coordinate of the pivot point P will be referred to as *pivot angle* φ and the radial polar coordinate as *pivot radius* r.

Three basic actions can be performed on the actuator: change of neutral position, change of stiffness, and deflection (cf. figure 3.5).

1. The neutral position is changed by equal rotation of motor 1 and 2. This causes a change of the pivot angle φ while keeping the pivot radius r constant.

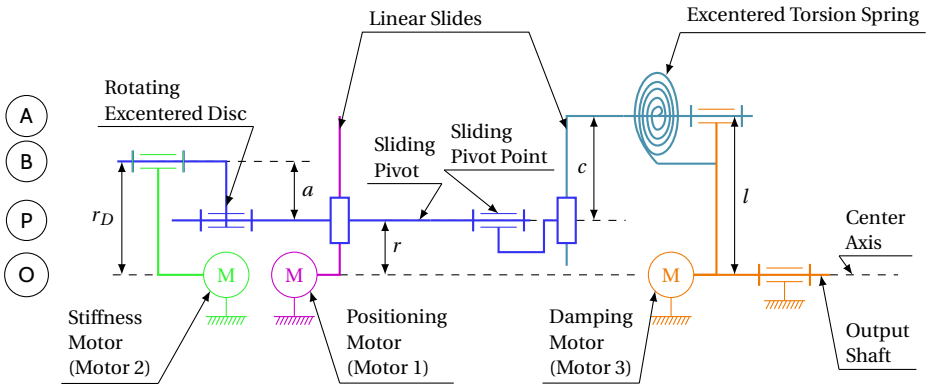

Figure 3.3: Schematic view of the kinematics of the actuator. Motor 1 sets the neutral position of the actuator. Moving motor 2 relative to motor 1 changes the sliding pivot's position through the slider-crank mechanism realized with the excentered disc connected to motor 2 and the linear slide connected to motor 1. The change of the pivot position on the linear slide, in turn, changes the position of the sliding pivot point on the linear slide mounted on the excentered torsion spring, which changes the effective stiffness of the actuator by changing the lever ratio between spring input (motor 1) and output (output shaft). A torque on the output shaft causes a deflection of the spring and a counter-force depending on the sliding pivot position. If the sliding pivot is aligned with the center axis, the actuator has zero stiffness as the output shaft can turn freely around the pivot point. If the sliding pivot is aligned with the spring axis, the actuator has infinite stiffness as the spring cannot be deflected. Generating a torque with motor 3 can be used to dampen oscillations on the output shaft. The dimensions r_D, a, and l are design parameters, whereas r and c change during actuator operation. The positions notated A, P, B, and O on the left refer to the projections of the points used in figure 3.4.

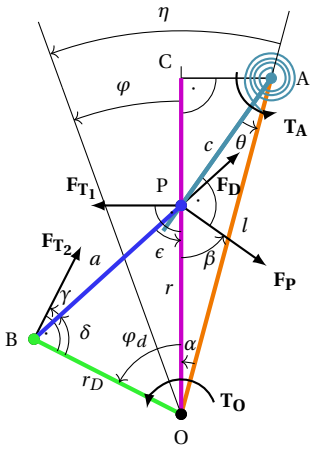

Figure 3.4: Geometric relations of the kinematics (view from the left compared to figure 3.3). The neutral position φ is controlled by motor 1 (purple). The angular position η of the output axis (orange) is the sum of neutral position φ and the deflection angle α. The triangle OBP is defined by the lengths a and r_D and the angle φ_d. Changing φ_d by moving motor 2 (green) relative to motor 1 will modify the pivot radius r. The triangle OPA is defined by the lengths r and l and the angle α. Changing α by deflecting the output axis (orange) compared to the neutral position will modify the spring deflection angle θ, and result in a counter-force from the spring deflection. The other measures in the figure are indicated to help obtain equations 3.4 to 3.10.

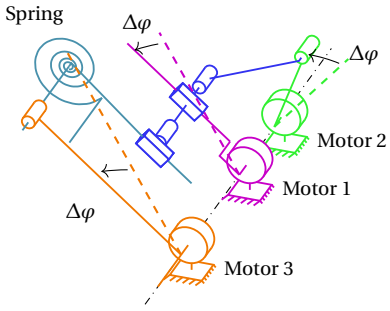

(a) Change of neutral position.

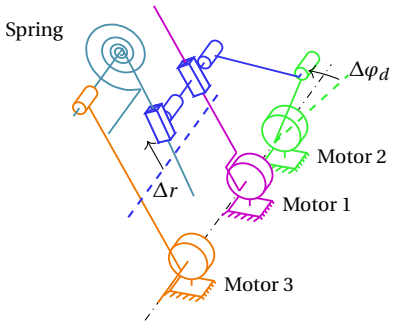

(b) Change of effective stiffness.

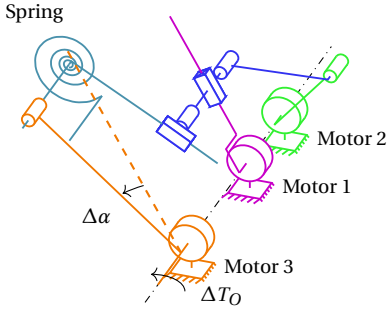

(c) Deflection by torque on the output axis.

Figure 3.5: 3D view of the kinematics of the actuator: Moving motor 1 (pink) and 2 (green) by the same angle $\Delta\varphi$ makes the output axis (orange) rotate by $\Delta\varphi$ without changing the effective stiffness (sub-figure (a)); Moving motor 2 by $\Delta\varphi_d$ with motor 1 fixed, changes the effective stiffness by changing the pivot radius (blue) by Δr without changing the output axis position (sub-figure (b)); A change of torque on the output axis by ΔT_O with motors 1 and 2 maintaining their position causes the spring to deflect by $\Delta\alpha$ (sub-figure (c)). Motor 3 is torque-controlled, and acts as variable damper.

2. The stiffness is changed by rotation of motor 2 relative to motor 1 (change of the angle φ_d) through the crankshaft mechanism formed by the excentered disc $\overline{BP}$ rotating relative to the link $\overline{OB}$ to motor 2. This causes P to move along the two linear slides represented by the lines going through $\overline{OC}$ and $\overline{PA}$. Notice that a movement of P along $\overline{OC}$ also requires a change of either α or θ to maintain the triangle OPA, corresponding to a change of the output shaft position or the spring deflection, *i.e.*, of the output torque. Changing the position of P and thus the length of $r = \overline{OP}$ changes the effective stiffness of the spring by changing the length of the spring lever length $c = \overline{AP}$. Indeed, if P is on one axis with the output axis going through O for $r = 0$, the output axis can rotate freely around the pivot axis, and the spring has no effect, which corresponds to an effective stiffness of zero. On the other hand, if P is on one axis with the spring rotation axis going through A for $r = l$, then the output axis is locked to the motor 1 axis, and the effective stiffness of the spring is infinite. For any other values of r between these two extremes, the effective stiffness has a certain finite value, with the special case of $r = l/2$, for which the effective stiffness equals the nominal stiffness of the spring.

3. A torque T_O on the output shaft while motor 1 and 2 maintain their positions causes a deflection of the spring by the angle θ and an output deflection angle α. The torque T_O required to cause a deflection of α is determined by the effective stiffness. Notice that this is only possible because c is not constant but can vary when the spring is deflected thanks to the linear slide. On the other hand, this also means that the stiffness is not constant over the deflection but decreases with increasing deflection.

Equations 3.1 to 3.16 describe the relationships to calculate the output torque T_O (eq. 3.10) and the torques T_1 and T_2 of motor 1 and 2 (eq. 3.15 and 3.16) depending on the design parameters r_D, a and l, the spring stiffness k, the stiffness setting angle φ_d, and the deflection α for static equilibrium of forces. Some helping variables β, γ, and δ can easily be obtained from the basic trigonometric relations:

$$\beta = \frac{\pi}{2} - \alpha - \theta\,, \tag{3.1}$$

$$\gamma = \frac{\pi}{2} - \delta\,, \tag{3.2}$$

and

$$\delta = \pi - \varphi_d - \epsilon\,. \tag{3.3}$$

From the law of sines, one obtains ϵ and r:

$$\epsilon = \arcsin\left(\frac{r_D}{a}\,\sin\varphi_d\right), \tag{3.4}$$

and

$$r = a\,\frac{\sin\delta}{\sin\varphi_d}\,. \tag{3.5}$$

Using Pythagoras' theorem in the triangle PAC allows to calculate c as

$$c = \sqrt{(l\,\cos\alpha - r)^2 + l^2\,\sin^2\alpha}\,, \tag{3.6}$$

which helps to calculate θ using the law of cosines:

$$\theta = \arccos\left(\frac{c^2 + l^2 - r^2}{2\,c\,l}\right). \tag{3.7}$$

With θ, the torque T_A produced by the spring is easily obtained from Hooke's law applied to torsion springs as

$$T_A = k\,\theta\,, \tag{3.8}$$

which gives the force of the spring in the point P by division through the lever length c:

$$F_P = \frac{T_A}{c}\,. \tag{3.9}$$

This needs to be projected into the tangential direction and multiplied with the lever arm to obtain the output torque:

$$T_O = k\,\theta\,\frac{r}{c}\,\sin\beta\,. \tag{3.10}$$

The effective stiffness k_e can be defined from this equation as

$$k_e = k\,\frac{r\,\theta}{c\,\alpha}\,\sin\beta\,, \tag{3.11}$$

such that $T_O = k_e\alpha$.

Further, the motor torques T_1 and T_2 can be obtained by projection of the forces and the relation between torque and force:

$$F_D = F_P\,\frac{\cos\beta}{\cos\epsilon}\,, \tag{3.12}$$

$$F_{T_1} = F_P\,\sin\beta + F_D\,\mathrm{sign}(\alpha)\,\sin\epsilon\,, \tag{3.13}$$

and

$$F_{T_2} = \frac{F_D}{\cos\gamma} \tag{3.14}$$

yield

$$T_1 = k\,\theta\,\frac{r}{c}\left(\sin\beta + \mathrm{sign}(\alpha)\,\sin\epsilon\,\frac{\cos\beta}{\cos\epsilon}\right), \tag{3.15}$$

and

$$T_2 = k\,\theta\,\frac{r_D\,\cos\beta}{c\,\cos\epsilon\,\cos\gamma}\,. \tag{3.16}$$

Fig. 3.6 shows a semi-logarithmic plot of the effective stiffness ratio over the pivot radius ratio. The stiffness ratio is defined as effective stiffness k_e over nominal spring stiffness k, and the pivot radius ratio is defined as pivot radius r over lever length l. For

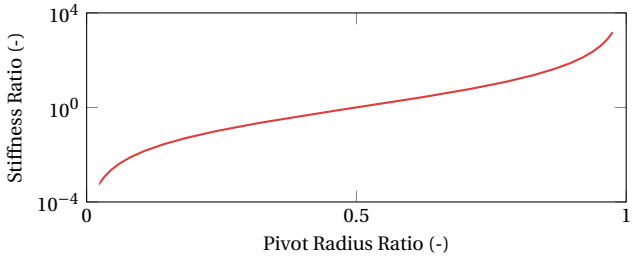

Figure 3.6: Semi-logarithmic plot for the proposed actuator kinematics of the effective stiffness ratio, defined as effective stiffness k_e divided by spring stiffness k, over the pivot radius ratio, defined as pivot radius r divided by lever length l. The plot is cropped as a pivot radius ratio of zero yields zero effective stiffness ratio, and a pivot radius ratio of 1 yields infinite effective stiffness ratio.

the pivot in the center position (pivot radius ratio of 0.5), the effective stiffness equals the nominal spring stiffness (stiffness ratio of 1). In practice, a pivot radius of zero is not useful to implement with a slider-crank linkage. It would result in a dead-lock position from which one cannot recover by changing the relative position of stiffness changer and positioning motors. In the final design, the design parameters were set to $r_D = 10\,\text{mm}$, $a = 9.5\,\text{mm}$, and $l = 20\,\text{mm}$, resulting in a theoretical stiffness ratio range from 0.0006 to 1500.

3.2.5. Component Selection and Assembly

Although the kinematics of the actuator are simple, its realization turned out to be rather complex. If the reachable pivot radius should be as small as possible, the pivot axis has to be very close to the motors' shared rotation axis. Thus, a hollow shaft approach was adopted. All bearings and driving components were placed on the outside of the actuator, leaving the center region for the pivot mechanism (cf. Figure 3.2). This was achieved using large-diameter thin section bearings (INA CSEA030) and frameless large-diameter thin section motors (ThinGap TG5151). The motors were placed in a direct drive configuration as a concession not to add further complexity by the necessity also to integrate gears.

The final design (cf. figure 3.7) consists of three disc-shaped modules for the positioning motor, the stiffness changer motor, and the damper, mounted on a two-parted chassis (cf. figure 3.8). For position sensing, large-diameter magnetic ring absolute position encoders were mounted directly to the respective discs (RLS AksIM). A CAD model of the actuator is provided as Solidworks files in the supplementary material [89].

3.2.6. Spring Design

A monolithic part consisting of a rigid cantilever section and an elastic torsion spring section was designed to act as the actuator's elastic element, as shown in Fig. 3.9. A nominal stiffness of $k = 60\,\text{N m/rad}$ was chosen as the design goal for the spring, resulting in a theoretical effective stiffness range of 0.06 N m/rad to 41 000 N m/rad. Considering the selected motors' maximum torque of 12 N m, this corresponds to a maximum spring deflection of 15.1° and a spring torque of 15.8 N m.

Titanium grade 5 (Ti6Al4V) was selected as the spring material because of its capacity

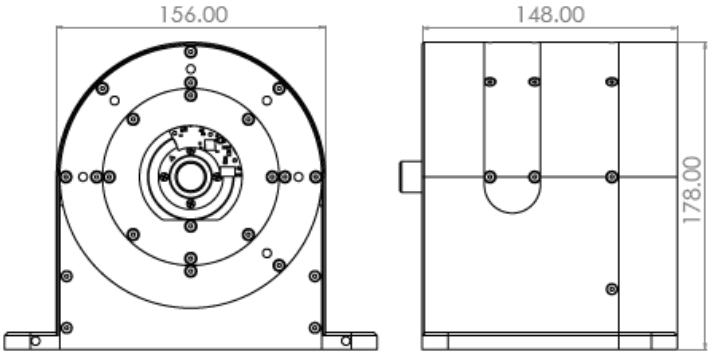

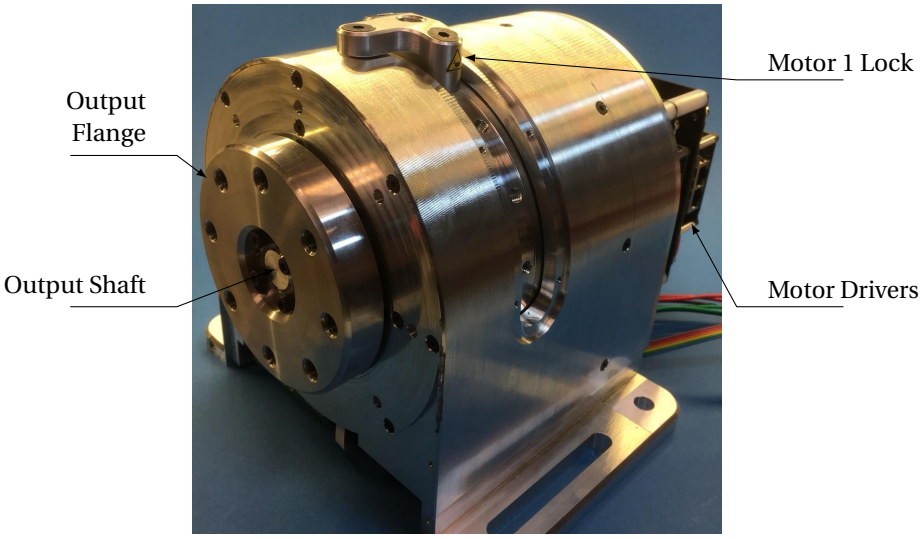

Figure 3.7: Drawing with external dimensions and photo of the actuator. The slot in the housing allows for locking the position of motor 1 for calibration purposes with the piece visible on top that can be screwed to the housing and to a ring with threaded holes that is attached to the motor. Alternatively, a handle can be screwed into one of the threaded holes for direct manipulation tests with the motor 1 disabled. The motor drivers are mounted to the back of the housing. A flange attached to the output shaft facilitates attaching an end-effector to the actuator.

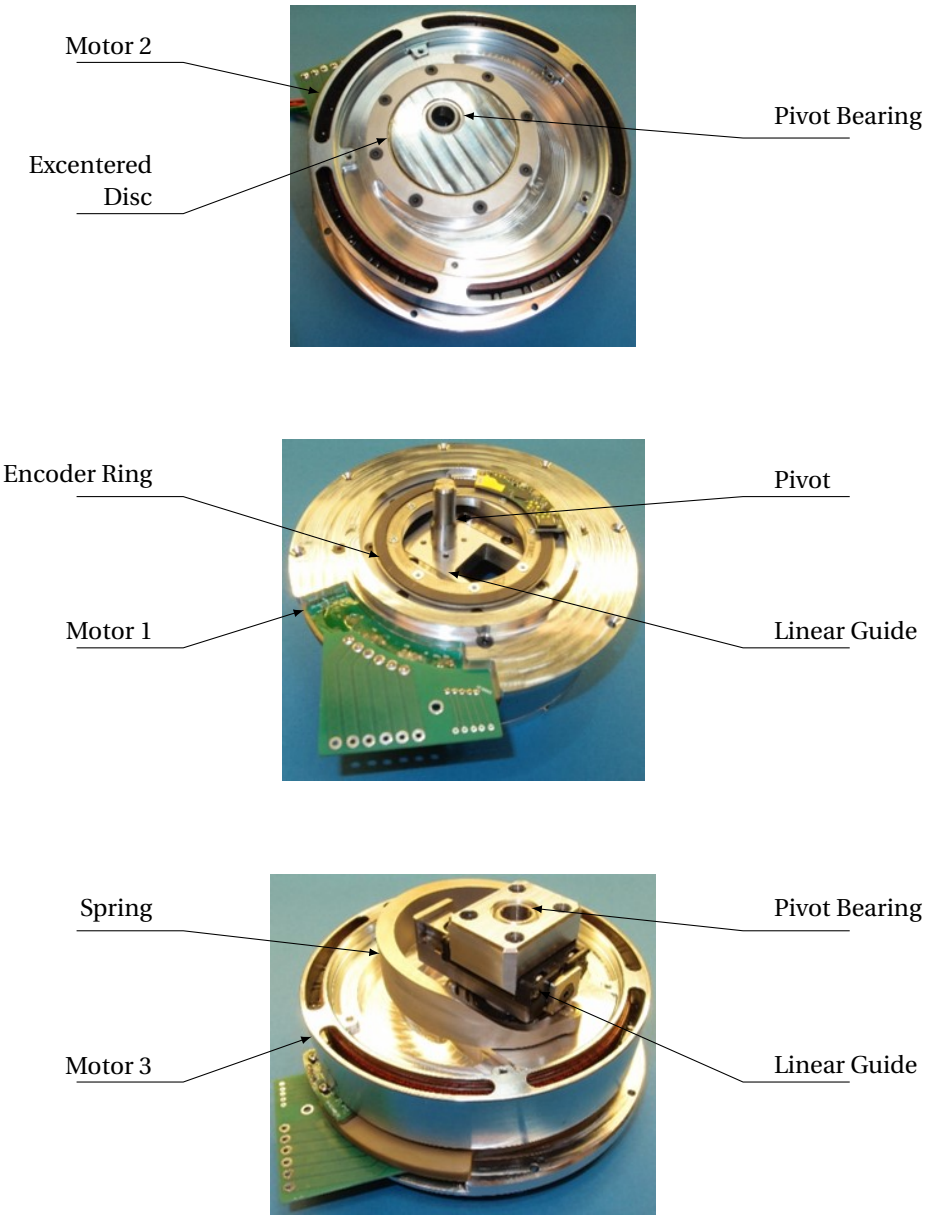

Figure 3.8: From top to bottom: photos of the prototype stiffness variation module (motor 2 with excentered disc), neutral position variation module (motor 1 with sliding pivot), and assembled elastic and output modules (motor 3, spring, and linear guide).

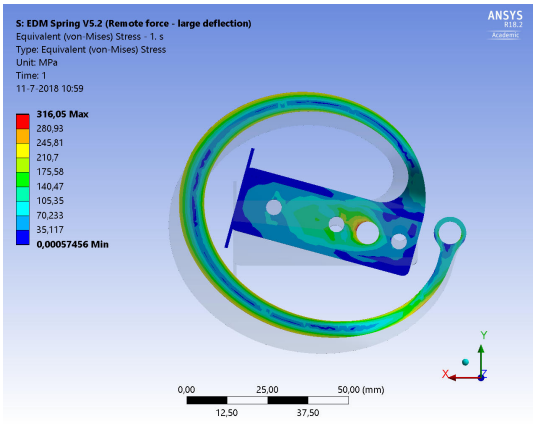

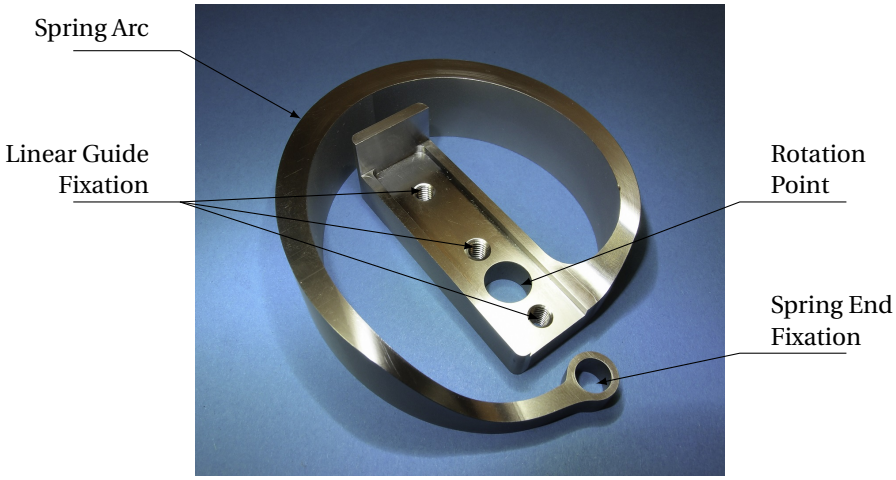

Figure 3.9: Finite elements simulation result and photo of the final spring design manufactured of titanium grade 5 (Ti6Al4V). The spring shape was iteratively optimized through finite element simulation to meet the desired stiffness of 60 N m/rad while ensuring not to exceed the material fatigue strength and not touching surrounding parts at maximum deformation in either direction as the spring is asymmetric.

to store high potential energy per volume elastically before being affected by plastic deformation. Several torsion spring shapes were considered. Because of spatial constraints, the resulting spring has only one winding. The diameter and thickness of the spring were determined to fit in the design when deformed. The spring thickness profile was dimensioned such that those values are achieved without exceeding material limits in the following procedure.

First, a finite element simulation was performed in ANSYS Workbench 18 on a spring model with a uniform thickness of 5 mm and a load of 15.8 N m. The simulation result indicated a non-uniform stress distribution over the circumference of the spring. The spring winding thickness was then altered iteratively until an even stress distribution was achieved. By doing so, the stress is uniform along the outer edge of the spring. Second, the spring shape and thickness was optimized further. The height, width, and thickness were changed iteratively until the spring had the desired deflection at maximum load (15.1°), the maximum stress did not exceed the titanium grade 5 fatigue strength (450 MPa), and the spring did not touch any surrounding parts at maximum deformation. Since the spring is asymmetric, these conditions were checked in both directions. The spring was manufactured through wire electric discharge machining (EDM) and CNC milling.

3.2.7. Variable Damper

Motor 3 acts as a variable damper with the stator mounted to the chassis, and the rotor mounted to the output axis. The motor torque T_3 is controlled to mimic the behavior of a variable damper with damping factor b between motor 1 and the output shaft:

$$T_3 = b\,(\dot{\varphi} - \dot{\eta})\,. \tag{3.17}$$

3.2.8. Controller

The motors are controlled by three motor drivers (Ingenia JUP-40/80-E) communicating via EtherCAT with a real-time Linux based high-level controller, as shown in figure 3.10. The EtherCAT loop runs at 1 kHz with the drivers of motor 1 and 2 configured in position control mode and the driver of motor 3 configured in torque control mode. The internal current controllers of the drivers run at 10 kHz.

For the controller, φ_d has to be calculated from the radius r to be set for a specific stiffness and the design parameters a and r_D through the law of cosines:

$$\varphi_d = \arccos\left(\frac{a^2 - {r_D}^2 - r^2}{2\,r_D\,r}\right). \tag{3.18}$$

Calling φ_1 and φ_2 the motor positions of motor 1 and motor 2, respectively, the following equations are also relevant for the controller:

$$\varphi_1 = \varphi\,, \tag{3.19}$$

and

$$\varphi_2 = \varphi_d - \varphi_1\,. \tag{3.20}$$

Finally, the controller uses a relationship between k_e and r that was fitted as following to the stiffness measurements of section 3.3:

$$r = (0.2273\,(\ln(k_e \mathrm{N\,m/rad}) + 5.9))^3\,\mathrm{mm}\,. \tag{3.21}$$

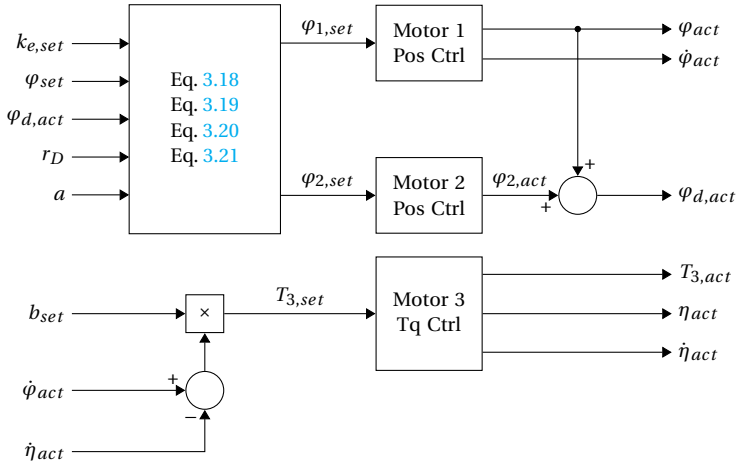

Figure 3.10: Control diagram of the actuator. The low-level position and torque control are implemented directly in the motor drivers of the respective motors, which receive the setpoints and return the actual values via EtherCAT to the high-level controller implemented in real-time Linux.

3.3. System Performance

Table 3.2 shows a summary of the mechanical performance. Figure 3.11 shows the measured output torque over output deflection plots for different pivot radii, showing the output torque hysteresis. Figure 3.12 shows the measured effective stiffness over torque plots for different pivot radii with the effective stiffness calculated as output torque over output deflection. Figure 3.13 shows the measured output torque over output deflection plots for different pivot radii. Figure 3.11 to 3.13 use the same measurement data collected with motor 1 fixed and an external torque applied at the output. The torque was measured with an ATI Gamma force-torque sensor mounted to the output axis (calibrated for ± 10 N m torque measurement in the z-axis). For figure 3.12 and 3.13, the data points were reduced for better visualization by calculating the centerline of the hysteresis and applying the Douglas-Peucker line simplification algorithm (Matlab function `reducem`). The dashed lines indicate the theoretical values for reference. Figure 3.14 shows the measured torque of motor 3 at different velocities for low and high damping settings. Figure 3.15 shows the measured pivot radius in response to a stiffness setpoint step, once for a small step and a large step. The 90 % step response time is 50 ms for a small step and 120 ms for a large step.

Figure 3.16 shows the measured step response of the actuator to a simultaneous position and stiffness change command (end-effector inertia of 0.0125 kg m^2, position change of 0.16 rad, stiffness change from 12 N m/rad to 350 N m/rad, constant damping of 0.5 N m s/rad). The measured 90 % step response time for this positioning motor change was 160 ms. The measured 90 % step response time for this stiffness motor change was 110 ms.

No.	Measure	Unit	Value Calculated	Value Measured
1	Cont. Output Power (pos.)	W	1085	
	Cont. Output Power (neg.)	W	1457	
2	Nominal Torque (pos.)	N m	7	
	Nominal Torque (neg.)	N m	9.4	
3	Nominal Speed	rad/s	155	
4	Nominal Stiffness Variation Time without load	s		0.09
5	Nominal Stiffness Variation Time with nominal load	s		0.12
6	Peak Torque (pos.)	N m	23	
	Peak Torque (neg.)	N m	33.4	
7	Maximum Speed	rad/s	1100	
8	Maximum Stiffness	N m/rad	41 000	313
9	Minimum Stiffness	N m/rad	0.06	0.2
10	Maximum Damping Torque	N m s/rad		3
11	Minimum Damping Torque	N m	0	
12	Damping Variation Time	s		0.01
13	Maximum Elastic Energy	J	5.7	0.7
14	Max. Torque Hysteresis	%		40
15	Maximum Deflection with max. stiffness	°		2.3
16	Maximum Deflection with min. stiffness (end stop)	°		120
17	Active Rotation Angle	°	∞	
18	Angular Resolution	°	6.87×10^{-4}	
19	Weight	kg		10.3

Table 3.2: Actuator mechanical performance summary

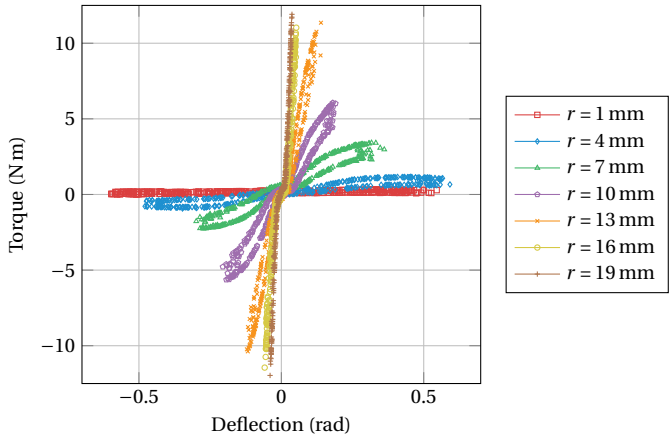

Figure 3.11: Measured torque over deflection hysteresis plot for different pivot radius settings.

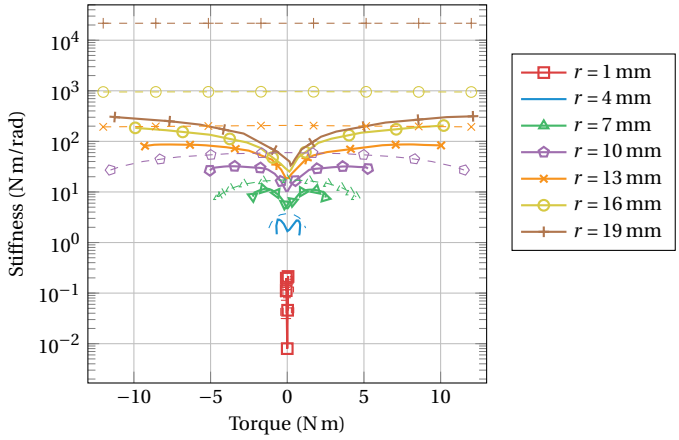

Figure 3.12: Semi-logarithmic plot of stiffness over external torque. Continuous lines show values extracted from measurement data and dashed lines values as calculated with the design parameters.

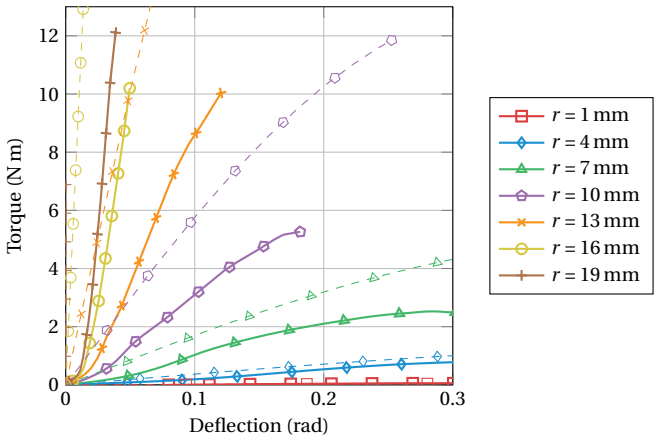

Figure 3.13: Torque over deflection plot. Continuous lines show values extracted from measurement data and dashed lines values as calculated with the design parameters.

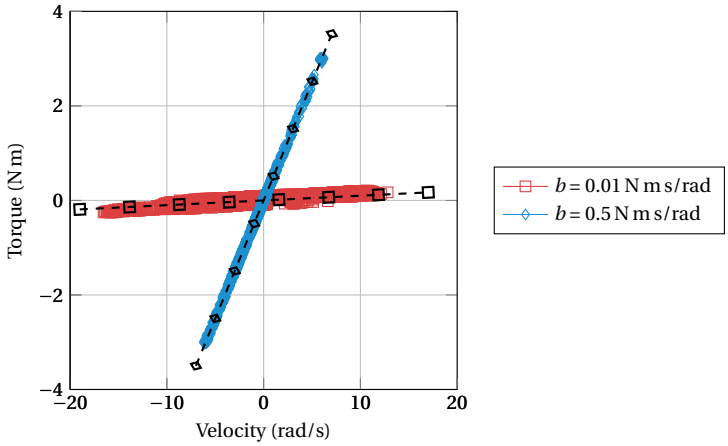

Figure 3.14: Torque over velocity for low and high damping settings. The dashed lines show the expected torque at the respective damping setting.

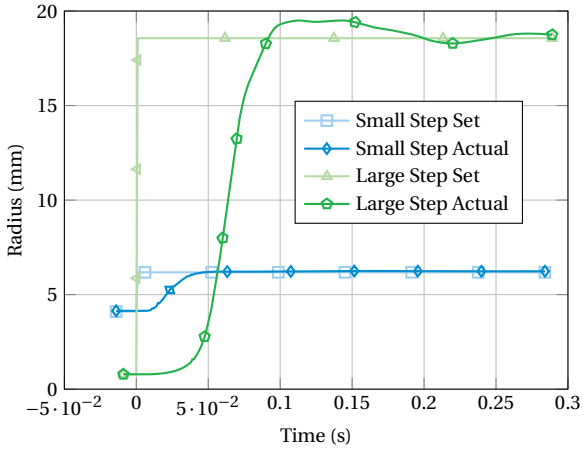

Figure 3.15: Pivot radius over time for a small and large setpoint step.

3.4. Application Example

As a simple application example, the actuator was programmed to execute a fast back-and-forth swinging motion similar to hammering at approximately 3.1 Hz with a cylindrical brass load of 1.6 kg at the output of the actuator. Together with the torque sensor, this resulted in an inertial load of approximately 0.0125 kg m^2.

The actuator was programmed to execute the motion once at a high stiffness setting with a pivot radius of 19.1 mm and once with changing the stiffness to a low setting with a pivot radius of 6.9 mm at the beginning of the motion. In both cases, the variable damping setting was set to a low value at the beginning of the motion (0.01 N m s/rad) and triggered to a high value (0.5 N m s/rad) at detection of a negative output position η_{act} to simulate an impact.

Figure 3.17 shows plots over time of the position, velocity, stiffness, and damping torque measured during execution of the motion (3.3 s of data were cropped at time 0.5 s, corresponding to a return to initial conditions and waiting for the manual start of the next run). At high stiffness (r_{set} = 19.1 mm), the deflection is lower than 0.03 rad, allowing for precise motions, whereas at low stiffness (r_{set} = 6.9 mm), the deflection is up to 0.3 rad, helping to reach a higher output velocity than with the stiff setting. The velocity gain obtained with low stiffness is 175 % from input velocity $\dot{\varphi}$ to output velocity $\dot{\eta}$. The stiffness changing time measured was 58 ms for this stiffness change.

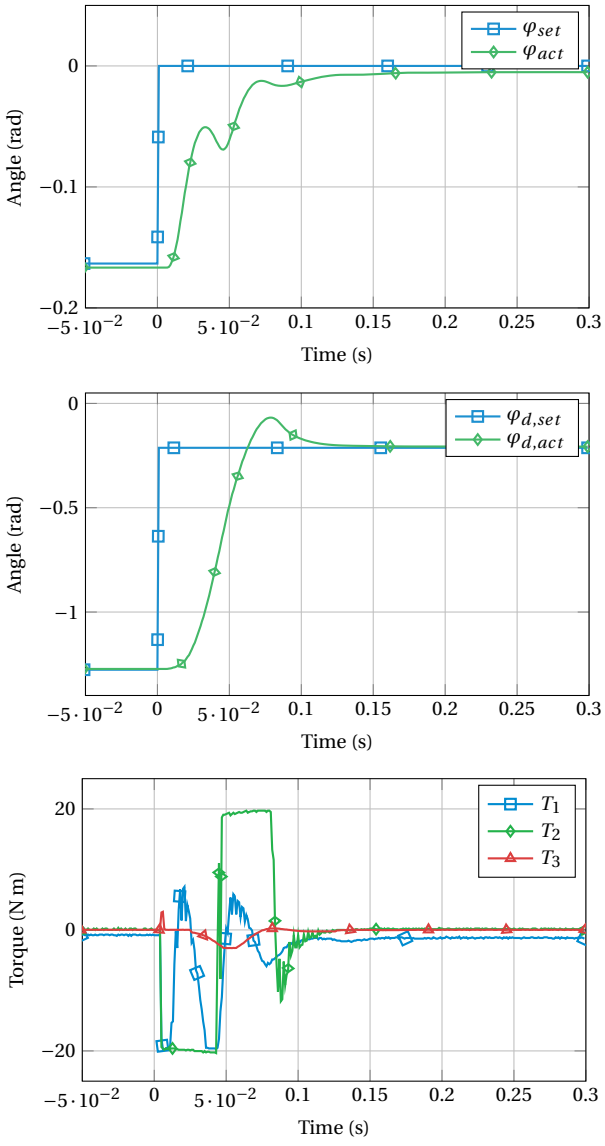

Figure 3.16: Angles and motor torques during a simultaneous position and stiffness change command (end-effector inertia of 0.0125 kg m^2, position change of 0.16 rad, stiffness change from 12 N m/rad to 350 N m/rad, constant damping of 0.5 N m s/rad).

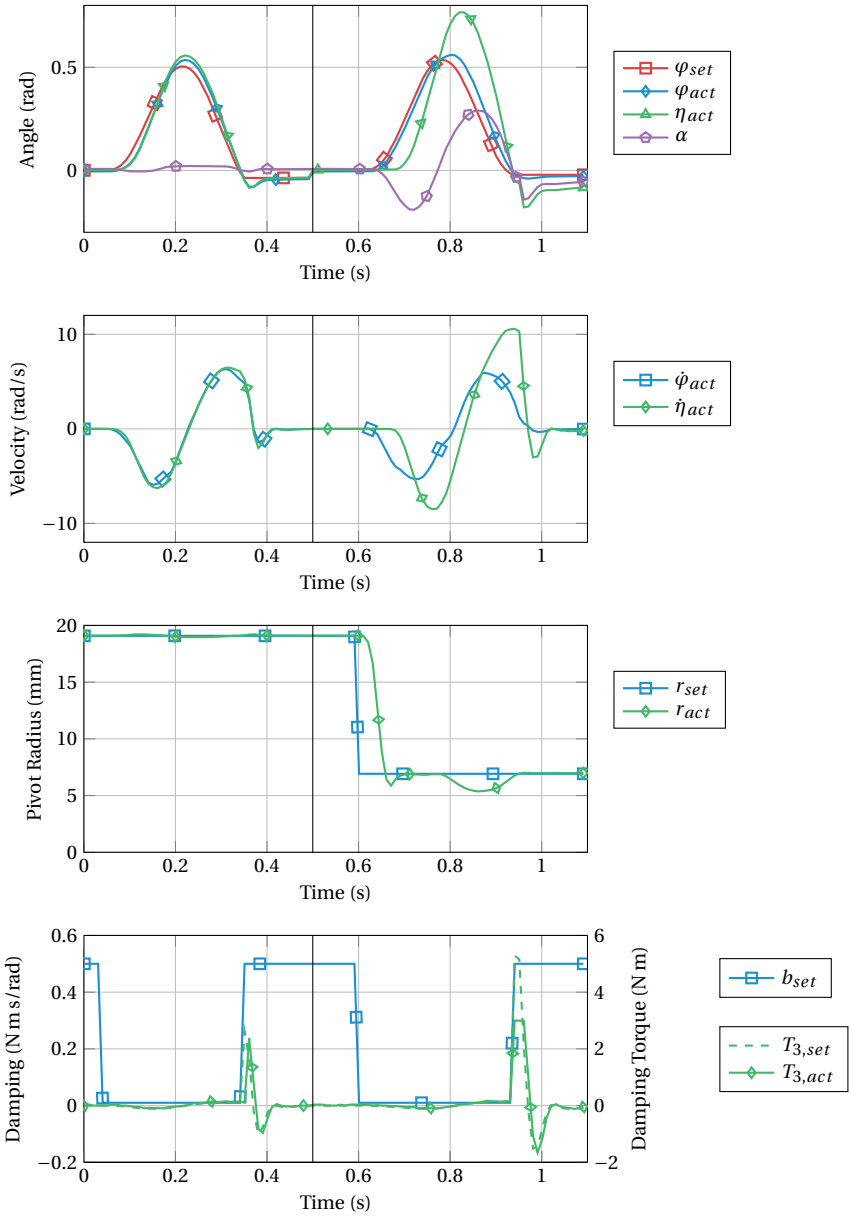

Figure 3.17: Application example measurements showing a fast back-and-forth swinging motion similar to hammering at approximately 3.1 Hz, once executed with high stiffness (pivot radius of 19.1 mm), and once with low stiffness (pivot radius of 6.9 mm). The high stiffness setting allows for precise motions with low deflection α. The low stiffness setting allows for exploiting the spring deflection to achieve a higher output velocity $\dot{\eta}$ than the input velocity $\dot{\varphi}$. The fast stiffness changing time of 58 ms shown by the plot of r_{act} allows for changing the stiffness dynamically within a motion. The variable damping is activated at the end of the motion to reduce oscillations, as shown by the plot of the damping setpoint b_{set}, the damping torque setpoint $T_{3,set}$, and the measured torque $T_{3,act}$. Some data were cropped at $t = 0.5$ s to skip resetting to the initial position and manual start of the next motion.

3.5. Discussion

In the analysis of whether the design meets the tasks' requirements, we differentiate between the design and the prototype implementation, which was slightly simplified for budgetary reasons. Most notably, the prototype was implemented without gears for motors 1 and 2, meaning that the position has to be held by the motors in stall operation. This is not an efficient operation mode for electric motors and negatively affects the actuator's positioning performance in the presence of external disturbances. However, this was deemed acceptable, as the main mode of operation aimed at with this actuator are highly dynamic tasks. For delicate tasks and highly dynamic tasks, a direct drive configuration is beneficial. The actuator can then be very soft and suffers less wear than an actuator with gears in unexpected high velocity impacts in a stiff actuator setting, which could occur due to misuse by the operator.

The requirement of 50 ms was only met by the prototype for small stiffness changes, whereas the time measured for large stiffness changes was up to 120 ms. We think that this is not an issue in our targeted bilateral hammering application because it only requires small stiffness changes as the maximum human arm stiffness was measured to be in the range of 40 N m/rad [90]. The measured damping variation time of 10 ms is due to the motor time constant of the torque-controlled motor used for damping.

Also, while the design's calculated maximum stiffness was 41 000 N m/rad, a maximum stiffness of only 313 N m/rad was measured. This difference is most likely due to play and deformations in the transmission mechanism. At maximum torque the difference between expected and measured stiffness corresponds to an additional deflection of 1.8° compared to the expected deflection angle.The calculations are based on the assumption that only the spring deforms which cannot be guaranteed for this prototype. However, the maximum actuator stiffness is still sufficiently high compared to the maximum human arm stiffness of 40 N m/rad, and therefore the use of Dyrac for bilateral teleoperation is not limited.

Play is an issue of the prototype's performance for explosive movements, as it induces a high torque hysteresis (cf. figure 3.11), resulting in energy losses in resonance mode. This can explain the lower velocity gain of 175 % in the example application compared to results measured with other VSAs of 272 % [42] and over 400 % [43].

Another effect of the design is that for equal motor torques, the output torque is higher in the negative direction than the positive direction (9.4 N m to 7 N m) because the respective torques of the position changing motor 1 and the stiffness changing motor 2 add up in the negative direction, whereas they subtract in the positive direction.This is a direct consequence of the crankshaft mechanism. The pivot is held at its position P on the linear guide of motor 1 through the tangential component of force F_D that the shaft linking motor 2 to the pivot exerts (cf. figure 3.4). This has to be always outwards as the tangential component of the external forces acting on the pivot F_P is always inwards. Thus, the radial component of the force F_D applied by the shaft is always in the same direction (to the right on figure 3.4 or to the left if the shaft was positioned on the other side of the linear guide). Therefore, to stabilize the angular position, the motor 1 has to either compensate for the radial component of F_D or exert less force F_{T_1} to achieve in total an equal force but in opposite direction to the radial component of the external force F_P. While this is in general undesirable, it might not be an issue in many practical applications

as there is often a working direction requiring a large force and a disengaging direction requiring much less force. Moreover, the configuration can be changed on-the-fly by setting φ_d to a negative value to swap the stronger and the weaker direction.

Mechanical end stops were added at ±120° deflection in the prototype to avoid situations that cannot be recovered from by the motors alone. This is mainly due to the crankshaft mechanism leading to very unfavorable configurations for low stiffness settings. As the deflection angle increases, the forces F_{T_1} and F_D become less efficient in compensating for F_P in figure 3.4. This effect is more predominant for low stiffness settings where the deflection is larger for equal external torque. Furthermore, in these settings, φ_d is large, thus a higher torque in motor 2 is required to maintain the equilibrium of forces as the cosine terms in the denominator of equation 3.16 tend to zero for small pivot radii.

The complexity of the mechanism resulted in a heavy actuator (10.3 kg) compared to existing variable stiffness actuators with similar performance, such as the FSJ or the AwAS-II (both 1.4 kg). However, the other actuators also do not have variable damping capability.Indeed, Dyrac is one of very few implemented actuators that allows full impedance variation (*i.e.*, stiffness and damping) with such high dynamics and over such a wide stiffness range.

The application example shows that the actuator is suitable for precision tasks and highly dynamic tasks and can adapt the stiffness dynamically. Also, the variable damping is very useful to suppress unwanted oscillations without affecting the desired ones. The main motivation of using VIAs for hammering is to exploit the mechanical resonance and for this it is crucial that very low damping can be realized. At the same time, the goal was to design a versatile robotic actuator and not a specialized hammering tool. Thus, oscillations have to be suppressed during precision tasks. The variable damper fulfills both requirements.

Overall, the measured actuator performance is very favorable for performing not only delicate and precision tasks but also human-like dynamic motions such as hammering, shaking, jolting, and throwing through teleoperation. Also, a human-subject study was successfully performed on a simulated VIA with similar dynamics to the Dyrac prototype [91]. It shows the usefulness of fast stiffness changing time and the variable damping to perform precision and dynamic tasks with one actuator. This could make performing different types of tasks through teleoperation more efficient and intuitive for the human operator in the sense that he or she would not need to change the mode of operation explicitly [91].

3.6. Conclusion

A new variable impedance actuator design was presented having some attractive performance features for dynamic actuation research:

1. fast impedance-changing time of 120 ms for full-range stiffness steps (50 ms for steps smaller up to 10 % of full scale pivot radius change) and 10 ms for full-range damping steps,
2. a wide effective stiffness range of 0.2 N m/rad to 313 N m/rad,
3. variable damping with a damping torque from 0 N m to 3 N m.

A prototype of the new design was manufactured and characterized to show the feasibility and validate the performance requirements in hardware, albeit with small limitations. The benefits of this actuator for teleoperated applications have also successfully been demonstrated in an application example. A simulated VIA based on the dynamics of the Dyrac prototype was used in a human-subject study [91], showing the potential of such a dynamic and versatile variable impedance actuator for both precise positioning tasks and highly dynamic tasks like hammering.

4

Self-Adapting Variable Impedance Actuator Control

Variable impedance actuators (VIAs) as tool devices for teleoperation could extend the range of tasks humans can perform through a teleoperated robot by mimicking the change of upper limb stiffness that humans intuitively perform for different tasks and thereby increasing the dynamic range of the robot. This requires that the impedance be controlled appropriately, which was often achieved by sensors measuring the operator's muscle tension. However, additional sensors mean increased system complexity and possibly longer donning time if the sensors need to be fixed and calibrated on the operator. This chapter aims to show the effectiveness of a controller that does not require additional sensors, thereby reducing system complexity and increasing ease of use. The controller should allow performing precision tasks and dynamic tasks like hammering through teleoperation with a VIA tool device without requiring the human user to change the VIA's impedance setting actively. This is achieved by a control law according to the principle "slow and stiff/fast and soft," tuned to the characteristics of human motion during precision tasks and dynamic tasks. The controller was tested in a human user study with 24 participants comparing the human-machine performance with the self-adapting controller in a bilateral telemanipulation experiment with two tasks (precision/dynamic) using three impedance settings (high/low/adaptive impedance). The results indicate that the proposed system performs equally well as state of the art stiff teleoperation devices for precision tasks while having benefits in terms of increased safety and reduced wear for dynamic tasks. This is a step towards teleoperation with a wide dynamic range, enabling intuitively performing tasks in the full human motion bandwidth without requiring the human operator to select a specific mode of operation.

4.1. Introduction

Variable Impedance Actuators (VIAs) [26, 27, 70] can be a powerful technology for teleoperation, as they allow for changing a robotic manipulator's impedance dynamically, in a similar way to humans adapting the impedance of their arms to the task at hand [92]. Compared to classical stiff actuators, VIAs thus have additional degrees of freedom (stiffness and damping) that need to be controlled on top of position control, which is not a trivial problem. Specifically, the scope of this study was to develop a control law for teleoperated actuators similar to the dynamic robotic actuator (Dyrac) that we developed, optimized for highly dynamic tasks like throwing or hammering [93].

For automatically executed tasks, optimal control laws for the impedance control have been presented, optimizing for maximum energy efficiency, maximum output velocity, or other criteria [49, 94, 95]. These apply to preplanned task execution. However, for teleoperated robots, an optimal control law cannot be determined the same way due to the unpredictable nature of the human trajectory that needs to be followed by the robot. Thus, an impedance controller is required that works without knowing the full trajectory beforehand.

One approach that has been explored in previous research is to estimate the stiffness of the limbs of the human operator interacting with the handle device of the teleoperation system and reproduce it in the tool device. Stiffness estimation of the limbs can be achieved, for example, through EMG measurement [96, 97], vibration based estimation [98], or grip force measurement [99]. This approach assumes correct stiffness intention and good body control by the human operator and correct estimation of the operator's limbs' stiffness by the teleoperation system. It also requires additional sensors, some of them (*e.g.*, EMG) needing to be fixed and calibrated to the operator's body. This increases the system complexity and the preparation time before using the system, making it cumbersome to implement and use.

The goal of this paper is to experimentally validate a control law for VIAs that does not require external impedance commands but continuously adapts the tool actuator impedance according to the instantaneous motion command. The control law is based on the "slow-stiff/fast-soft" principle inspired by "Fast and "Soft-Arm" Tactics" of Bicchi *et al.* [31]. It should allow efficient execution of precision tasks and highly dynamic tasks like hammering, throwing, shaking, jolting, etc., without requiring an explicit task selection. Related approaches to adapt the impedance of a teleoperator system have been studied [100, 101], but not in the context of explosive movements.

We have shown in previous research through two experiments how SEAs could increase the output velocity compared to stiff actuators for highly dynamic tasks [71]. However, soft SEAs are less practical for precision tasks as they are difficult to control in position and quickly start oscillating in free air. Nevertheless, precision tasks are crucial to teleoperation as they include prevalent tasks like pick-and-place tasks, insertion, inspection, etc. This chapter shows through a third experiment how precision tasks and highly dynamic tasks can be performed efficiently and intuitively by a human operator through one teleoperated robotic actuator.

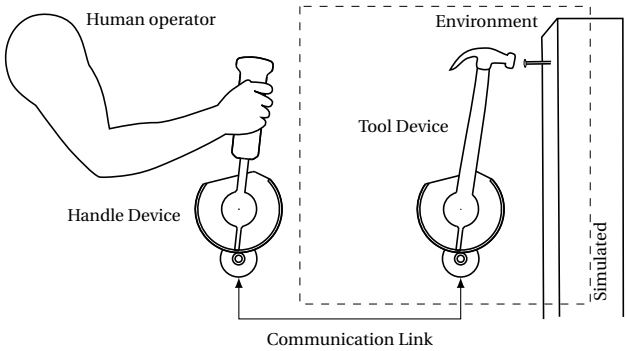

Figure 4.1: The scenario considered for this study is a human operator interacting with the environment through a bilateral teleoperation system. The teleoperator consists of a handle device and a tool device coupled to each other through a communication link and tuned to mirror velocity and force as accurately as possible. The tool device in this experiment was a simulated VIA with dynamics similar to the Dyrac actuator [93] interacting with a simulated environment.

4.2. Experiment 3: Method

4.2.1. Scenario

The study is based on a teleoperation setup, as illustrated in figure 4.1 with parts of the setup being simulated. A human operator interacts with the teleoperation system through the handle device, and the teleoperation system interacts with the simulated environment through the simulated tool device. The teleoperation system mirrors the velocity and force between the handle and the tool device, ideally with full transparency allowing the human operators to interact with the environment as if it was through their own arm. The tasks to be performed are either a precision task, consisting of moving the tool device from one position to another as fast as possible while stopping precisely at the target position, or a dynamic task, consisting of hitting a target with the tool device with as much impact velocity as possible (cf. section 4.2.8).

In this study, the handle device and tool device are not equal mechanically, but the handle device is rigid, whereas the tool device consists of a simulated VIA with similar dynamics as the wide impedance range actuator Dyrac [93]. A simulation was used instead of the physical actuator to make the experiment outcome independent of some flaws in the Dyrac prototype [93]. Mainly, considerable hysteresis was measured in the prototype of up to 40 %. Further, as the prototype had been built without gears, the position holding accuracy of the joint position motor was deemed insufficient in situations with dynamic external loads, *e.g.*, impacts, most likely due to controller bandwidth limitations. The VIA can be configured with a permanently high impedance setting, permanently low impedance setting, or continuously self-adapting impedance (cf. section 4.2.4). The permanently high impedance setting is equivalent to classical robots and best-suited for precision tasks when the influence of external forces and end-effector inertia should affect the end-effector position the least possible. The permanently low impedance setting is equivalent to SEAs and best-suited for highly dynamic tasks when impact forces should be reduced, and which benefit from energy storage in the actuator's elastic element. The

self-adapting impedance setting uses the proposed "slow-stiff/fast-soft" control law to be validated. It should allow the human operator to perform both types of tasks with comparable performance to the best-suited setting without requiring an explicit mode change.

4.2.2. Hypotheses

The study was based on the following hypotheses:
Hypothesis B1: A permanently high impedance tool device setting allows a human operator to perform better in telemanipulated precision tasks than a permanently low impedance setting (according to state of the art robot design).

Hypothesis B2: A permanently low impedance tool device setting allows a human operator to perform better in telemanipulated dynamic tasks than a permanently high impedance setting (according to our previous research [51]).

Hypotheses B1 and B2 are the basic assumptions on which the experiment is designed. Checking them serves as a sanity check for the experiment method and apparatus.

The hypotheses for validating the new self-adapting impedance variation algorithm were:

Hypothesis H1: A self-adapting control law that increases the tool device impedance at low velocity and decreases its impedance at high velocity allows a human operator to perform telemanipulated precision and dynamic tasks equally well as with the best-suited permanent impedance setting for the respective task while achieving significantly better performance than with the alternative permanent impedance setting for the respective task.

Hypothesis H1 translates into:

> *Hypothesis H1.1*: There is no significant difference in performance achieved in precision tasks with the self-adapting impedance setting or the permanently high impedance setting.
>
> *Hypothesis H1.2*: Significantly better performance can be achieved in precision tasks with the self-adapting impedance setting than with the permanently low impedance setting.
>
> *Hypothesis H1.3*: Significantly better performance can be achieved in dynamic tasks with the self-adapting impedance setting than with the permanently high impedance setting.
>
> *Hypothesis H1.4*: There is no significant difference in performance achieved in dynamic tasks with the self-adapting impedance setting or the permanently low impedance setting.

Hypothesis H2: The performance achieved with the self-adapting impedance setting does not depend on whether the type of task performed is the same over many repetitions or few repetitions.

Hypothesis H2 thus suggests that hypotheses H1.1 to H1.4 are also valid if precision and dynamic tasks are performed in quick succession. Hypotheses H1.1 to H1.4 will be referred to as H2.1 to H2.4 if used for quickly succeeding precision and dynamic tasks.

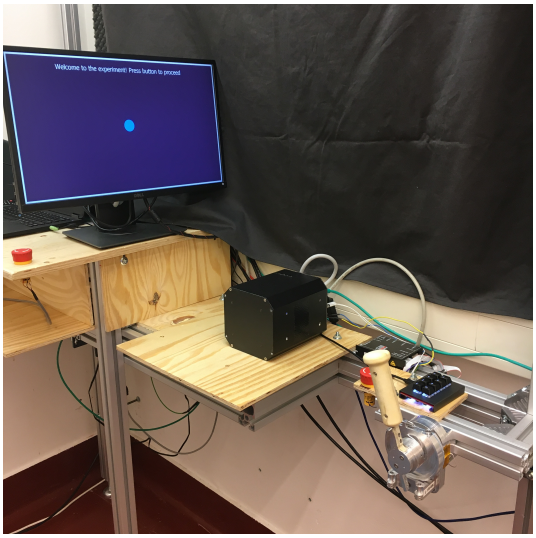

Figure 4.2: Photo of the setup used for the experiment. The white handle in front is the handle of the 1-DOF haptic joystick. The black box in the center is the control computer running real-time Linux. The screen visualizes the GUI with the instructions and feedback for the participants (controlled by a second computer not visible on the picture).

4.2.3. Experiment Apparatus

Hardware

The experiment apparatus consisted of a haptic bilateral teleoperation setup with one degree of freedom, where the handle device consisted of a stiff actuator device (cf. figure 4.2, the handle device was a modified version of one of the units described by Rebelo *et al.* [52] and the same as in chapter 2) and the tool device of a simulated VIA actuator, similar to the architecture proposed by Christiansson [48], but with a VIA instead of a permanently soft tool device.

A computer screen connected to a second computer showed the user interface (GUI) to the participants, leading them through the experiment (cf. figure 4.3). The computer showing the GUI was connected through a UDP connection over Gigabit Ethernet with the real-time Linux computer.

The simulation model was built according to the system identification of the Dyrac prototype and included a model of the kinematics of the stiffness changing mechanism (end-effector inertia 0.0125 kg m^2, joint motor set position to actual position transfer function as second-order Butterworth filter with 20 Hz cut-off frequency, stiffness changing motor set position to actual position transfer function as second-order Butterworth filter with 10 Hz cut-off frequency). However, the simulation model did not exhibit hysteresis, position was not affected by load, and the effective spring constant was not affected by the deflection. The simulation model ran at 1 kHz on a real-time Linux computer. Figure 4.4 to 4.8 compare measurements of the simulation to the measurements of the prototype to show the differences and similarities between them.

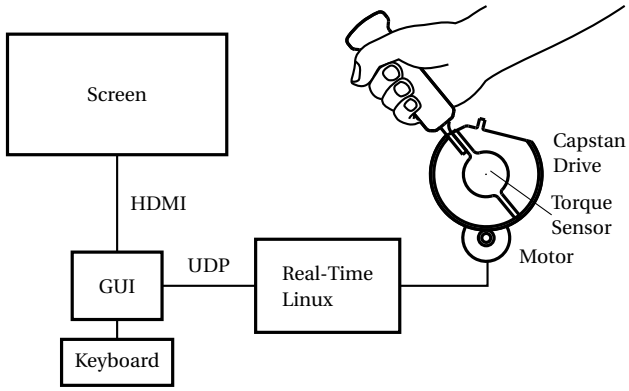

Figure 4.3: Schematic of the setup used for the experiment

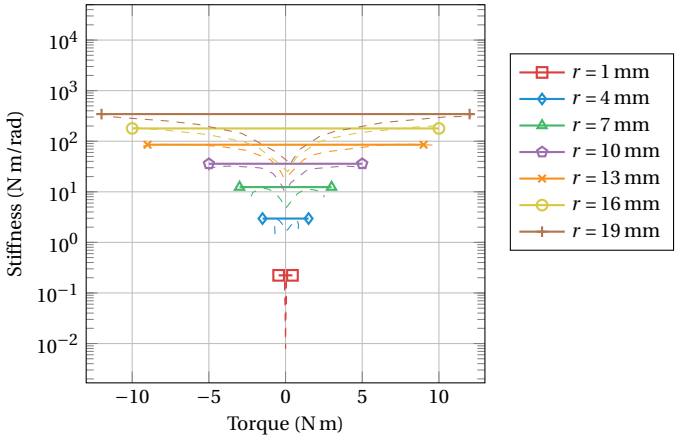

Figure 4.4: Semi-logarithmic plot of stiffness over external torque of the simulated actuator compared to the Dyrac prototype. Continuous lines show values extracted from measurements on the simulation. Dashed lines show values extracted from measurements on the Dyrac prototype (cf. figure 3.12).

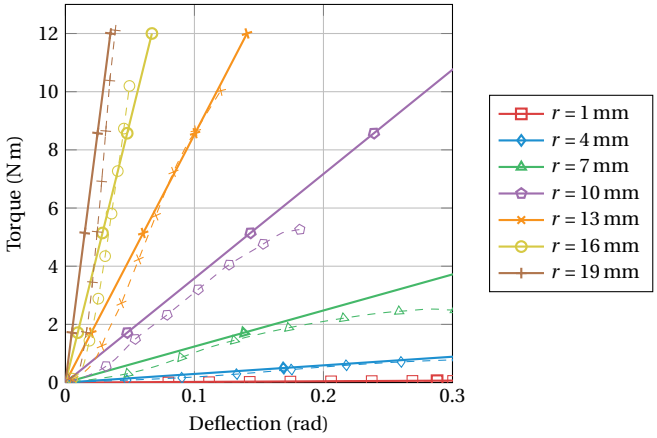

Figure 4.5: Torque over deflection plot of the simulated actuator compared to the Dyrac prototype. Continuous lines show values extracted from measurements on the simulation. Dashed lines show values extracted from measurements on the Dyrac prototype (cf. figure 3.13).

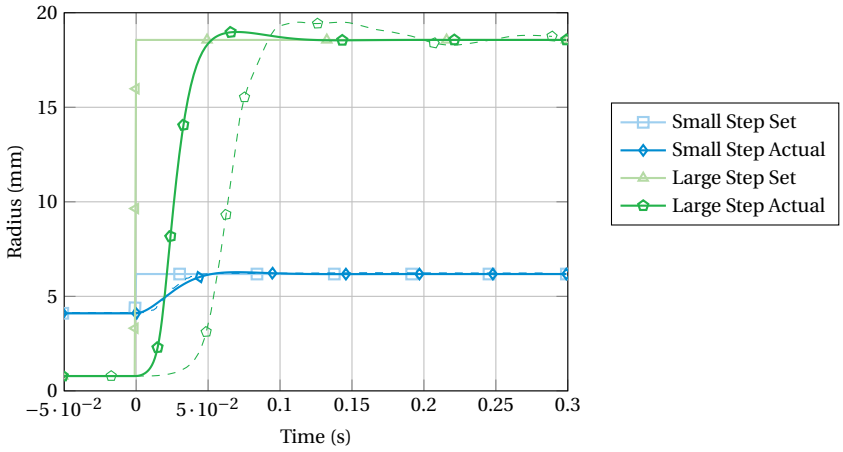

Figure 4.6: Pivot radius over time for a small and large set point step of the simulated actuator compared to the Dyrac prototype. Continuous lines show measurements on the simulation. Dashed lines show measurements on the Dyrac prototype (cf. figure 3.15).

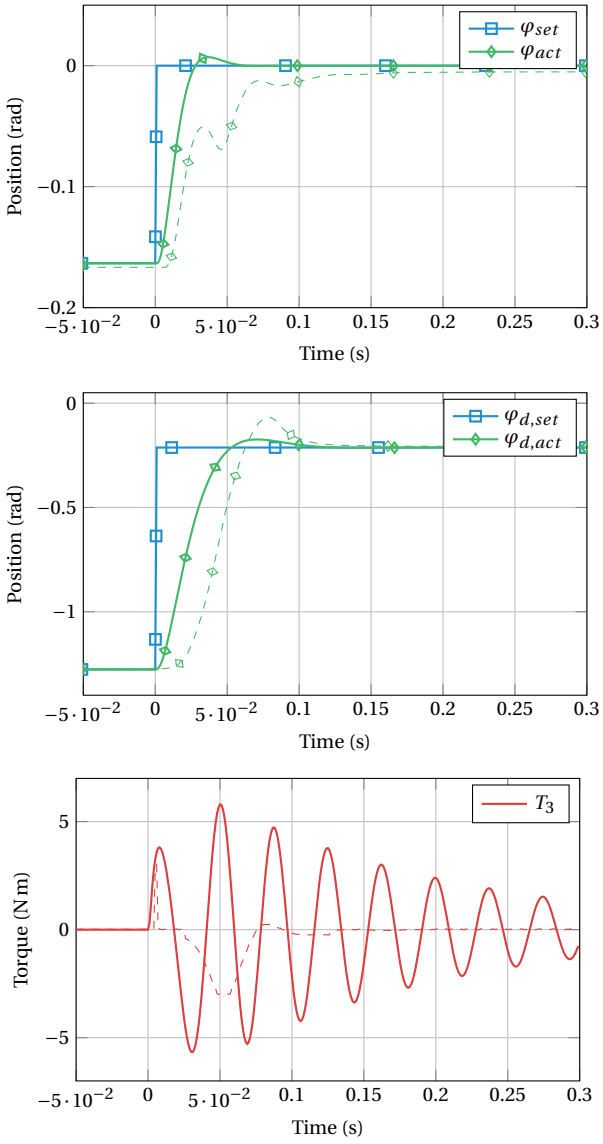

Figure 4.7: Angles and motor torques during a simultaneous position and stiffness change command of the simulated actuator compared to the Dyrac prototype (end-effector inertia of 0.0125 kg m^2, position change of 0.16 rad, stiffness change from 12 N m/rad to 350 N m/rad, constant damping of 0.5 N m s/rad, motor torques of motor 1 and 2 not simulated). Continuous lines show measurements on the simulation. Dashed lines show measurements on the Dyrac prototype (cf. figure 3.16).

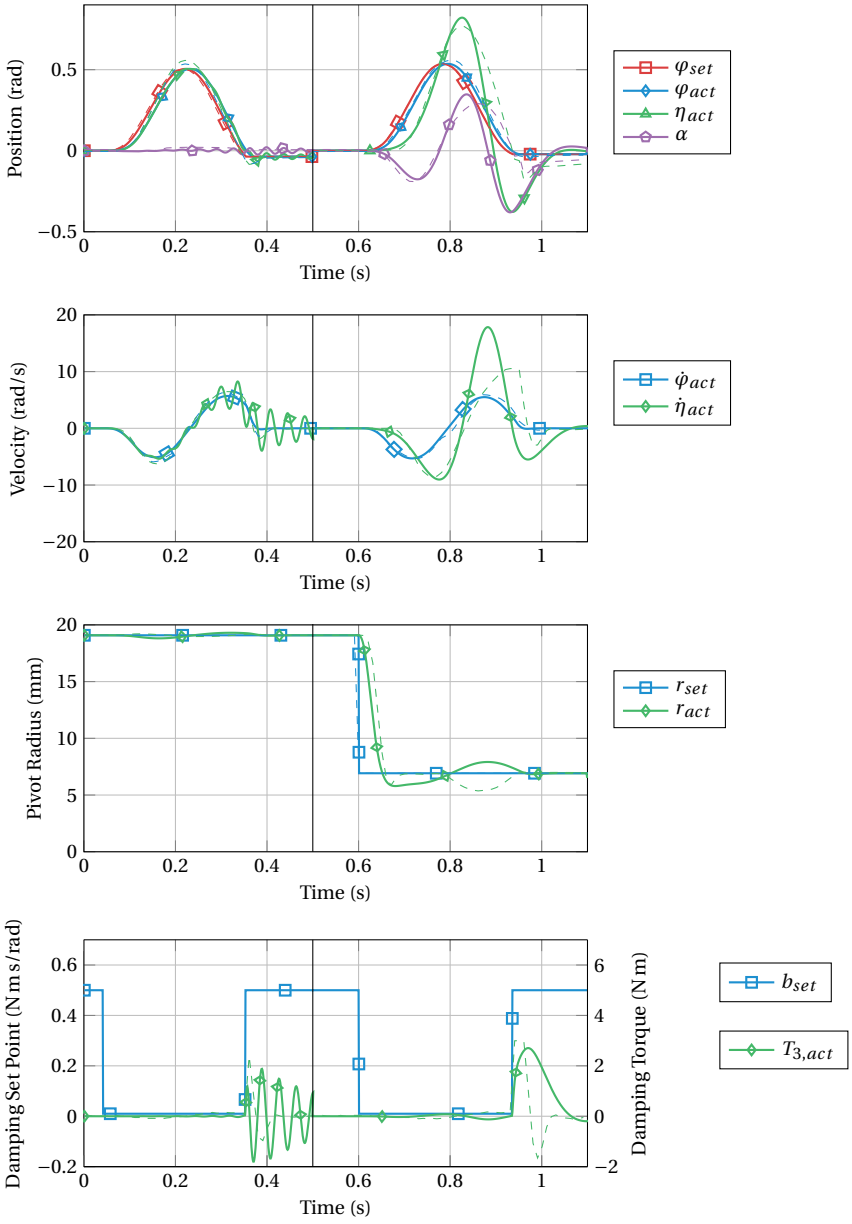

Figure 4.8: Application example measurements of the simulated actuator compared to the Dyrac prototype showing a fast back and forth swinging motion similar to hammering at approximately 3.1 Hz, once executed with high stiffness (pivot radius of 19.1 mm) and once with low stiffness (pivot radius of 6.9 mm). Continuous lines show measurements on the simulation. Dashed lines show measurements on the Dyrac prototype (cf. figure 3.17).

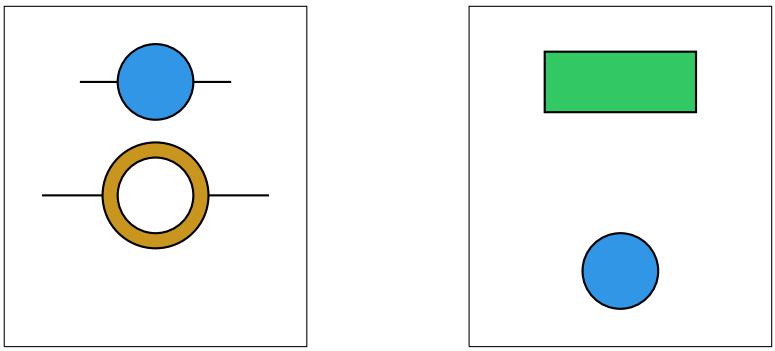

(a) Precision Task (b) Dynamic Task

Figure 4.9: Essential elements of the user interface: the blue circle visualizes the tool device position, the brown circle visualizes the target position for the precision task, and the green box visualizes the impact position for the dynamic task.

User Interface

The user interface was a full screen application (cf. figure 4.2) with one line for instructions, a user cursor whose position corresponded to the position of the VIA output position, and a target whose appearance changed depending on the current task (cf. the instruction video of the experiment in the complementary material [102]). The rotatory position of the handle was mapped linearly to a linear position on the screen. For the precision task, the target was a moving ring, and the participants were instructed to follow the target as closely as possible, such that the user cursor filled the ring as much as possible at any time (cf. Fig. 4.9). For the dynamic task, the target was a rectangle, and the participants were instructed to hit the target with the speed of the user cursor as high as possible. After every trial, the result achieved in that trial was displayed to the participants in the instruction line.

4.2.4. Self-Adapting Teleoperation System Tuning and Identification

Fig. 4.10 shows the controller architecture of the teleoperation system. The control laws C_m, C_1, C_2, and C_4 were tuned for optimal transparency according to the rules of Hashtrudi-Zaad and Salcudean [61]. The tool device and the environment were simulated. The tool device was position-controlled, so C_3 from the four-channel architecture was not used. In the diagram, TF_{motor} is the transfer function modeling the time behavior of the VIA's position-controlled joint position motor. The tool device impedance Z_s was not constant but was modified depending on the handle device velocity $\dot{x}_m$ through the parameter C_{Z_s}, as indicated by the signal z_{sc}. This implemented the self-adapting impedance variation algorithm. The simulated environment force $f_{\tilde{e}}$ was zero for the precision task in free air or rendered a contact at the target position during the dynamic task ($k_{wall} = 10\,000$ N m/rad, $b_{wall} = 20$ N m s/rad).

The control law C_{Z_s} could be changed to switch between the low impedance setting (mode L), the high impedance setting (mode H), and the adaptive setting (mode A).

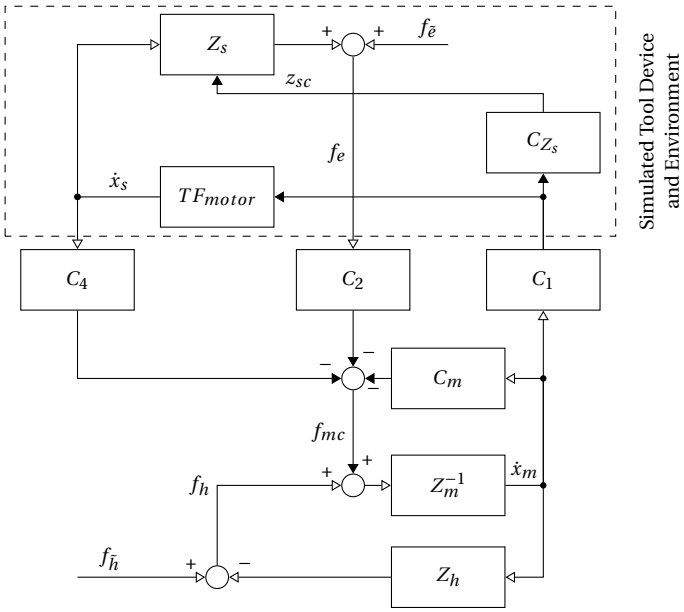

Figure 4.10: Controller architecture of the teleoperator (Adapted from [61]). The tool device and the environment were simulated. TF_{motor} is the transfer function modeling the time behavior of the VIA's position-controlled joint position motor. The tool device impedance Z_s was not constant but was modified depending on the handle device velocity $\dot{x}_m$ through the parameter C_{Z_s}, as indicated by the signal z_{sc}. This implemented the self-adapting impedance variation algorithm. The simulated environment force $f_{\tilde{e}}$ was zero for the precision task in free air or rendered a contact at the target position during the dynamic task.

Table 4.1 shows the controller gains used for the different modes. The low impedance setting was chosen such that a resonance frequency of 4.5 Hz was achieved ($k = 10$ N m/rad, $b = 0.01$ N m s/rad). The high impedance setting corresponded to the actuator's highest stable impedance setting ($k = 100$ N m/rad, $b = 0.8$ N m s/rad). In the adaptive setting, the control law mapped the handle velocity $\dot{x}_m$ to the tool device impedance. The mapping law was such that the lowest impedance setting corresponded to the impedance of mode L, and the highest impedance setting corresponded to the impedance of mode H.

The velocity ranges for the adaptive impedance variation for distinguishing between precision task and dynamic task were based on our previous experiments on teleoperated hammering for the dynamic task [71] and were refined in the pilot phase to an upper velocity of a precision task of $\dot{x}_{m,min} = 1$ rad/s, and a lower velocity of a dynamic task of $\dot{x}_{m,max} = 6$ rad/s. An exponential transition was chosen between these two points in order to map the relatively small velocity range (1 rad/s to 6 rad/s) to the high actuator stiffness range (10 N m/rad to 100 N m/rad). These constraints resulted in the following equations for the control law:

$$k(\dot{x}_m) = \min\left(k_{max},\quad (k_{max} - k_{min}) \exp\left(-a \frac{|\dot{x}_m| - \dot{x}_{m,min}}{\dot{x}_{m,max} - \dot{x}_{m,min}}\right) + k_{min}\right), \qquad (4.1)$$

Contr.	Parameter			
	C_m = - C_4	C_1	C_2	C_{Z_s}
H	$0.8 + \frac{10}{s}$	1	1	$k = 100\,\mathrm{N\,m/rad}$, $b = 0.8\,\mathrm{N\,m\,s/rad}$
L	$0.8 + \frac{10}{s}$	1	1	$k = 10\,\mathrm{N\,m/rad}$, $b = 0.01\,\mathrm{N\,m\,s/rad}$
A	$0.8 + \frac{10}{s}$	1	1	$k = f(\dot{x}_m)$, $b = f(\dot{x}_m)$

Table 4.1: Controller gains of the system shown in Fig. 4.10

$$b(\dot{x}_m) = \min\left(0.8, \quad 2\,D(\dot{x}_m)\,\sqrt{km}\right), \tag{4.2}$$

with

$$D(\dot{x}_m) = (D_{max} - D_{min}) \exp\left(-a\frac{|\dot{x}_m| - \dot{x}_{m,min}}{\dot{x}_{m,max} - \dot{x}_{m,min}}\right) + D_{min}, \tag{4.3}$$

and $k_{max} = 100\,\mathrm{N\,m/rad}$, $k_{min} = 10\,\mathrm{N\,m/rad}$, $D_{max} = 0.7$, $D_{min} = 0.01$, $a = 6$, $m = 0.0125\,\mathrm{kg\,m^2}$. Before being passed to the impedance variation control law, the velocity signal $\dot{x}_m$ was filtered with a least-squares low-pass filter of order 80, pass frequency of 0.2 Hz, and stop frequency of 2 Hz. The filter introduced a 80 ms delay to a velocity step change. This was done to prevent that the impedance was lowered too quickly during precision tasks, and to prevent that the impedance returned to a high value before the impact during the dynamic task.

Figure 4.11 shows the magnitude over frequency of the resulting transfer function at the different settings obtained through system identification measurements. As shown, the adaptive setting follows the "slow-stiff/fast-soft" principle: the curve corresponding to the adaptive setting is close to that of the high impedance setting at low frequencies and close to that of the low impedance setting at high frequencies. There is also a narrow region with high gain showing the resonance, although at a higher frequency of approximately 6.5 Hz than the low impedance resonance (4.5 Hz).

4.2.5. Conditions

Six different conditions were compared in the experiment:

PR Precision task reference condition: The participants performed the precision task while the VIA was set to the permanently high impedance setting.

PC Precision task counter-reference condition: The participants performed the precision task while the VIA was set to the permanently low impedance setting.

PA Precision task adaptive condition: The participants performed the precision task while the VIA was set to the self-adapting impedance setting.

DR Dynamic task reference condition: The participants performed the dynamic task while the VIA was set to the permanently low impedance setting.

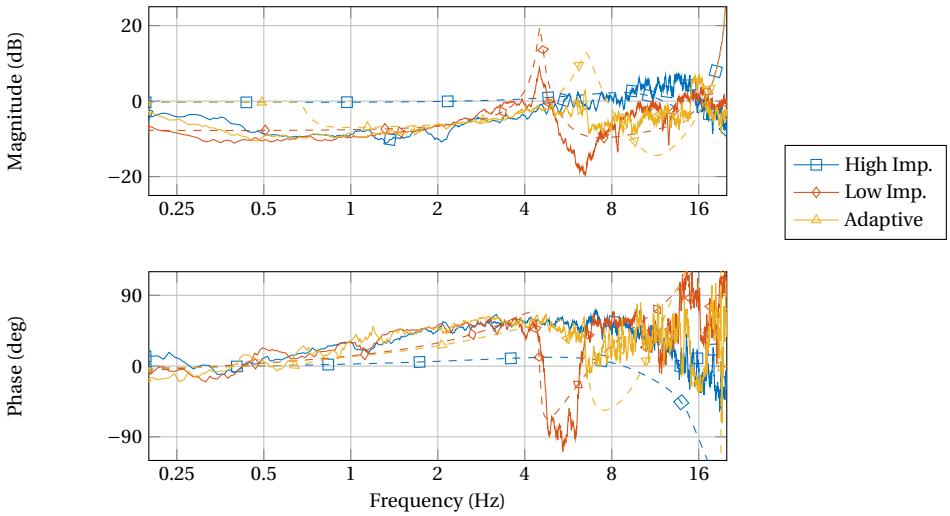

Figure 4.11: Bode plots of the transmitted impedance at the different stiffness settings. The dashed lines show the results as expected from the analytical solution of the system behavior. The continuous lines show the measured results.

DC Dynamic task counter-reference condition: The participants performed the dynamic task while the VIA was set to the permanently high impedance setting.

DA Dynamic task adaptive condition: The participants performed the dynamic task while the VIA was set to the self-adapting impedance setting.

Additionally, participants were given the opportunity to familiarize with the device in permanently high impedance (FH condition), low impedance (FL condition), and self-adapting impedance setting (FA condition) before starting the measurements. No specific objective was given to the participants for the familiarization.

4.2.6. Participants

The experiment was performed by 24 participants (16 male, 8 female, age 17 - 64 median 23.5) grouped in four groups of six participants each. The participants were students and researchers with a higher-education background. None of the participants had prior experience with the experiment. The experiment had been approved by the human research ethics committee of TU Delft, and all participants gave written informed consent before participation.

The participants watched a 3 min instruction video before the experiment explaining the goal and giving instructions [102]. In previous experiments, the instructions included extensive explanations about an elastic tool's resonance and how to exploit it to achieve higher output velocities [71]. In this experiment, this kind of explanation was left out on purpose. The motivation was to evaluate whether the participants could reproduce the results of the previous experiments with even less knowledge about the tool device. The target instructed to the participants was to reach a travel time of less than 300 ms travel

time for the precision task and to reach an output velocity of more than 10 rad/s for the dynamic task (cf. section 4.2.9). The result per trial was displayed to the participants after each trial (cf. section 4.2.3).

4.2.7. Experiment Procedure

Fig. 4.12 shows the experiment procedure divided into four phases: I. familiarization, II. training trials, III. reference measurement, and IV. task switch test. The familiarization phase gave the participants time to familiarize with the experiment device and with the dynamics of the actuator in high impedance (FH), low impedance (FL), and adaptive (FA) settings. The training trials and the reference measurement phases were identical except for the target positions (see below), but only the reference measurement was taken into account for the analysis. Training trials and reference measurement consisted of a series of six blocks with twenty trials per block. The target positions changed between the trials, such that every second trial was at the same distance of 0.3 rad of the previous trial, either forward or backward. In contrast, the other trials were at varying distance compared to the previous trial. This was done for three reasons:

1. the target positions should be spread over the full range of motion in order to compensate for a possible influence of the working point on the outcome (the positions were spread equally from –0.1789 rad to 0.5 rad with 0 rad corresponding to the vertical handle position, positive angles forward; one position at –0.42 rad was added, which resulted in a pose of the participants with the hand very close to the own body to have a data point with an adverse pose);

2. the next target position should not be easily anticipated in order to avoid a possible influence of repetitive motions on the outcome;

3. the travel distance of some measurements should be equal for the precision task to make the measurements comparable.

The last two reasons do not apply to the dynamic task, but the same target positions were used for both tasks for simplicity. However, this means that only ten trials per block were effectively used in the analysis of the precision task (those with a difference of ±0.3 rad to the previous target position), whereas twenty trials per block were used in the analysis of the dynamic task.

The order of positions was the same for all groups and all trial blocks, but different between the phases II and III to prevent prior knowledge of the next target position during phase III. The order of condition blocks during phases II and III was assigned to the groups according to the Latin square method as shown in Fig. 4.13. The goal of phase IV, the task switch test, was to test how easily the participants could switch from one task to another with the adaptive impedance variation of the tool device. According to hypothesis H2, we expected phase III and phase IV to have the same outcome. For phase IV, ten blocks of the PA and DA condition (precision or dynamic task with adaptive stiffness) were performed in an order randomized per group, where each block consisted of two trials with the first trial at a varying distance from the zero position and the second trial at ±0.3 rad of the previous position.

I. Familiarization:

Condition:	FH	FL	FA
Time:	2 min	2 min	2 min

II. Trainig Trials:

Condition:	1	2	3	4	5	6
Trials:	20	20	20	20	20	20

III. Reference Measurement:

Condition:	1	2	3	4	5	6
Trials:	20	20	20	20	20	20

IV. Task Switch Test:

Condition:	PA	DA
Trials:	2	2

10 x in randomized order

Figure 4.12: Order of experiment conditions grouped by objective. The order was shown for participants of group 1. The order of conditions during phase II was altered according to the Latin square method (cf. figure 4.13). The order of conditions during phases III and IV was changed for groups 3 and 4 by swapping PA and DA.

Before every block, the participants had to bring the handle to the zero position to start. Before the first trial of every block, the participants had to press a key on a keyboard to indicate that they were ready. Thus, the participants could rest between blocks if they wanted and mentally prepare for the next task. The type of task of a block was always announced on the screen before the participants pressed the key to indicate their readiness. This was particularly important for phase IV, where each block consisted only of two trials, but the type of task was selected per block in a pattern not disclosed to the participants.

4.2.8. Experiment Task

In both tasks, the instructions for a new block of trials were shown to the participants until they indicated that they were ready by pressing a keyboard key. For the precision task, the target cursor then appeared every 2 s at a new position, and the participants had to follow the cursor to its new position. For the dynamic task, the participants moved to a new starting position before every trial, located close below the new target position, while the target box was still invisible to the participants. Once the participants had reached the starting position, the target appeared, and the participants could perform one hammering strike. The starting position was on purpose close to the target position, to ensure that the participants performed the hammering motion as a backward-forward strike instead of trying to hit the target in a straight forward motion. A hammering trial was over when the tool device had reached the target. This was indicated to the participants by changing the color of the target from green to orange. In both tasks, data were collected during the trial, and the result was shown on the screen to the participants immediately after each trial.

Group \ Trial Block	1	2	3	4	5	6
A	PA	PR	PC	DC	DR	DA
B	DR	PC	PA	DA	DC	PR
C	DC	PA	DR	PR	DA	PC
D	DA	DR	DC	PC	PR	PA
E	PR	DC	DA	PA	PC	DR
F	PC	DA	PR	DR	PA	DC

Figure 4.13: Latin square showing the order of conditions in the trial blocks (1-6) per participant group (A-F): PA = position–adaptive, PR = position–reference (high impedance), PC = position–counter-reference (low impedance), DA = dynamic–adaptive, DR = dynamic–reference (low impedance), DC = dynamic–counter-reference (high impedance).

Precision Task	Dynamic Task
Performance Measures	
Travel time (s) ★	Maximum output velocity (rad/s) ★
ITAE (rad s^2) ♦	Gain (-)
Analytic Measures	
—	Excitation Frequency (Hz)
	Actual Stiffness (N m/rad)
	Actual Damping (N m s/rad)

★ Result shown to participants immediately after every trial
♦ Integral of time-weighted absolute error

Table 4.2: Dependent Measures of the experiment for the precision task and the dynamic task

4.2.9. Dependent Measures

All relevant data were captured at 1 kHz directly from the experiment apparatus' built-in sensors and logged for later analysis. Task performance was calculated on-the-fly in the control system and communicated via UDP to the user interface for display. Table 4.2 lists the dependent measures used in the analysis of the experiment outcome. Travel time and integral of time-weighted absolute error (ITAE) were chosen as metrics for the precision task, similar to the settling time and ITAE known from control theory as indicators for the step-response positioning performance of a controller through a plant. For this, the travel time was defined as settling time minus dead time, calculated from the moment that the participants start moving to the moment that the tool position settled at the target position. This calculation method was chosen instead of the classical settling time to compensate for possible effects of different reaction times of the participants. The threshold for moving was defined as 0.03 rad from the handle position when the target

position jumped to its new value. Settling was defined as maintaining an absolute error from the target position of less than 0.03 rad for a duration of 0.5 s. The travel time was calculated during each trial and displayed to the participants at the end of each trial.

The ITAE is an indicator of the controller performance favoring fast initial response even at the cost of slightly overshooting. It was added as pilot participants often could not reliably judge whether they had already reached the target position corridor, resulting in very long calculated travel times even for negligible residual errors just above the settling threshold. The ITAE metric corresponds more to an operator's intuition where a small remaining error or small oscillations around the target position are considered less critical than a slow initial response. It was calculated in the post-processing analysis as

$$ITAE = \int_0^T t\,|x - x_0|\,dt \tag{4.4}$$

with t the time variable, T the travel time, x the actual tool position, and x_0 the target position [103].

For the dynamic task, the maximum output velocity was calculated and displayed to the participants as the peak forward velocity of the tool device before impact. Furthermore, the velocity gain was calculated in the post-processing analysis as the ratio of maximum output velocity over maximum handle velocity (as done in [71]). The maximum output velocity measures how effective the strike was, as a higher velocity means more energy on impact, whereas the gain measures how efficient the strike was, as a higher gain means that more energy from the backward motion could be recovered into the forward motion through the elastic actuator.

The previously mentioned four measures (travel time, ITAE, maximum output velocity, and gain) were used to asses the performance of the participants in the task and test the experiment hypotheses. Three more measures were considered for analytic purposes: excitation frequency, actual stiffness, and actual damping. The estimated excitation frequency on the handle device during the dynamic task was used to analyze whether participants that obtained significantly higher gains with the low impedance than the high impedance setting moved differently than those who did not. As explained in chapter 2, the excitation frequency should be close to the resonance frequency of the tool device. However, in this experiment, this was not explained to the participants. Thus, the participants could either exploit the resonance of the tool device to achieve a significant output velocity gain or not. The hypothesis was that participants achieving a significantly higher gain with the soft impedance setting than the high impedance setting correlates with them using a different excitation frequency.[1] The same method as in chapter 2 was used for estimating the excitation frequency: the time difference between handle velocity minimum and maximum was assumed to equal half the period of the excitation frequency.

Actual stiffness and damping were used to assess how the self-adapting impedance variation algorithm changed the tool device impedance during the tasks. The actual impedance should be different between participants performing the precision task and

[1] Whether the participants that achieved a significantly higher gain consciously used a different excitation frequency is not part of this hypothesis.

the dynamic task with the adaptive setting, otherwise the algorithm would most likely not have any benefit compared to a constant impedance setting.

4.2.10. Statistical Evaluation

As explained in section 4.2.7, 10 values were obtained per trial block per participant for the precision task, and 20 values were obtained per trial block per participant for the dynamic task. Wilcoxon's signed-rank test [54] was used for testing the experiment hypotheses. It allows for pairwise testing of related samples for whether the difference of the values of one sample and the other are significantly different from zero without assuming a normal distribution of the data. The rank-biserial correlation coefficient r for Wilcoxon's signed-rank test was calculated according to Kerby [104] to indicate the effect size. Assuming that samples are related compensates for per-participant effects on the results. The data could not be assumed to be normally distributed as it was always more difficult to achieve "good" performance (low travel time, low ITAE, high output velocity, or high gain) than "bad" performance.

Comparing the results of low impedance setting and high impedance setting served to verify the basic assumptions B1 and B2. Further, the following pairs of settings were compared: adaptive impedance – high impedance, and adaptive impedance – low impedance. The test was applied to the precision task and the dynamic task results, corresponding to the four hypotheses H1.1-H1.4.

H1.1 and H1.4 (no significant difference in performance between adaptive setting and reference setting results) are supported if the null-hypothesis of Wilcoxon's signed-rank test could not be rejected at the 5 %-level. H1.2 and H1.3 (significantly better performance of adaptive setting results than counter-reference setting results) are supported if the null-hypothesis of Wilcoxon's signed-rank test could be rejected at a level better than 5 %. The same tests were performed for the task switch test phase results to verify hypothesis 2 stating that hypotheses H1.1 to H1.4 (then referred to as H2.1 to H2.4) also hold for quick succession of precision and dynamic tasks. These results are labeled with "Adaptive*" or "A*" for short in the result tables and figures.

The statistical tests were applied once on the per-participant medians per condition and once on per-participant outstanding trials per condition. The per-participant 10^{th} percentiles per condition were considered a measure for outstanding trials of the precision task (lower is better for travel time and ITAE measures). The per-participant 90^{th} percentiles per condition were considered a measure for outstanding trials of the dynamic task (higher is better for maximum output velocity and gain measures). With 10 trials, the 10^{th} or 90^{th} percentile corresponds to the middle between the best and second trials. With 20 trials, the 10^{th} or 90^{th} percentile corresponds to the middle between the second and third trials. Using the 10^{th} or 90^{th} percentiles instead of the minima or maxima adds some basic robustness to the evaluation towards outliers. Comparing the outstanding trials of the participants in addition to the median gives an impression of how much effort was required from the participants to obtain a certain result with a specific impedance setting (cf. the discussion section 4.4).

For the analysis of the correlation between excitation frequency and gain, the participants were assigned to two groups (A or B), based on the gains achieved during the dynamic task with the high impedance and the low impedance settings. Group A con-

tained those participants who achieved significantly higher gains with the low impedance setting than the high impedance setting according to the Wilcoxon signed-rank test (significance level $\alpha = 5\,\%$). Group B contained the other participants. Wilcoxon's rank-sum test [54] (equivalent in terms of outcome to the Mann-Whitney U test [105]) was then used to test whether the per-participant median gains of the participants of group A were significantly different than those of group B. It allows testing of independent samples for whether the values of one sample are significantly larger than those of the other sample without assuming normal distribution of the data. The rank-biserial correlation coefficient r for the Wilcoxon rank-sum test was calculated according to Wendt [106] to indicate the effect size.

A linear fit was performed over the per-participant median gains and excitation frequencies to give a rough approximation of the effect of the excitation frequency on the achieved gain depending on the impedance setting.[2]

The average of the actual stiffness and damping were calculated for every trial over the period of activity to analyse the effect of the self-adapting impedance variation algorithm. The travel period as used to calculate the travel time was considered as the period of activity for the precision task. The period from the handle velocity crossing the threshold of –0.1 rad/s to impact was considered as the period of activity for the dynamic task. Wilcoxon's rank-sum test was then used to test whether the median over all trials of the adaptive setting were significantly different between the precision task and the dynamic task. The rank-biserial correlation coefficient r for the Wilcoxon rank-sum test was calculated according to Wendt [106] to indicate the effect size.

[2] This can only be a rough approximation as the frequency-gain relationship of the tool device is not linear (cf. figure 4.11).

4.3. Experiment 3: Results

The experiment measurement data are available in the supplementary material [107].

4.3.1. Precision task

Fig. 4.14 shows the plots of some position error measurements during the reference measurement phase and the task switch test phase. It gives a qualitative impression of the system behavior with the three settings of the reference measurement and the task switch test (Adaptive*). As shown in the plots for the low impedance setting, in many cases, there are more oscillations, and it takes more time to settle below the threshold of 0.03 rad compared to the high and adaptive impedance settings.

Fig. 4.15 to 4.18 show the per-participant median and 10^{th} percentile results of the measured travel time and ITAE with 95 % confidence intervals (lower is better). The expected outcome according to the experiment hypotheses was that the lowest value of travel time and ITAE would be achieved with the high impedance setting (blue), the highest with the low impedance (red) and that the results with the adaptive (yellow) and adaptive* (purple) settings would not be significantly different from the results with the high impedance settings.

The grouped statistical comparison over all participants of travel time medians (cf. table 4.3) showed a significant difference at the 0.1 %-level between low and high impedance settings (supporting hypothesis B1[3]). It showed no significant difference at the 20 %-level between adaptive and high impedance settings, and adaptive* and high impedance settings, but a significant difference at the 0.1 %-level between adaptive and low impedance settings and adaptive* and low impedance settings (supporting hypotheses H1.1, H1.2, H2.1, and H2.2[4]).

The grouped statistical comparison over all participants of ITAE medians (cf. table 4.4) showed a significant difference at the 0.5 %-level between low and high impedance settings (supporting hypothesis B1). It showed no significant difference at the 20 %-level between adaptive and high impedance settings, and adaptive* and high impedance settings, but a significant difference at the 0.5 %-level between adaptive and low impedance settings and adaptive* and low impedance settings (supporting hypotheses H1.1, H1.2, H2.1, and H2.2).

The grouped statistical comparison over all participants of travel time 10^{th} percentiles (cf. table 4.5) showed no significant difference at the 5 %-level between low and high impedance setting (contradicting hypothesis B1). It showed no significant difference at the 20 %-level between adaptive and high impedance settings, and the 10 %-level between adaptive and low impedance settings, but a significant difference at the 0.1 %-level between the adaptive* and high impedance settings and adaptive* and low impedance settings (supporting hypotheses H1.2 and H2.2, but contradicting hypotheses H1.1 and H2.1).

[3] Hypothesis B1: Better performance is achieved in precision tasks with a permanently high impedance setting than a permanently low impedance setting.

[4] Hypothesis H1.1/H2.1: The same performance is achieved in precision tasks with the self-adapting impedance setting and the permanently high impedance setting.
Hypothesis H1.2/H2.2: Better performance is achieved in precision tasks with the self-adapting impedance setting than with the permanently low impedance setting.

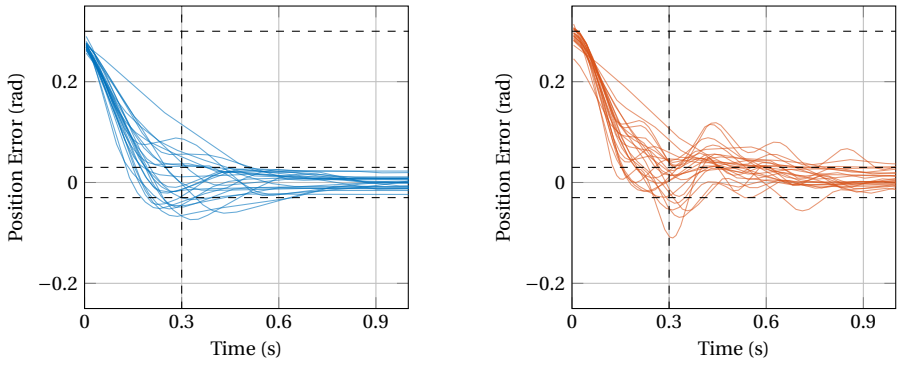

(a) High Impedance

(b) Low Impedance

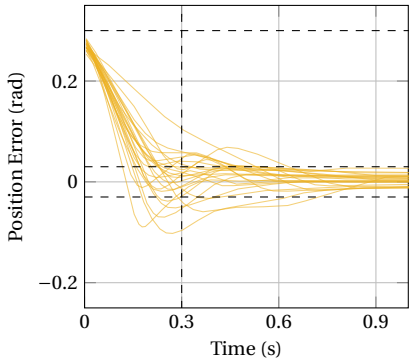

(c) Adaptive

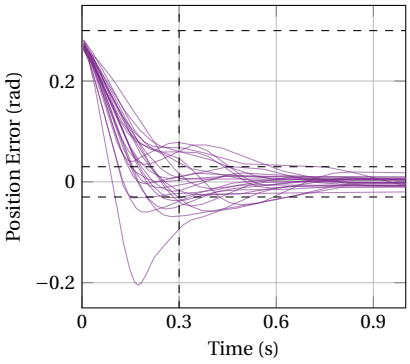

(d) Adaptive*

Figure 4.14: Precision task position error plot of some measurements giving a qualitative impression of the system behavior during the reference measurement phase for trials in high, low, and adaptive settings, and of the task switch test phase for trials in the adaptive* setting. The dashed lines show the experiment criteria: the initial absolute error was 0.3 rad, and the goal communicated to the participants was to achieve a travel time of less than 0.3 s. The criterion for the end of the travel time was to keep the absolute error under 0.03 rad for at least 0.5 s.

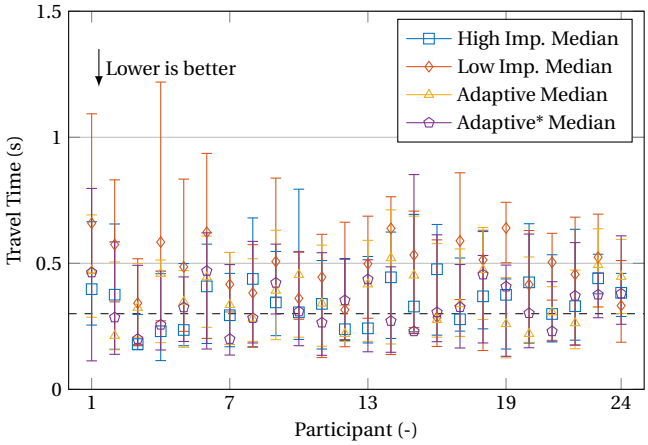

Figure 4.15: Per-participant median results of travel time measured during the precision task with 95 % confidence intervals (lower is better). It was communicated to the participants that they should try to achieve a travel time of less than 0.3 s. This is indicated by the dashed line. The expected outcome according to the experiment hypotheses was that the shortest travel times would be achieved with the high impedance setting (blue), the longest with the low impedance (red) and that the results with the adaptive (yellow) and adaptive* (purple) settings would not be significantly different from the results with the high impedance settings.

Table 4.3: Grouped results over all participants of pairwise comparison of per-participant median travel times measured during the precision task, given as effect size of median difference and 95 % confidence interval (negative difference indicates better performance of the first setting compared to the second, $n = 24$, p-values refer to Wilcoxon's signed-rank test results). The last column indicates which experiment hypothesis was checked by the statistical test and whether the outcome supports (green) or contradicts (red) the hypothesis (significance level $\alpha = 5\,\%$).

Impedance Setting Pair		Median Diff. (ms)	$CI_{95\%}$ (ms)	p	r	Hyp.
Low – High		162	[106, 205]	< 0.001	0.87	B1
Adaptive – High		50	[2, 77]	0.29	0.25	H1.1
Adaptive – Low		-110	[-178, -81]	< 0.001	-0.86	H1.2
Adaptive* – High		12	[-75, 48]	0.56	-0.14	H2.1
Adaptive* – Low		-151	[-217, -85]	< 0.001	-0.96	H2.2

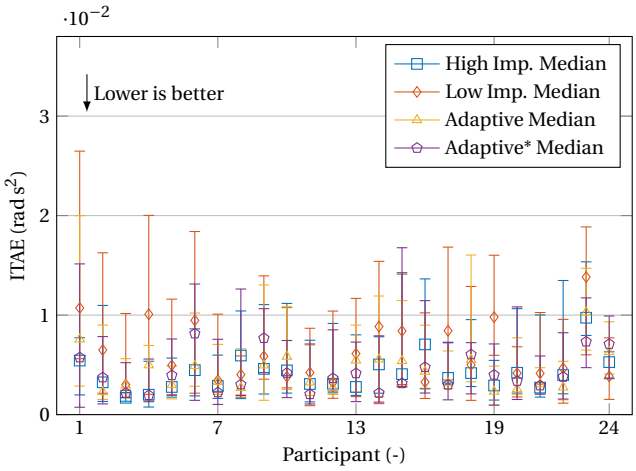

Figure 4.16: Per-participant median results of ITAE measured during the precision task with 95 % confidence intervals (lower is better). The expected outcome according to the experiment hypotheses was that the lowest ITAE would be achieved with the high impedance setting (blue), the highest with the low impedance (red) and that the results with the adaptive (yellow) and adaptive* (purple) settings would not be significantly different from the results with the high impedance settings.

Table 4.4: Grouped results over all participants of pairwise comparison of per-participant median ITAE measured during the precision task, given as effect size of median difference and 95 % confidence interval (negative difference indicates better performance of the first setting compared to the second, $n = 24$, p-values refer to Wilcoxon's signed-rank test results). The last column indicates which experiment hypothesis was checked by the statistical test and whether the outcome supports (green) or contradicts (red) the hypothesis (significance level $\alpha = 5\,\%$).

Impedance Setting Pair	Median Diff. (mrad s^2)	$CI_{95\%}$ (mrad s^2)	p	r	Hyp.
Low – High	1.4	[0.68, 3.8]	0.0016	0.71	B1
Adaptive – High	0.39	[-0.38, 1.0]	0.34	0.23	H1.1
Adaptive – Low	-1.5	[-3.1, -0.67]	0.0011	-0.73	H1.2
Adaptive* – High	0.076	[-0.69, 0.54]	0.88	0.040	H2.1
Adaptive* – Low	-1.2	[-2.8, -0.85]	0.0043	-0.65	H2.2

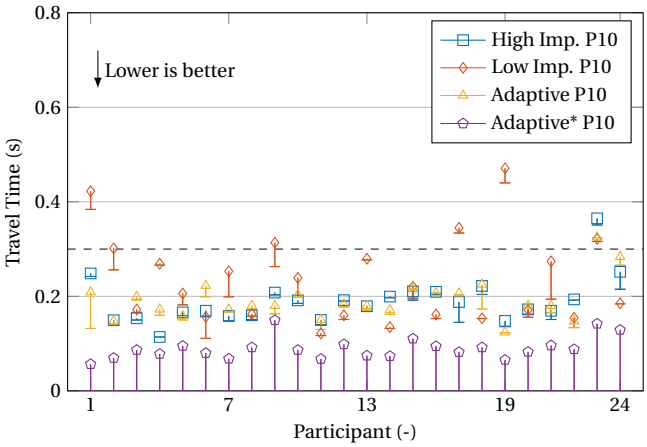

Figure 4.17: Per-participant 10^{th} percentile results of travel time measured during the precision task with 95 % confidence intervals (lower is better). It was communicated to the participants that they should try to achieve a travel time of less than 0.3 s. This is indicated by the dashed line. The expected outcome according to the experiment hypotheses was that the shortest travel times would be achieved with the high impedance setting (blue), the longest with the low impedance (red) and that the results with the adaptive (yellow) and adaptive* (purple) settings would not be significantly different from the results with the high impedance settings.

Table 4.5: Grouped results over all participants of pairwise comparison of per-participant 10^{th} percentile travel times measured during the precision task, given as effect size of median difference and 95 % confidence interval (negative difference indicates better performance of the first setting compared to the second, $n = 24$, p-values refer to Wilcoxon's signed-rank test results). The last column indicates which experiment hypothesis was checked by the statistical test and whether the outcome supports (green) or contradicts (red) the hypothesis (significance level $\alpha = 5\,\%$).

Impedance Setting Pair	Median Diff. (ms)	$CI_{95\%}$ (ms)	p	r	Hyp.
Low – High	14	[-29, 101]	0.089	0.40	B1
Adaptive – High	2	[-8, 12]	0.58	0.13	H1.1
Adaptive – Low	-5	[-94, 24]	0.14	-0.34	H1.2
Adaptive* – High	-92	[-106, -83]	< 0.001	-1	H2.1
Adaptive* – Low	-111	[-180, -71]	< 0.001	-1	H2.2

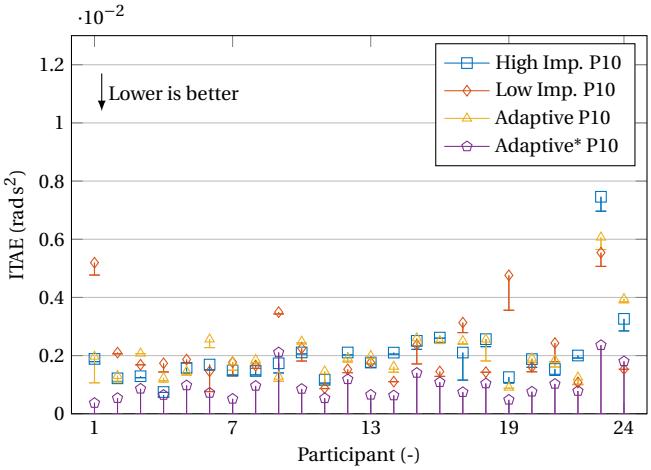

Figure 4.18: Per-participant 10^{th} percentile results of ITAE measured during the precision task with 95 % confidence intervals (lower is better). The expected outcome according to the experiment hypotheses was that the shortest travel times would be achieved with the high impedance setting (blue), the longest with the low impedance (red) and that the results with the adaptive (yellow) and adaptive* (purple) settings would not be significantly different from the results with the high impedance settings.

Table 4.6: Grouped results of pairwise comparison of per-participant 10^{th} percentile ITAE measured during the precision task, given as effect size of median difference and 95 % confidence intervals (negative difference indicates better performance of the first setting compared to the second, $n = 24$, p-values refer to Wilcoxon's signed-rank test results). The last column indicates which experiment hypothesis was checked by the statistical test and whether the outcome supports (green) or contradicts (red) the hypothesis (significance level $\alpha = 5\,\%$).

Impedance Setting Pair		Median Diff. (mrad s^2)	$CI_{95\%}$ (mrad s^2)	p	r	Hyp.
Low – High		0.071	[-0.29, 0.39]	0.81	0.060	B1
Adaptive – High		0.091	[-0.11, 0.31]	0.33	0.23	H1.1
Adaptive – Low		0.23	[-0.41, 0.39]	0.73	0.087	H1.2
Adaptive* – High		-1.0	[-1.3, -0.68]	< 0.001	-0.99	H2.1
Adaptive* – Low		-0.93	[-1.4, -0.70]	< 0.001	-0.99	H2.2

The grouped statistical comparison over all participants of ITAE 10^{th} percentiles (cf. table 4.6) showed no significant difference at the 20 %-level between low and high impedance settings (contradicting hypothesis B1). It showed no significant difference at the 20 %-level between adaptive and high impedance settings, and adaptive and low impedance settings (supporting hypothesis H1.1, but contradicting hypothesis H1.2), but a significant difference at the 0.1 %-level between adaptive* and high impedance settings and adaptive* and low impedance settings (supporting hypotheses H1.1 and H2.2, but contradicting hypotheses H1.2 and H2.1).

4.3.2. Dynamic task

Fig. 4.19 shows the plots of some handle and tool velocity measurements during the reference measurement phase and the task switch test phase. It gives a qualitative impression of the system behavior with the three settings of the reference measurement and the task switch test (Adaptive*). As shown in the plots for the low impedance and adaptive settings, the tool velocity on impact at time zero is often considerably higher than the handle velocity. In contrast, it is very close to the handle velocity for the stiff setting.

Fig. 4.20 to 4.23 show the per-participant median and 90^{th} percentiles results of maximum output velocities and gains with 95 % confidence intervals (higher is better). The expected outcome according to the experiment hypotheses was that the highest maximum output velocity and gain would be achieved with the low impedance setting (red), the lowest with the high impedance (blue) and that the results with the adaptive (yellow) and adaptive* (purple) settings would not be significantly different from the results with the low impedance settings.

The grouped statistical comparison over all participants of maximum output velocity medians (cf. table 4.7) showed a significant difference at the 5 %-level between low and high impedance settings (supporting hypothesis B2[5]). It showed no significant difference at the 20 %-level between adaptive and high impedance settings, and adaptive* and high impedance settings, but a significant difference at the 5 %-level between adaptive and low impedance settings and the 1 %-level between adaptive* and low impedance settings (contradicting hypotheses H1.3, H1.4, H2.3, and H2.4).

The grouped statistical comparison over all participants of gain medians (cf. table 4.8) showed a significant difference at the 0.1 %-level between low and high impedance settings (supporting hypothesis B2). It showed no significant difference at the 10 %-level between adaptive and high impedance settings, but a significant difference at the 5 %-level between adaptive* and high impedance settings, at the 0.5 %-level between adaptive and low impedance settings, and at the 5 %-level between adaptive* and low impedance settings (supporting hypothesis H2.3, but contradicting hypotheses H1.3, H1.4, and H2.4[6]).

The grouped statistical comparison over all participants of maximum output velocity 90^{th} percentiles (cf. table 4.9) showed a significant difference at the 0.5 %-level between

[5] Hypothesis B2: Better performance is achieved in dynamic tasks with a permanently low impedance setting than a permanently high impedance setting.

[6] Hypothesis H1.3/H2.3: Better performance is achieved in dynamic tasks with the self-adapting impedance setting than with the permanently high impedance setting.
Hypothesis H1.4/H2.4: The same performance is achieved in dynamic tasks with the self-adapting impedance setting and the permanently low impedance setting.

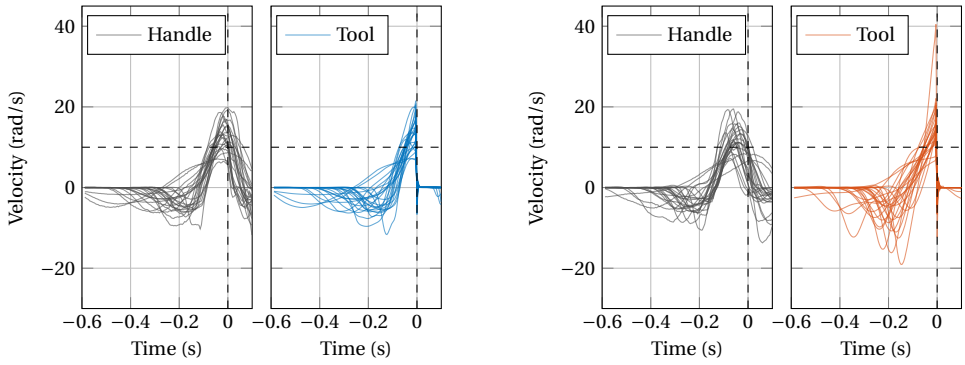

(a) High Impedance

(b) Low Impedance

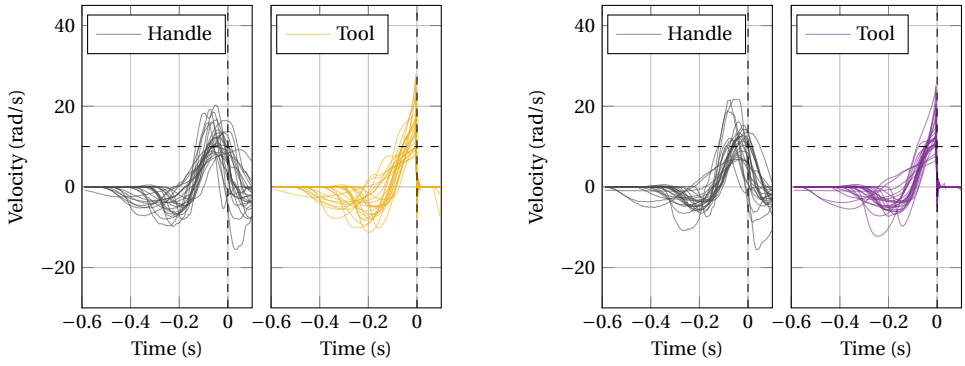

(c) Adaptive

(d) Adaptive*

Figure 4.19: Dynamic task handle and tool velocity plots of some measurements giving a qualitative impression of the system behavior during the reference measurement phase for trials in high, low, and adaptive impedance setting and the task switch test for trials in the adaptive* setting. The dashed lines show the experiment criteria: the goal communicated to the participants was to achieve a maximum output velocity of at least 10 rad/s. The time axis was adjusted such that the time 0 s corresponded to the impact (the blue circle reaching the green box in Fig. 4.9.

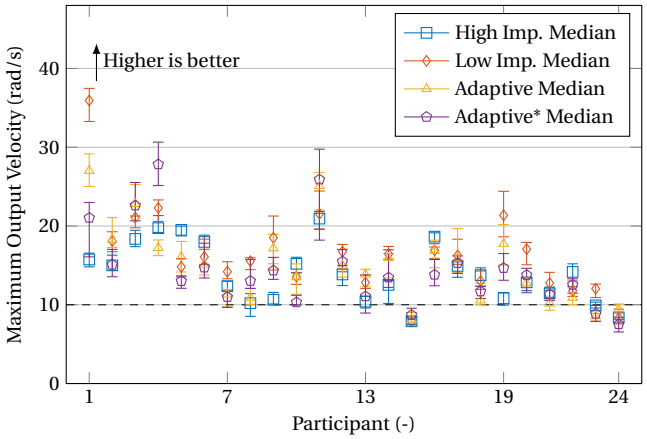

Figure 4.20: Per-participant median results of maximum output velocity measured during the dynamic task with 95 % confidence intervals (higher is better). It was communicated to the participants that they should try to achieve a maximum output velocity of more than 10 rad/s. This is indicated by the dashed line. The expected outcome according to the experiment hypotheses was that the highest maximum output velocity would be achieved with the low impedance setting (red), the lowest with the low impedance (blue) and that the results with the adaptive (yellow) and adaptive* (purple) settings would not be significantly different from the results with the low impedance settings.

Table 4.7: Grouped results over all participants of pairwise comparison of per-participant median maximum output velocities measured during the dynamic task, given as effect size of median difference and 95 % confidence interval (positive difference indicates better performance of the first setting compared to the second, $n = 24$, p-values refer to Wilcoxon's signed-rank test results). The last column indicates which experiment hypothesis was checked by the statistical test and whether the outcome supports (green) or contradicts (red) the hypothesis (significance level $\alpha = 5\,\%$).

Impedance Setting Pair		Median Diff. (rad/s)	$CI_{95\%}$ (rad/s)	p	r	Hyp.
Low – High		2.0	[-0.017, 2.9]	0.013	0.57	B2
Adaptive – High		0.48	[-1.4, 3.3]	0.34	0.23	1.3
Adaptive – Low		-0.92	[-2.6, -0.074]	0.019	-0.54	1.4
Adaptive* – High		0.51	[-1.1, 1.6]	0.55	0.15	2.3
Adaptive* – Low		-1.8	[-3.1, -1.3]	0.0059	-0.63	2.4

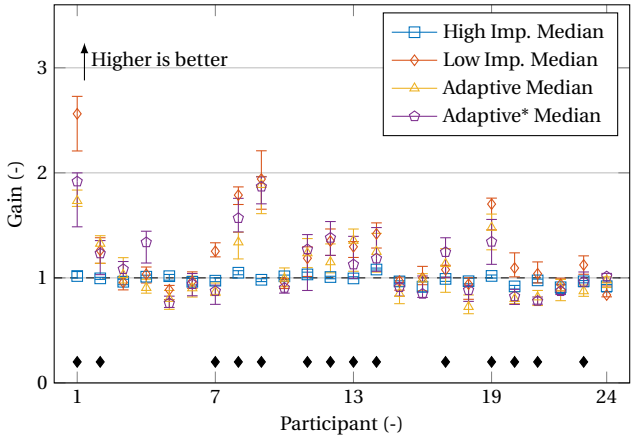

Figure 4.21: Per-participant median results of gain measured during the dynamic task with 95 % confidence intervals (higher is better). The dashed line indicates a gain of 1, which corresponds to the gain of a rigid actuator. The expected outcome according to the experiment hypotheses was that the highest gain would be achieved with the low impedance setting (red), the lowest with the low impedance (blue) and that the results with the adaptive (yellow) and adaptive* (purple) settings would not be significantly different from the results with the low impedance settings. Diamonds indicate participants that achieved significantly higher median gains with the low impedance than the high impedance setting and were considered for the separate analysis (cf. tables 4.11 and 4.11)

Table 4.8: Grouped results over all participants of pairwise comparison of per-participant median gains measured during the dynamic task, given as effect size of median difference and 95 % confidence interval (positive difference indicates better performance of the first setting compared to the second, $n = 24$, p-values refer to Wilcoxon's signed-rank test results). The last column indicates which experiment hypothesis was checked by the statistical test and whether the outcome supports (green) or contradicts (red) the hypothesis (significance level $\alpha = 5\,\%$).

Impedance Setting Pair	Median Diff. (-)	$CI_{95\%}$ (-)	p	r	Hyp.
Low – High	0.12	[0.024, 0.28]	< 0.001	0.75	B2
Adaptive – High	0.061	[-0.093, 0.17]	0.17	0.32	H1.3
Adaptive – Low	-0.10	[-0.22, -0.014]	0.0035	-0.66	H1.4
Adaptive* – High	0.098	[-0.054, 0.24]	0.049	0.46	H2.3
Adaptive* – Low	-0.070	[-0.17, -0.029]	0.027	-0.51	H2.4

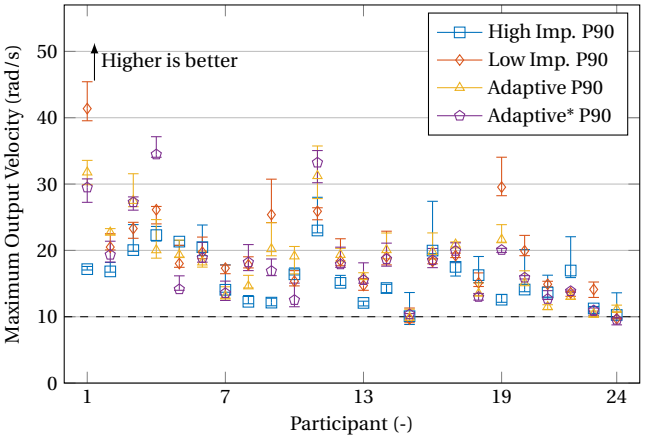

Figure 4.22: Per-participant 90^{th} percentile of maximum output velocity measured during the dynamic task with 95 % confidence intervals (higher is better). It was communicated to the participants that they should try to achieve a maximum output velocity of more than 10 rad/s. This is indicated by the dashed line. The expected outcome according to the experiment hypotheses was that the highest maximum output velocity would be achieved with the low impedance setting (red), the lowest with the low impedance (blue) and that the results with the adaptive (yellow) and adaptive* (purple) settings would not be significantly different from the results with the low impedance settings.

Table 4.9: Grouped results over all participants of pairwise comparison of per-participant 90^{th} percentile maximum output velocities measured during the dynamic task, given as effect size of median difference and 95 % confidence interval (positive difference indicates better performance of the first setting compared to the second, $n = 24$, p-values refer to Wilcoxon's signed-rank test results). The last column indicates which experiment hypothesis was checked by the statistical test and whether the outcome supports (green) or contradicts (red) the hypothesis (significance level $\alpha = 5\,\%$).

Impedance Setting Pair		Median Diff. (rad/s)	$CI_{95\%}$ (rad/s)	p	r	Hyp.
Low – High		2.9	[-0.43, 3.7]	0.0039	0.65	B2
Adaptive – High		1.7	[-0.83, 4.2]	0.032	0.5	H1.3
Adaptive – Low		-0.18	[-3.4, 1.3]	0.28	-0.26	H1.4
Adaptive* – High		2.1	[-0.72, 4.4]	0.069	0.43	H2.3
Adaptive* – Low		-0.70	[-2.8, 0.25]	0.11	-0.38	H2.4

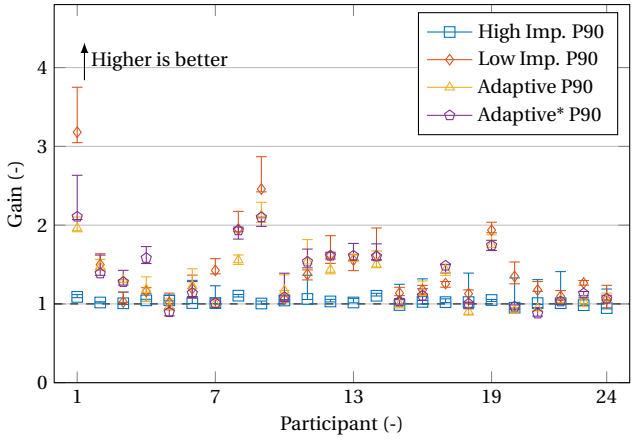

Figure 4.23: Per-participant 90^{th} percentile of gain measured during the dynamic task with 95 % confidence intervals (higher is better). The dashed line indicates a gain of 1, which corresponds to the gain of a rigid actuator. The expected outcome according to the experiment hypotheses was that the highest gain would be achieved with the low impedance setting (red), the lowest with the low impedance (blue) and that the results with the adaptive (yellow) and adaptive* (purple) settings would not be significantly different from the results with the low impedance settings.

Table 4.10: Grouped results over all participants of pairwise comparison of per-participant 90^{th} percentile gains measured during the dynamic task, given as effect size of median difference and 95 % confidence interval (positive difference indicates better performance of the first setting compared to the second, $n = 24$, p-values refer to Wilcoxon's signed-rank test results). The last column indicates which experiment hypothesis was checked by the statistical test and whether the outcome supports (green) or contradicts (red) the hypothesis (significance level $\alpha = 5\,\%$).

Impedance Setting Pair	Median Diff. (-)	$CI_{95\%}$ (-)	p	r	Hyp.
Low – High	0.26	[0.15, 0.48]	< 0.001	0.98	B2
Adaptive – High	0.18	[0.051, 0.41]	< 0.001	0.82	H1.3
Adaptive – Low	-0.082	[-0.23, -0.0045]	0.013	-0.57	H1.4
Adaptive* – High	0.21	[0.043, 0.50]	< 0.001	0.82	H2.3
Adaptive* – Low	-0.069	[-0.13, -0.0051]	0.069	-0.43	H2.4

low and high impedance settings (supporting hypothesis B2). It showed a significant difference at the 5 %-level between adaptive and high impedance setting, but no significant difference at the 5 %-level between adaptive and low impedance settings, at the 5 %-level between adaptive* and high impedance settings, and at the 10 %-level between adaptive* and low impedance settings (supporting hypotheses H1.3, H1.4 and H2.4, but contradicting hypothesis H2.3).

The grouped statistical comparison over all participants of gain 90^{th} percentiles (cf. table 4.10) showed a significant difference at the 0.1 %-level between low and high impedance settings (supporting hypothesis B2). It showed a significant difference at the 0.1 %-level between adaptive and high impedance settings, and at the 0.1 %-level between adaptive* and high impedance settings, a significant difference at the 5 %-level between adaptive and low impedance settings, but no significant difference at the 5 %-level between adaptive* and low impedance settings (supporting hypotheses H1.3, H2.3 and H2.4, but contradicting hypothesis H1.4).

The comparison between the participants that achieved significantly higher gains with the low impedance setting than the high impedance setting (group A, $n = 14$) and those who did not (group B, $n = 10$) shows significantly higher excitation frequencies in group A than in group B across all impedance settings (cf. table 4.11, significance level $\alpha = 5\,\%$).

Table 4.12 shows the results of the grouped statistical comparison over the group A participants of gain medians (cf. also table 4.8). It shows that the group of participants that achieved significantly higher gains with the low compared to the high impedance setting also achieved higher gains with the adaptive than the high impedance setting at the 1 %-level. However, they did not reach the same median gains with the adaptive as with the low impedance setting at the 5 %-level.

Figure 4.25 shows the per-participant median gains plotted over the per-participant median estimated excitation frequencies and the result of the linear regression performed per impedance setting. It shows that the effect of the frequency on the gain is the strongest with the low impedance setting (0.38/Hz) and close to zero with the high impedance setting (0.027/Hz). The effect of the frequency on the gain is approximately half as strong with the adaptive and adaptive* impedance settings (0.23/Hz and 0.22/Hz)compared to the low impedance setting.

4.3.3. Impedance Variation Comparison

Figure 4.26 shows the plots of some stiffness and damping measurements during the reference measurement phase. It gives a qualitative impression of the effect of the self-adapting impedance variation algorithm on the impedance during the precision and the dynamic task. As shown, the impedance drops less from its initial value (stiffness of 100 N m/rad, damping of 0.8 N m s/rad) during the precision task than during the dynamic task and for a shorter duration.

Tables 4.13 and 4.14 show the results of the statistical comparison on the average stiffness and damping. The values measured with the high and low impedance settings are given as reference, but were not part of the statistical evaluation. The measured average impedance was significantly lower at the 0.1 %-level during the dynamic task trials than during the precision task trials. The difference between the medians was of

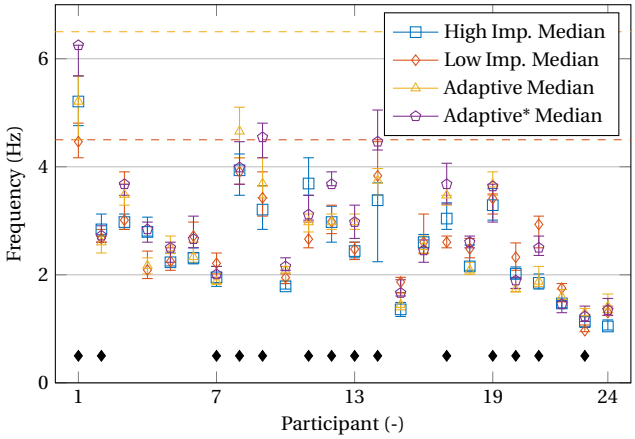

Figure 4.24: Per-participant median of excitation frequency estimated from measurements during the dynamic task with 95 % confidence intervals. The dashed lines indicate the resonance frequency of the low and adaptive impedance settings according to the system identification (cf. figure 4.11, resonance frequency of low impedance setting: 4.5 Hz, resonance frequency of adaptive impedance setting: 6.5 Hz). Diamonds indicate participants that achieved significantly higher median gains with the low impedance than the high impedance setting.

Table 4.11: Comparison of the estimated excitation frequency used by the particicpants of group A (significantly higher gain with low impedance setting than with high impedance setting during dynamic task, $n = 14$) and group B (other participants, $n = 10$). The p-level of the Wilcoxon rank-sum test and its rank-biserial correlation r are given per test.

Impedance Setting	Group A ($n = 14$)		Group B ($n = 10$)		p	r
	Median (Hz)	$CI_{95\%}$ (Hz)	Median (Hz)	$CI_{95\%}$ (Hz)		
High	3.0	[2.0, 3.4]	2.2	[1.4, 2.8]	0.023	0.55
Low	2.8	[2.5, 3.4]	2.2	[1.8, 2.7]	0.023	0.55
Adaptive	3.0	[1.9, 3.7]	2.1	[1.4, 2.5]	0.046	0.49
Adaptive*	3.4	[2.5, 4.0]	2.5	[1.5, 2.8]	0.037	0.51

Table 4.12: Grouped results over the group A participants of pairwise comparison of per-participant median gains measured during the dynamic task, given as effect size of median difference and 95 % confidence interval (positive difference indicates better performance of the first setting compared to the second, $n = 14$, p-values refer to Wilcoxon's signed-rank test results). The last column indicates which experiment hypothesis was checked by the statistical test and whether the outcome supports (green) or contradicts (red) the hypothesis for the participants of group A (significance level $\alpha = 5\,\%$).

Impedance Setting Pair	Median Diff. (-)	$CI_{95\%}$ (-)	p	r	Hyp.
Adaptive – High	0.18	[-0.093, 0.36]	0.0085	0.38	H1.3
Adaptive – Low	-0.21	[-0.29, 0.094]	0.011	-0.91	H1.4

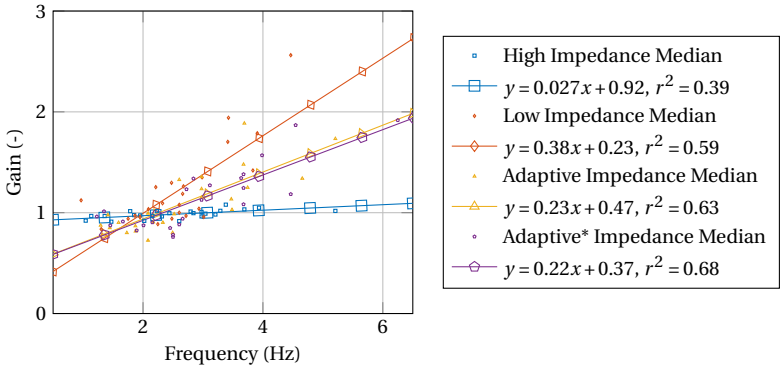

Figure 4.25: Per-participant median gains plotted over per-participant median estimated excitation frequency and linear regression per impedance setting.

42.4 N m/rad ($CI_{95\%}$ = [39.1, 45.0] N m/rad) for the stiffness and 0.48 N m s/rad ($CI_{95\%}$ = [0.45, 0.51] N m s/rad) for the damping. Thus, the self-adapting impedance variation algorithm made the tool device behave clearly different during the precision task than during the dynamic task. At the same time, the impedance was much higher with the adaptive than with the low impedance setting (median stiffness of 41.9 N m/rad, $CI_{95\%}$ = [39.2, 45.6] N m/rad instead of 10 N m/rad; median damping of 0.25 N m s/rad, $CI_{95\%}$ = [0.23, 0.29] N m s/rad instead of 0.01 N m s/rad).

4.4. Discussion

This study shows the potential and the limits of the proposed self-adapting impedance variation algorithm for the telemanipulation of variable impedance tool devices. It is also the first human-user study with a simulated VIA with similar dynamics to the new Dyrac actuator [93], evaluating a possibility to use one actuator for precision and dynamic tasks instead of using a dedicated actuator for each type of tasks.

Using the median results as the reference for normal performance, the study shows that normally high impedance tool devices are more appropriate for free air precision tasks, and low impedance tool devices are more appropriate for dynamic tasks (hypotheses B1 and B2). This is not surprising, as the first is the well-established state of the art in robot design, and we showed the second in two previous experimental studies with SEAs [71]. The results also strongly indicate that the experiment participants were able to achieve the same median performance in the precision task with the new adaptive impedance as with the conventional high impedance. This is an encouraging result as precision tasks play a significant role in teleoperation (*e.g.*, for pick-and-place tasks, inspection, insertion, etc.). Thus, it can be argued that a tool device not performing well in precision tasks would be very impractical for teleoperated use.

On the other hand, it is surprising that the human users seem to have been able to achieve similar performance on the precision task with the tool device in low impedance setting as in high impedance setting in their outstanding trials (10^{th} percentile results). Apparently, they were able in the outstanding trials to sufficiently suppress the

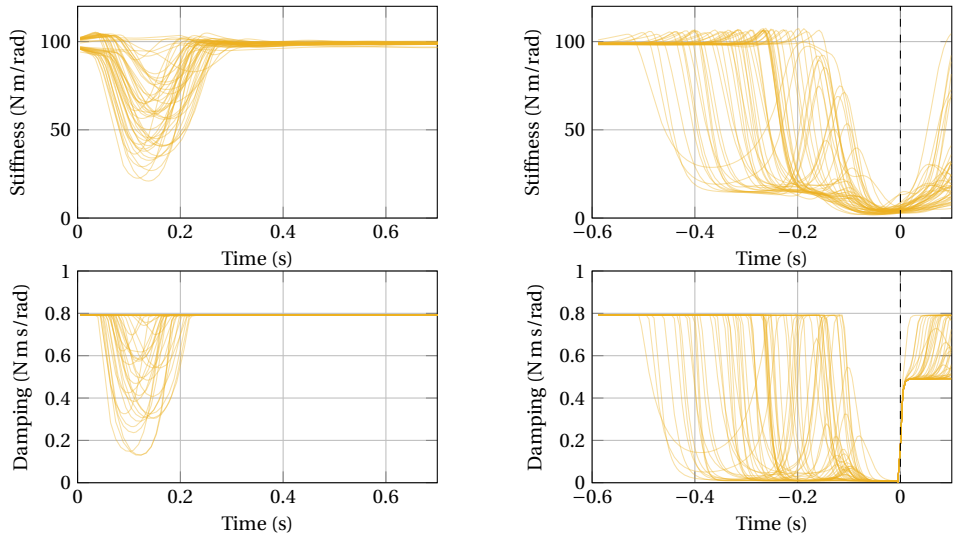

(a) Precision Task

(b) Dynamic Task

Figure 4.26: Actual stiffness and damping measured during the precision task and the dynamic task with the adaptive stiffness setting. In the precision task plots, $t = 0$ s corresponds to the start of the travel. The dashed line at $t = 0$ s in the dynamic task plots shows the moment of impact.

Table 4.13: Comparison of the effective stiffness measured during trials performed with the high, low, and adaptive impedance settings of the reference measurement phase. The p-value and rank-biserial correlation coefficient are indicated for Wilcoxon's rank-sum test between trials performed with the adaptive setting. The stiffness measured during the trials performed with the high and low impedance settings are given as reference, without calculations of statistical significance.

Impedance Setting	Precision Task		Dynamic Task		p	r
	Median (N m/rad)	$CI_{95\%}$ (N m/rad)	Median (N m/rad)	$CI_{95\%}$ (N m/rad)		
High	100	[99.9, 100.5]	100.8	[100.4, 101.1]		
Low	10	[10, 10]	10.1	[9.9, 10.2]		
Adaptive	**83.7**	**[83.1, 87.8]**	**41.9**	**[39.2, 45.6]**	**< 0.001**	**1**

Table 4.14: Comparison of the effective damping measured during trials performed with the high, low, and adaptive impedance settings of the reference measurement phase. The p-value and rank-biserial correlation coefficient are indicated for Wilcoxon's rank-sum test between trials performed with the adaptive setting. The stiffness measured during the trials performed with the high and low impedance settings are given as reference, without calculations of statistical significance.

Impedance Setting	Precision Task		Dynamic Task		p	r
	Median (N m s/rad)	$CI_{95\%}$ (N m s/rad)	Median (N m s/rad)	$CI_{95\%}$ (N m s/rad)		
High	0.8	[0.8, 0.8]	0.8	[0.8, 0.8]		
Low	0.01	[0.01, 0.01]	0.01	[0.01, 0.01]		
Adaptive	**0.77**	**[0.73, 0.78]**	**0.25**	**[0.23, 0.29]**	**< 0.001**	**1**

oscillations of the low impedance tool device to come to rest at the target position in a comparable time to the outstanding trials with the high impedance tool device. The observation that they only achieved this in their outstanding trials suggests that reaching better performance required more effort with low tool device impedance than high tool device impedance. However, this doubt on the basic assumption (hypothesis B1) for the precision task in the case of outstanding trials makes it difficult to conclude about the performance with the adaptive setting on the precision task for outstanding trials.

This might also have been influenced by the bounded by zero nature of the metrics, that gave a lower limit to the travel time and integral of time-weighted absolute error (ITAE) even under perfect conditions (10^{th} percentile of high impedance setting, cf. figure 4.17, table 4.5, figure 4.18 and table 4.6). This could have facilitated that the participants achieved similar performance for their outstanding trials of less good conditions. The particularly good performance on the precision task during the task switch phase of the experiment could be because the participants had performed more trials at this point of the experiment or performed less repetitive trials in a row, helping them to focus better. However, no concluding explanation was found on why they reached even better performance than the reference measurement phase's high impedance performance.

Although a significantly better median performance in terms of maximum output velocity and gain was measured on the dynamic task with low tool device impedance than with high tool impedance, the observed effect sizes were much smaller than in the experiments with SEAs [71]. The effect size on the maximum output velocity in Experiment 1 of [71] was 14.34 rad/s, $CI_{95\%} = [11.30, 15.43]$ rad/s at a resonance frequency of 4.8 Hz and 9.88 rad/s, $CI_{95\%} = [8.00, 16.72]$ rad/s at 6.9 Hz. The effect size on the gain was 1.16, $CI_{95\%} = [0.93, 1.36]$ at 4.8 Hz and 1.31, $CI_{95\%} = [0.73, 1.51]$ at 6.9 Hz. The effect size on the maximum output velocity in the median performance measurement of this study as indicated by table 4.7 was only 2 rad/s, $CI_{95\%} = [-0.017, 2.9]$ rad/s at a resonance frequency of 4.5 Hz (low impedance), and 0.48 rad/s, $CI_{95\%} = [-1.4, 3.3]$ rad/s at 6.5 Hz (no significant effect for the adaptive impedance). The effect size on the gain in this study as indicated by table 4.8 was only 0.12, $CI_{95\%} = [0.024, 0.28]$ at 4.5 Hz (low impedance), and 0.061, $CI_{95\%} = [-0.093, 0.17]$ 1 at 6.5 Hz (no significant effect for the adaptive impedance), and also only 0.18, $CI_{95\%} = [-0.093, 0.36]$ at 6.5 Hz (adaptive setting) for group A (cf. table 4.12).

Testing each participant's results on the dynamic task separately for significant difference between the per-setting median gains, revealed that 14 out of 24 participants achieved significantly higher gains with the low than with the high impedance settings (group A), whereas 10 participants did not (group B). The participants of group A used significantly higher excitation frequencies at the 5 %-level than those of group B, although the effect was only moderate (cf. table 4.11, difference of medians in the range from 0.6 Hz to 0.9 Hz, r in the range from 0.49 to 0.55). The participants of group A also achieved higher gains with the adaptive than with the high impedance setting, although not as high as with the low impedance setting (cf. table 4.12), suggesting that the adaptive setting could be more efficient than the high impedance setting for sufficiently high excitation frequencies.

Combined with the results of the linear regression of the gain over frequency (cf. figure 4.25), it can be hypothesized that the participants, and especially those of group B,

could have achieved higher gains with the adaptive setting if they had been made aware that they should use higher excitation frequencies (4.5 Hz for the low impedance setting and 6.5 Hz for the adaptive impedance setting). This suggests that it was not obvious to the participants how they could use the tool's elasticity to their advantage.The elasticity is only beneficial for achieving a higher gain if the motion profile is such that the spring deflection and unwinding aid in accelerating the end-effector in the forward direction after the backswing motion. In this experiment, no instructions were given specifically about this mechanism, whereas in the previous study, the participants saw an instruction video explaining the principles of resonance extensively [60]. That could indicate that the elastic hammering task is less intuitive than we concluded previously, requiring some understanding of the resonance effect even if no extensive training.

The experiment apparatus and the impedance variation algorithm probably also influenced the dynamic task performance negatively. The much higher impedance measured with the adaptive compared to the low impedance setting (median stiffness of 41.9 N m/rad, $CI_{95\%} = [39.2, 45.6]$ N m/rad instead of 10 N m/rad; median damping of 0.25 N m s/rad, $CI_{95\%} = [0.23, 0.29]$ N m s/rad instead of 0.01 N m s/rad) most likely contributed to the lower performance in terms of gain during the dynamic task compared to Experiment 1 and 2 of [71].

Also, the adaptive setting system identification showed a resonance frequency close to 6.5 Hz instead of the 4.5 Hz resonance frequency of the low impedance setting. This might have made it more difficult for the participants to achieve high gains with the adaptive setting compared to the low impedance setting, as a different, faster motion was required to optimally excite the actuator's resonance under the adaptive setting than under the low impedance setting. The experiment results suggest that the uninstructed participants would have achieved higher gains had the tool device been tuned to a resonance frequency beetween 2 and 3 Hz. Indeed, in Experiment 1 of [71] the confidence intervals of the effect sizes were larger at a resonance frequency of 6.9 Hz, which supports the hypothesis that such high excitation frequencies are difficult to produce for human operators. This seems coherent with the indications of this study that the experiment participants could only achieve significantly better performance in some cases with the adaptive setting compared to the high impedance setting.

However, the effect sizes are also small for those measures that show a significant effect (cf. table 4.9 and 4.10), making it impossible to formulate strong statements of any performance improvements with the adaptive setting such as configured in this experiment. Especially, the relatively high damping with the adaptive impedance setting probably hindered exploiting the resonance effect, masking the effect of the excitation frequency. It seems important to the author to put the focus on the damping adaptation of the self-adapting impedance variation algorithm for future experiments if the actuator should be optimized more for dynamic tasks. However, care needs to be taken as this can easily lead to bad precision task performance.

Overall, the experiment results could only partially support the experiment hypotheses. Namely, the median results of the precision task strongly indicate that the participants could achieve equal performance with the adaptive setting as with the high impedance setting. Even if the adaptive setting did not yield consistent results for the dynamic task, it also has the advantage that it has a low impedance on high-speed impacts, thereby

increasing safety in human-robot cooperation [31] and helping to reduce wear on the actuator [15]. As shown in figure 4.26, the impedance is consistently low at the moment of impact of the dynamic task trials. From a system point of view, these can be considered positive results for the self-adapting impedance variation principle for dynamic teleoperation compared to the state-of-the-art rigid tool devices.

4.5. Conclusion

This study demonstrated the proof of principle for self-adapting impedance control without additional sensors measuring the operator's limb stiffness, where the operator does not need to consciously change from one mode of operation to another to perform different kinds of tasks. A self-adapting impedance variation control law was presented, and its use was demonstrated by a human-subject experiment. This control law automatically changes the impedance of a variable impedance actuator tool device in a teleoperation system depending on the handle device's velocity. The experiment validated this control law for the use of one VIA tool device for precision tasks and dynamic tasks without the need for additional sensors for measuring the intended stiffness, reducing system complexity. The performance obtained during the precision task was comparable with the performance achieved with a high impedance actuator. The performance obtained during the dynamic tasks was not as good as observed in previous experiments with a permanently soft actuator.

Hence, the system can be used equally well as a rigid system for precision tasks, which constitute the classic domain for teleoperation. Additionally, the system is better suited for dynamic tasks than rigid teleoperation systems, as the safety is increased in human-robot cooperation scenarios, and the wear on the VIA is reduced by automatically decreasing the impedance when operating at a higher speed. These are promising results for the development of wide-range teleoperation systems, covering the full dynamic spectrum of the human motion bandwidth.

5

Conclusions & Discussion

5.1. Summary of Research Goals and Approach

The vision of this research was to develop an efficient (requiring little energy for explosive motions), intuitive (usable to operators without training), and versatile (suited for precision tasks and dynamic tasks alike) teleoperation system suited for tasks of a wide dynamic range with a focus on dynamic tasks such as hammering, which cannot be performed well with rigid teleoperation systems. The criterion for efficiency was the ability to exploit the resonance of elastic tools to obtain a higher output velocity than input velocity. The criterion for intuitiveness was that operators do not require extensive training but can use the system in the first session. The criterion for versatility was that precision and dynamic tasks, which are at the two extremes of the dynamic range (slow and stiff/fast and soft), can both be executed well with one system without requiring reconfiguration by the user.

This problem was approached from two sides. First, the human capabilities were explored in their interaction with elastic tools for explosive movement tasks to characterize the human motion profile in such tasks and test their capability to adapt to the imperfections of a teleoperation system, *e.g.*, reduced fidelity in visual and force feedback, and time delay. Then, a teleoperation system was developed, suitable for human dynamic motions and precision tasks alike. This part of the thesis consisted of designing, building, and characterizing an actuator, and implementing a self-adapting impedance variation control method. The goal of this control method was to allow human operators to intuitively perform precision tasks and dynamic tasks without explicitly changing the configuration of the system. Finally, a human user study was performed to experimentally show that humans can handle and appreciate this combination of teleoperated (simulated) variable impedance tool device with self-adapting impedance variation.

5.2. Main Conclusions

The following main conclusions can be taken from this thesis. Their significance and limitations are discussed subsequently.

Humans executing explosive movement tasks with elastic tools

1. Humans can appreciate tool elasticity in direct manipulation and in teleoperation to obtain a doubled output velocity during explosive movement tasks compared to rigid tools.
2. The observed gain in output velocity was reproduced even in the absence of visual feedback, force feedback, or in the presence of significant time delay.
3. Humans can match an elastic tool's resonance frequency in the range of 3 Hz to 5 Hz with more than 10 % accuracy.
4. Hammering with an elastic tool is sufficiently intuitive for untrained participants to achieve significantly higher gains with the elastic tool than with the rigid tool in the first session of using the system, whether in direct manipulation or through a teleoperation system.

Variable impedance actuators as tool devices for teleoperation

5. Variable impedance actuators are suitable tool devices for humans to perform teleoperated precision and dynamic tasks with the same actuator.
6. The variable impedance actuator Dyrac combines three attractive features for dynamic teleoperation: fast impedance changing time (120 ms for full-range steps and 50 ms for small steps; 10 ms for full-range damping steps), wide effective stiffness range (0.2 N m/rad to 313 N m/rad), and variable damping (damping torque from 0 N m to 3 N m).
7. The self-adapting impedance variation algorithm based on the "slow and stiff/fast and soft" principle was validated to make it intuitive for humans to interact with teleoperated variable impedance actuators for precision and dynamic tasks without explicit mode changes, and without additional sensors to measure the operator's limb stiffness.

5.3. Discussion

5.3.1. Human use of tool elasticity

This section discusses to what extent the conclusion "Humans can appreciate tool elasticity in direct manipulation and in teleoperation to obtain a doubled output velocity during explosive movement tasks compared to rigid tools" can be utilized for dynamic tasks in telerobotics.

This thesis showed through three experiments (chapter 2 and chapter 4) that human operators can exploit an elastic hammer to achieve higher peak velocities in a hammering task than they can with a rigid hammer. While the experiments were only performed with one specific task, the nature of other dynamic tasks like throwing, shaking, or jolting is very similar to hammering, making it plausible that such tasks could also benefit from tool elasticity in terms of efficiency. They all have in common that the motion is performed in a fast alternation of backward and forward direction. Rigid actuators are usually inefficient for motions of this kind, where the end-effector needs to be accelerated and then stopped and accelerated in the opposite direction as the kinetic energy is dissipated during the inversion of motion direction.[1] Elastic actuators, however, are not only more robust to shock loads than rigid actuators, but they can also store kinetic energy as potential energy and again release it as kinetic energy for a motion in the opposite direction. This principle is easy to exploit in automatic task execution, as had repeatedly been studied before [43, 75, 78]. However, with the additional findings of the experiments of this thesis related to human interaction with elastic tools, one can imagine that dynamic tasks also become more important in future teleoperation applications.

5.3.2. Effects of degraded feedback

This section discusses the sensitivity of the resonance effect in elastic tools to non-optimal excitation in order to give an indication about the span of the conclusion "The observed gain in output velocity was reproduced even in the absence of visual feedback, force feedback or in the presence of significant time delay."

[1] In theory, the energy could be recuperated electrically, but this is rarely done in robotics.

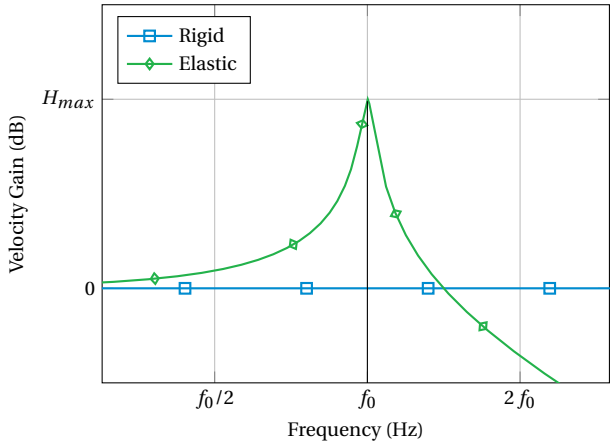

Figure 5.1: Velocity transfer function magnitude of an elastic hammer compared to a rigid hammer as obtained analytically from an underdamped mass-spring-damper model with f_0 the resonance frequency and $H_{max} = \max \left| H_{elastic}(s) \right|$ the maximum gain of the elastic hammer (repeated from chapter 2).

5

In Experiment 2 (chapter 2) of this thesis, no significant effects could be observed related to either the absence of force-feedback, absence of visual feedback, or the presence of time delay (cf. section 2.4.6). One possible explanation for this result is that participants have an intuitive understanding of the dynamic system properties and actively adapt their excitation input to exploit the resonance of the elastic hammer (cf. section 5.3.3). At the same time, it is interesting to consider the sensitivity to non-optimal excitation of the elastic hammering task. Indeed, the gain of the velocity transfer function (cf. figure 5.1) shows that the response for any frequency below approximately 140 % of the resonance frequency yields a gain larger than 1. Thus, some positive effects of the elastic tool, even though not the maximum theoretically possible ones, can be expected for a rather broad range of excitation frequencies.

At the same time, a significant difference in the achieved velocity gain was observed between Experiment 1 and 2 (chapter 2, section 2.3.11) compared to Experiment 3 (chapter 4, table 4.8), which is not explained well by the transfer function. Figure 5.1 shows the transfer function with a perfect velocity source after reaching a stationary condition. This helps choose the excitation frequency for a continuous sinusoidal excitation to achieve the highest output velocity: the resonance frequency f_0. However, in the experiments of this dissertation, the stationary oscillation condition was never reached because the motion was a hammering motion, *i.e.*, a single backward-forward motion followed by an impact. Some effects of this motion can be better understood by analyzing the system from an energetic point of view.

In the following, a simplified energy analysis of the system is discussed to give a possible explanation for the ease of the participants to achieve high gains during the experiment. Figure 5.2 shows a network representation of the elastic hammering experiment setup inspired by the representation of Ryu *et al.* [108]. Energy can be transferred between the operator arm holding the handle and the spring, either directly or through a

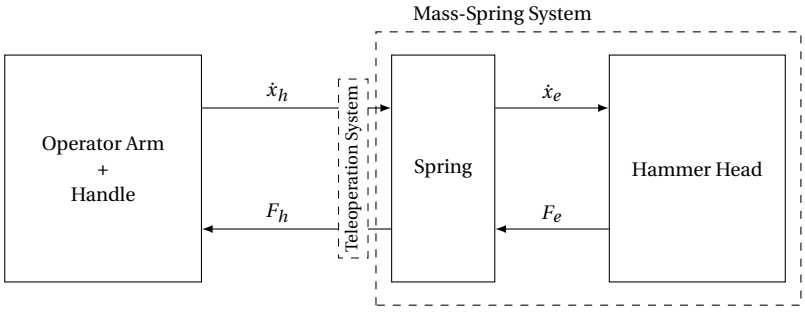

Figure 5.2: Network representation of elastic hammering interaction. Power is transferred between the operator arm and the spring and between the spring and the hammer head as the product of the velocity $\dot{x}$ and the force F. The teleoperation system in the case of teleoperated operation is indicated with dashed lines as it is considered perfectly transparent, exactly transferring the power between arm and spring. Power can be transferred in both directions, the arrow heads indicating the sign convention.

transparent bilateral teleoperation system. Energy can also be transferred between the spring and the hammer head. The spring and the hammer head build a mass-spring system conserving energy with negligible damping. The spring stores energy as potential energy, the hammer head conserves energy as kinetic energy neglecting the drag of the hammer head in air. The operator arm can induce or dissipate energy.

A higher velocity gain of hammer head velocity compared to handle velocity means that more energy is accumulated in the mass-spring system. A smaller gain means that less energy is accumulated in the mass-spring system, *i.e.*, some energy is transferred back to the operator arm at the moment when the operator slows down before inversion of the direction of motion.[2] Let us therefore analyze the energy transfer from the mass-spring system to the operator arm.

The principle of impedance matching states that reflection-less power/energy transfer occurs if the source impedance is equal to the complex conjugate of the load impedance [109, 110]. Otherwise, some energy is reflected, back to the source. Impedance matching is mostly used in electronics, but the principle can be transferred by analogy to mechanics with the mechanical complex impedance Z linking force F and velocity v such that

$$F(\omega) = Z(\omega)\, v(\omega)\,, \tag{5.1}$$

with ω the angular frequency (cf. [111]). The source impedance for an energy transfer from the mass-spring system to the operator arm is composed of the spring stiffness, the load impedance by the mass of the human arm, and the stiffness and damping of its muscles. As the source impedance in Experiment 1 and 2 was small due to the small inertia and small spring stiffness (inertia of 2.6×10^{-3} kg m^2, stiffness of 2.3 N m/rad for the reference condition with 4.8 Hz resonance frequency), it is possible that large portions of the kinetic energy of the hammer head were not transferred to the operator arm but reflected and conserved in the mass-spring system (assuming similar arm characteristics as those measured by Tanaka *et al.* in task readiness for a virtual ball-catching task [112]:

[2] Energy could be dissipated in the teleoperation system, but here it is assumed to be transparent with negligible energy dissipation.

inertia of approximately 0.8 kg to 1.9 kg, stiffness of approximately 57 N/m to 189 N/m, damping of approximately 17 N m s/rad to 28 N m s/rad, corresponding approximately to an inertia of 18×10^{-3} kg m^2 to 43×10^{-3} kg m^2, stiffness of 380 N m/rad to 1260 N m/rad, and damping of 113 N m s/rad to 186 N m s/rad, when applied on a handle at 15 cm of the rotation axis). More energy in the mass-spring system corresponds to a higher peak hammer head velocity at the moment when all potential energy in the spring is converted into kinetic energy of the hammer head.

In contrast, the (simulated) inertia and spring stiffness were much higher in Experiment 3 (inertia of 12.5×10^{-3} kg m^2; stiffness of 10 N m/rad). Thus, in this simplified model, a much larger part of the kinetic energy could be transferred back to the operator in Experiment 3.[3] Consequently, more energy would be transferred from the tool device to the operator at the moment of inversion of direction in Experiment 3 than in Experiment 1 and 2, leading to less energy in the mass-spring system for the forward motion. The result would be a lower peak hammer head velocity with the setup of Experiment 3 than with the setup of Experiment 1 and 2, as it was measured.

This could explain why it was apparently easier than expected for the participants to exploit the elastic tool's resonance in terms of peak output velocity and gain, even under the sub-optimal conditions of Experiment 2. Furthermore, this could be part of an explanation why in Experiment 3, the effect of the elastic tool was much less pronounced in terms of peak output velocity and gain than in Experiment 1 and 2 (effect size maximum output velocity Experiment 1: 14.34 rad/s, $CI_{95\%}$ = [11.30, 15.43] rad/s at a resonance frequency of 4.8 Hz, Experiment 3: 2 rad/s, $CI_{95\%}$ = [−0.017, 2.9] rad/s at 4.5 Hz (low impedance setting); effect size gain Experiment 1: 1.16, $CI_{95\%}$ = [0.93, 1.36] at 4.8 Hz, Experiment 3: 0.12, $CI_{95\%}$ = [0.024, 0.28] at 4.5 Hz; cf. sections 2.3.11 and 2.3.11, and tables 4.7 and 4.8).

This would also be coherent with the results of Experiment 3 that the participants performed better in the low impedance condition of the precision task than expected. The measurements of the travel time show that the participants were able to stop the end-effector after only a few oscillations (cf. the plots of the time series in fig. 4.14 for a qualitative impression of the results), nearly as quickly as with the permanently high impedance setting for the best trials (14 ms median difference with $CI_{95\%}$ = [-29, 101] ms of 10^{th} percentile results, cf. table 4.5). This suggests that the sensitivity to degraded feedback for achieving a high output velocity gain is reduced at lower mechanical impedance of the elastic hammer compared to the human arm impedance as less energy is transferred back to the arm during task execution, *i.e.*, it could be easier to achieve a high gain with a light and soft elastic hammer than with a heavy and stiffer elastic hammer (resonance frequency alike) because the energy "stays better in the elastic hammer."

5.3.3. Matching of the resonance frequency

This section places the conclusion "Humans can match the resonance frequency of an elastic tool in the range of 3 Hz to 5 Hz with more than 10 % accuracy" in relation to previous research.

[3] This can be compared figuratively to a collision between marbles. If a light marble collides with a heavier one, the lighter marble will bounce back. If both marbles have equal mass, the initially moving marble will be at a standstill after the collision.

In chapter 2, the participants used significantly different excitation frequencies between the conditions with 3 Hz and 4.8 Hz resonance frequency. As a result, they matched the resonance frequencies rather precisely with a relative error of +2.3 % and –6.3 %, respectively (cf. figure 2.11c). Thus, the participants seemed to adapt to the different resonance frequencies to some extent, adopting higher excitation frequencies for stiffer springs. This result is consistent with Hatsopoulos *et al.*, who concluded that "one senses and exploits the resonances of the musculoskeletal system to establish the frequency and amplitude of rhythmic movement. Thus, the physical dynamics provide constraints or anchoring points around which motor behavior is organized" [64], and with the neuromusculoskeletal model proposed by Verdaasdonk *et al.* to explain resonance tuning in human rhythmic limb movement [63]. However, the relative error was much higher for the higher resonance frequencies of 6.9 Hz and 9.9 Hz, suggesting that it is more difficult for humans to precisely match resonance frequencies above a maximum resonance frequency that probably lies between 4.8 Hz and 6.9 Hz.

5.3.4. Intuitiveness of the elastic tool for hammering

This section discusses what role learning effects could have played in the different experiments in order to assess the intuitiveness in the conclusion "Hammering with an elastic tool is sufficiently intuitive for untrained participants to achieve significantly higher gains with the elastic tool than with the rigid tool in the first session of using the system, whether in direct manipulation or through a teleoperation system."

Experiment 1 included a learning phase of 100 trials before each performance phase of a condition (20 trials) to examine learning effects over the experiment duration (cf. figure 2.3). Each participant therefore performed 600 trials. No significant improvement was observed in the grouped analysis of all participants. The only effect, if any, was observed in the first two to three blocks of ten trials of a new condition, thereby indicating that saturation is reached on average after 20 to 30 trials (cf. chapter 2, figure 2.10). This can only be a rough indication for short-term adaptation effects, as profound neuromuscular learning processes of new motions might take many more repetitions split into sessions over a longer period. However, it seems legitimate to assume that a simple task such as hammering is sufficiently well-known to most people that it does not require long training to perform the same task with an elastic tool. Also, as discussed above, the apparatus used in Experiment 1 and 2 was presumably not very sensitive to slightly sub-optimal task execution. Experiment 2 did not have a learning phase, but a detailed instruction video explaining the principle of resonance, a short familiarization phase, and 40 trials per condition for a total of 160 trials (cf. figure 2.12). The measured performance in terms of velocity gain was similar in Experiment 2 as in Experiment 1 (cf. figure 2.15). Thus, the shorter familiarization phase and smaller total number of trials did not seem to have made a difference on the outcome of Experiment 2 compared to Experiment 1.

The participants of Experiment 3 did not receive explanations about resonance and had only a short familiarization phase. They then performed only 20 hammering trials during the training phase, 20 during the reference measurement, and 20 during the task switch phase for a total of 260 hammering trials (cf. figure 4.12). They achieved only slightly higher gains with the low impedance setting than the high impedance setting, with a median difference of 0.12 ($CI_{95\%}$ = [0.024, 0.28]) over the grouped analysis

of all participants, which is a smaller effect than that observed in Experiment 1 and 2 (cf. section 2.3.11 and table 4.8). This suggests that basic knowledge about the system behavior helps to use the tool's elasticity, even if no extensive training might be required. However, the different actuator of Experiment 3 could also have been an important factor for these different results between Experiment 3 and Experiment 1 and 2 (cf. also section 5.3.2).

Nevertheless, the common goal of all experiments was not to teach the participants how to hammer efficiently with an elastic tool, but to examine how a teleoperation system with an elastic tool needs to be designed to be intuitive to use for untrained operators. Experiment 1 and 2 showed that the untrained participants can achieve significantly higher gains with the elastic tool than with the rigid tool in the first session of using the system. These results seem sufficiently strong to hold the conclusion, albeit with the insight of Experiment 3 that the actuator probably has a strong effect on the achievable gains, and that better explanations and some training trials certainly positively affect the achieved gain and output velocity.[4]

5.3.5. VIAs for teleoperated precision and dynamic tasks

After a theoretic introduction about the desired characteristics of a VIA for teleoperated precision and dynamic tasks, this section compares four VIA architectures to give indications about which architecture should be favored in the conclusion "Variable impedance actuators are suitable tool devices for humans to perform teleoperated precision and dynamic tasks with the same actuator."

The findings presented in chapter 2 support the notion of using SEAs as tool devices for teleoperated dynamic tasks. However, a teleoperation system with large oscillations, as used in Experiment 1 and Experiment 2, is not practical for positioning tasks. Thus, Experiment 3 used a VIA to perform positioning tasks and explosive movement tasks with one actuator. While a simulation of one specific actuator design was successfully used for the experiment, it leaves the question of which architecture should be favored in general for dynamic teleoperation. In the following, four different VIA architectures are compared, concerning their strengths and weaknesses for their use in dynamic teleoperation, in order to give some indications to this question.

In this discussion, only actuator architectures are included that are capable of providing variable impedance control, and of storing energy as potential energy in a spring. Variable impedance control is considered hereinafter as the ability of the actuator to, at any time t, render a torque $F(t)$ given by

$$F(t) = b(t)\,(\dot{x}(t) - \dot{x}_0(t)) + k(t)\,(x(t) - x_0(t))\,, \tag{5.2}$$

with b being the virtual viscous damping factor, $\dot{x}$ the end-effector velocity, $\dot{x}_0$ the virtual joint velocity, k the virtual spring stiffness, x the end-effector position, and x_0 the virtual neutral position. The *virtual* measures indicate that some architectures might not allow a physical change of the actuator characteristics, but can imitate the characteristics through control. The most extreme example of virtual variable impedance would be a completely

[4] Section 5.3.7 again discusses the results of Experiment 3 with respect to intuitiveness in the broader scope of covering precision tasks and dynamics tasks with one system.

rigid actively compliant robot actuator that can render the same forces as a VIA within the dynamic limitations of the motor. The actuator should allow changing the damping factor $b(t)$ and the stiffness $k(t)$ dynamically, continuously, and in a controlled way. The actuator should be able to store potential energy $E_p(t) = \frac{1}{2} k_0 (x(t) - x_1(t))^2$, with k_0 the mechanical spring stiffness and x_1 the mechanical joint position. The actuator should then allow the transformation of stored potential energy to kinetic energy at the end-effector without requiring to add energy from the actuator's motors. The energy storage capability requires a physical elastic element in the power train from the neutral position motor to the end-effector, thus excluding actively compliant actuators.

The importance of controlled damping for compliant robotic joints has been underlined by several researchers in the field [80, 113–117]. Its main reason lies in resolving the conflict of interest between the elastic actuator's desired functionality to store energy, and the necessity to keep the actuator stable. The latter requires that energy can be dissipated in a controlled way after it has been accumulated. Indeed, the actuator can either accumulate kinetic energy by acceleration of the end-effector, or potential energy by deflection of the actuator's elastic element. Variable damping is an effective way to switch between energy accumulation and energy dissipation by applying low or high damping as required.

The main methods of variable damping are either active, *i.e.*, by rendering a viscous damping torque $F(t) = b(t)\dot{x}(t)$ through torque control, or physical variable damping, *e.g.*, based on friction, Eddy currents, fluids led through valves, magneto-rheologic fluids, etc. [70]. With multiple joints, more advanced techniques can be applied, as the one presented by Petit *et al.* using an eigenmode decoupling approach for actively controlling the damping [115]. Active damping through an appropriate torque control has the important advantage of avoiding a physical damping mechanism's hardware complexity and weight. However, it comes with the drawbacks of torque control due to the actuator's dynamic limitations, namely potential stability issues in highly dynamic motions and higher residual forces in impact situations. These are especially disadvantageous for the hammering task considered in this thesis. Furthermore, the additional degree of freedom provided by the physical damping mechanism allows more freedom in the impedance shaping, *i.e.*, the impedance that can be controlled at any point in time depends less on the dynamics and external factors (*e.g.*, contact with the environment).

Four combinations are possible for VIAs with energy storage capability with virtual or physical stiffness and damping variation (cf. Figure 5.3):

1. SEA with torque control, *e.g.*, the systems described in [25, 118–121]
2. VSA with virtual damping: *e.g.*, DLR FSJ [78], IIT Awas-II [29], etc.
3. SEA with variable physical damping: *e.g.*, IIT CompAct [86]
4. VIA with full physical impedance variation (stiffness and damping): *e.g.*, University of Pisa/IIT VSA-Cube with variable damping module [85], Dyrac (chapter 3)

The SEA with torque control is essentially a classic robotic actuator with a physical spring added at its output. This architecture has been discussed extensively, among others by Howard [118] and by Pratt *et al.* [15]. SEAs with torque control are simple to

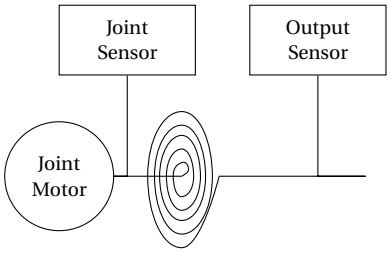

(a) SEA with torque control

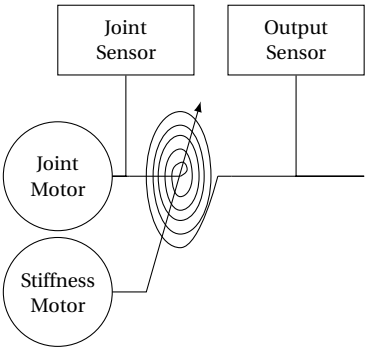

(b) VSA with virtual damping

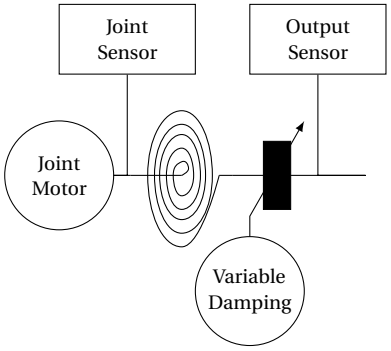

(c) SEA with variable physical damping

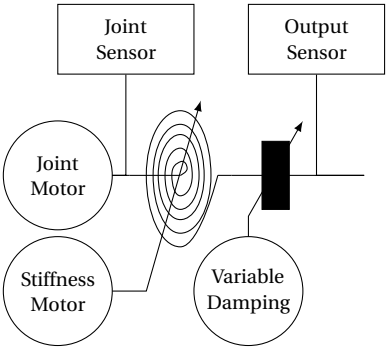

(d) VIA with physical impedance variation (stiffness and damping)

Figure 5.3: Actuator architectures with energy storage capability with virtual or physical stiffness and damping variation

design, compact, and light. They require only one motor, an elastic element, and two position sensors for the joint position and the end-effector position. The added spring element makes the actuator compliant, and not only soft in contact and suffering less wear through impacts, but also capable of storing energy for highly dynamic tasks. With known joint position, end-effector position, and spring stiffness, accurate (precise and close to the true value) and wide-range torque control can be achieved even with high-ratio gears on the motor. This enables designers to choose the gear ratio appropriately to ensure that the motors work at their most efficient working point, independently of the drawbacks induced by high-ratio gears such as friction and reduced back-driveability. The impedance of such actuators can be shaped freely in the low-frequency range, but is limited by the motor dynamics at higher frequencies, as any torque control at the end-effector is achieved by motor position control through the spring equation $F(t) = k_0(x(t) - x_1(t))$.

Due to the motor dynamic limitations, the resonance frequency of the end-effector needs to be within the frequency range of the motor, *i.e.*, low enough to obtain a system that can be stabilized in free air by the controller. More precisely, the criterion given by Howard is that the controller bandwidth needs to exceed the reciprocal of the oscillation decay time to help damp out the oscillations [118]. For a given motor-gear combination and end-effector mass, this imposes an upper limit on the spring stiffness to keep the end-effector as light as possible, and its inertia and the total mass of the actuator low ($\omega_0 = \sqrt{k_0/m}$ means the resonance frequency is higher for higher spring stiffness and lower for higher end-effector mass m). If the load on the actuator can change, *e.g.*, because the actuator is part of a robotic arm with gripper, the resonance frequency will depend on the load without the possibility to compensate by changing the actuator configuration, contrary to a VSA. Thus, for most applications, an SEA with torque control will be a limiting choice as it can easily become unstable in free air movements.[5]

The difference between VSAs and SEAs is that their effective spring stiffness can be varied mechanically. This helps in harmonizing torque control bandwidth and stability of the actuator. In a low stiffness configuration, the torque control bandwidth at the end-effector is smaller than in a high stiffness configuration, because the required motor position changes are larger for equal torque changes than at high stiffness. However, the stability in contact situations is better in a low stiffness configuration as the resonance frequency is lower. Thus, the contact with hard surfaces is more gentle in soft configurations than in stiff configurations. The controller sample rate necessary to keep the system stable is also lower for soft contacts than for hard contacts. In free air, a stiff configuration is advantageous as it allows better position control. Therefore, the VSA allows dynamically adapting the effective stiffness to the current environment: stiff for free air position control and soft for hard contact torque control.

With a VSA, the resonance frequency can also be kept constant through changing loads by changing the stiffness. Consequently, in teleoperated explosive movement tasks, VSAs can help keep the resonance frequency in a range in which the human operator can exploit the resonance (approximately 3 Hz to 6 Hz according to the findings of Experiment 1).

[5] SEAs can be stable in free air if they have sufficient (constant) damping. However, in this discussion, it is assumed that the damping is negligible as the actuator would be less interesting for explosive movement tasks otherwise.

Furthermore, Garabini *et al.* have shown that varying a VSA's stiffness during backward-forward motion can also significantly increase the peak output velocity compared to an actuator with constant stiffness, which is a unique feature of VSAs [43]. This comes at the cost of a much more complicated design with a mechanism for varying the effective spring stiffness, two motors, and three position sensors.

The difference between SEAs with variable physical damping and simple SEAs is that they are equipped with some damping mechanism at the end-effector, which largely extends their stable control bandwidth. Thus, SEAs with variable physical damping are especially valuable for dynamic teleoperation as even large energy can be dissipated through the damping mechanism efficiently and while maintaining stability. Furthermore, this architecture can often be implemented more simply than VSAs. Only one motor is required, and damping variation mechanisms can be as simple as a brake (*e.g.*, the CompAct [86]). As for simple SEAs, variable stiffness is implemented virtually through the torque controller.

A potential disadvantage is that the torque applied by the damping mechanism in parallel to the spring torque might be difficult to measure accurately, but needs to be taken into account in the estimate of the end-effector torque additionally to the torque produced by the spring deflection. If very accurate torque control is required at the same time as the actuator needs to be configured for high damping, a torque sensor might be needed at the end-effector, increasing system complexity, size, and costs. Without a torque sensor, the accuracy of the torque estimation can be degraded at non-zero damping. In practice, both requirements (accurate torque measurement and high damping) rarely occur simultaneously. Accurate torque control is primarily important in dexterous tasks, when the actuator moves slowly, and physical damping is not necessary, because the controller can stabilize the system. High physical damping is mostly required in dynamic tasks (*e.g.*, to stop oscillations after an explosive movement), when accurate torque control is less important than stabilizing the system quickly. Thus, both requirements could often be fulfilled in SEAs with variable physical damping.

A distributed variable damping SEA architecture similar to the distributed-macro-mini architecture by Zinn *et al.* [122] can be imagined for multi-joint robot manipulators. It would combine powerful but heavy SEAs with small and light variable damping modules. The heavy SEAs could be located at the robot base, connected to the joints by Bowden cables or a similar force transmission, providing high power to the manipulator [123]. The light damping modules, on the other hand, could be located directly at the joints to dampen oscillations and ensure stability. Overall, SEAs with variable physical damping appear to be a good compromise for dynamic teleoperation with a relatively simple, small and lightweight hardware, and good dynamic and stability characteristics (Özparpucu *et al.* have for example discussed optimal control strategies of this type of actuators [113]).

A VIA with physical impedance variation (stiffness and damping) such as the Dyrac actuator or the VSA-Cube coupled with the variable damping module [85] allows control over the mechanical impedance without suffering the bandwidth limitations of virtual impedance rendering. As a result, the impedance is affected less by controller and motor bandwidth limitations than in the previously discussed architectures, except during impedance changes. Unfortunately, VIAs with physical impedance variation are complex

to implement and necessarily bulkier and heavier than the other three architectures at equal power output, because they require additional motors and mechanisms. Hence, their practical usage is probably mostly restricted to single-joint testbeds that allow for the additional size and weight.

5.3.6. Dyrac actuator characteristics

This section discusses the characteristics of the Dyrac actuator as stated in the conclusion "The variable impedance actuator Dyrac combines three attractive features for dynamic teleoperation: fast impedance changing time (120 ms for full-range steps and 50 ms for small steps; 10 ms for full-range damping steps), wide effective stiffness range (0.2 N m/rad to 313 N m/rad), and variable damping (damping torque from 0 N m to 3 N m)".

In chapter 3, the Dyrac VIA was presented whose impedance can be varied dynamically over a wide range. The novelty of the Dyrac actuator is to combine wide stiffness range (0.2 N m/rad to 313 N m/rad) with fast stiffness changing time (120 ms for full-range steps and 50 ms for small steps) and variable damping (damping torque from 0 N m to 3 N m) with fast damping changing time (10 ms). The fast impedance changing time gives the actuator the versatility to smoothly change from precision to dynamic tasks in a similar way to what we are used to as humans with our arms. The self-adapting impedance variation algorithm presented in chapter 4 on a simulated actuator with similar dynamics as the Dyrac prototype gave an impression of how this versatility might be exploited in practice for an intuitive-to-use teleoperation system.

As discussed in the previous section, a SEA with variable physical damping might have similar versatility for teleoperation in a much more simple and more power-dense design. Thus, a future actuator for wide-range dynamic teleoperation would most likely be designed differently. However, as one of the Dyrac design goals was to be able to explore the parameter space of variable impedance teleoperation as widely as possible in a one degree of freedom testbed, the design with a less optimal power density and power-to-weight ratio was deemed acceptable in this case.

5.3.7. Self-adapting impedance variation for teleoperated precision and dynamic tasks

This section relates the conclusion "The self-adapting impedance variation algorithm based on the 'slow and stiff/fast and soft' principle was validated to make it intuitive for humans to interact with teleoperated variable impedance actuators for precision and dynamic tasks without explicit mode changes and without additional sensors to measure the operator's limb stiffness" to previous research.

As humans, we are used to switching smoothly from one task to another without paying attention to how the tension in our muscles influences the stiffness of our limbs. The muscular tension regulation is offloaded from our consciousness to our central nervous system [124, 125]. For reaching the same intuitiveness when performing tasks through a teleoperation system, it seems desirable that the teleoperation system takes care of any required system configuration changes and does not load this onto the operator. Previous research has achieved this goal by adding additional sensors to the handle device, measuring the operator's limb stiffness or grip strength [97–99].

In chapter 4, a self-adapting impedance variation algorithm was presented and validated experimentally to achieve this goal without additional sensors. The results of Experiment 3 showed that humans appreciate the automatic impedance adaptations. The self-adapting impedance variation algorithm follows a simple rule for relating the impedance of the tool device to the velocity of the handle device of the teleoperation system: *slow and stiff/fast and soft*. Although, in this thesis, the motivation behind adapting the impedance according to this principle was to allow switching easily between precision and dynamic tasks, this rule was originally established by Bicchi *et al.* [31] to assure the safety of human-robot interaction (with focus on the "fast and soft" aspect). Starting from the head injury criterion (HIC), which gives a measure of the severity for an impact suffered by the human head, they derived an equation for the safe travel speed of a robot with given inertia and stiffness. In turn, they calculated the optimum safe travel speed and stiffness for a rest-to-rest positioning task [31]. In Experiment 3 of this thesis, the safety aspect was not verified, but the "slow and stiff/fast and soft" principle was used in a new manner. The experiment showed that better performance was achieved in a precision task than with a permanently soft actuator, while the actuator impedance was lower during impact in a dynamic task, potentially reducing material fatigue.

Clearly, there is a conflict of interest between hammering and safe human-robot interaction. The goal of hammering is to transmit as much energy as possible during impact. In contrast, the constraint of safe human-robot interaction is to transmit as little energy as possible during an accidental collision. Still, it can be calculated that the kinetic energy of a hammer impact under safe conditions according to the equations of Bicchi *et al.* is higher if the hammer is held by a soft robot than if it is held by a stiff robot.

Using the equations of Bicchi *et al.* [31] to compute the kinetic energy for different values of the link inertia[6] over the joint stiffness with the constants as given there (HIC = 100, rotor inertia $m_{rot} = 1.2\,\text{kg}$, contact stiffness $k_{cov} = 5000\,\text{N/m}$, and operator head mass $m_{oper} = 4\,\text{kg}$), the plots in figure 5.4 are obtained. The plots show that the kinetic energy at maximum safe velocity is slightly higher at low joint stiffness, under the condition that the link mass is smaller than the rotor inertia. The curves have been plotted with the velocity limited to 3 m/s to show the effect of motor velocity saturation. The equations would yield that the link mass should be as small as possible to achieve the highest kinetic energy if actuator limitations were not considered.

This calculation indicates that, under the constraint of guaranteeing human safety, the soft actuator has no disadvantage compared to the stiff actuator concerning the goal of maximizing kinetic energy. Furthermore, even if human safety does not need to be taken into account as it would typically be the case for teleoperated robots deployed at places too dangerous or unreachable for humans, robot lifetime also benefits from low actuator impedance at high velocities, because material fatigue is reduced by higher compliance in the robot joints during collisions [15]. Overall, this thesis signals that what was already a well-founded principle for VIAs regarding human safety and robot lifetime reasons can also be beneficial for making a VIA intuitive to use in teleoperation, covering positioning tasks as well as explosive movement tasks without explicit mode change from

[6] With *link inertia*, Bicchi *et al.* refer to the inertia of the actuator end-effector attached to the elastic element of a VIA, *i.e.*, the inertia that transmits momentum in an impact even if the actuator impedance was to be zero [31].

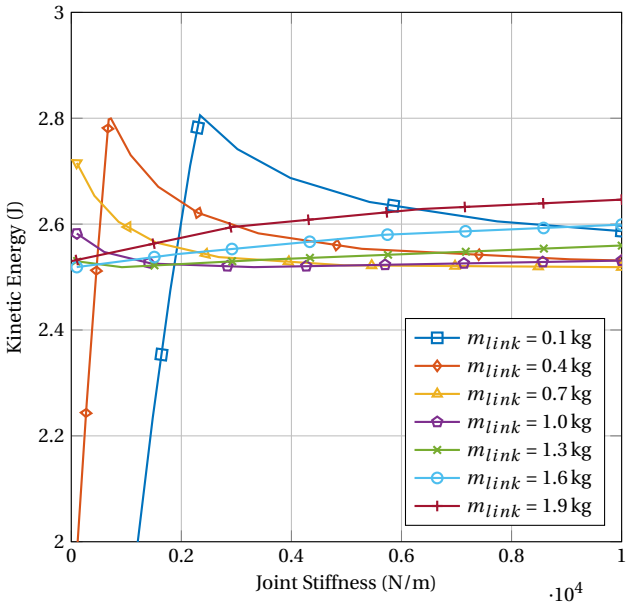

Figure 5.4: Kinetic energy E_k according to Bicchi *et al.* [31] for robot end-effectors with different masses m_{link} moving with maximum safe velocity v_{safe} (HIC = 100) coupled to a robot actuator with rotor inertia m_{rot} = 1.2 kg, contact stiffness k_{cov} = 5000 N/m, and operator head mass m_{oper} = 4 kg. The velocity was limited to 3 m/s to illustrate the effect of motor velocity saturation. This is visible in the curves for m_{link} of 0.1 kg and 0.4 kg, which would otherwise be continuously decreasing over the full range. The plot was cropped to the range 2 J to 3 J on the y-axis to make the small difference better visible between the different curves.

one to the other.

5.4. Limitations

Although the results obtained in this thesis are encouraging for dynamic teleoperation with variable impedance tool devices, some limitations have to be taken into account:

- The experiments of this thesis were performed with tens of participants instead of hundreds. It could be that the experiment results are untypical of the general population, even though the performed significance calculations take into account the sample size in order to reduce the chance of wrong statistical inference. The rather young age distribution of the participants reinforces this limitation. In Experiment 3, the instructions given to the participants were much less detailed than in Experiment 1 and 2, and the spread between participants of the results was bigger for the achieved gain. This could indicate that some people are less used to or less adept at explosive movement tasks with elastic tools than others. At the extreme, this could mean that some (otherwise able-bodied) people cannot perform explosive movement tasks efficiently at all with elastic tools.

- The effects of force feedback, visual feedback, time delay, and self-adapting impedance variation were tested one by one, but not in all possible combinations. Thus, cross-couplings from some effects to others cannot be excluded.

- Only hammering was considered in the experiments. Therefore, the effect of elastic tools cannot be generalized easily to other tasks without further experimentation. However, the fundamental principles of resonance and conversion from kinetic to potential energy may be the same for throwing, shaking, and similar tasks.

- All analyses and experiments that were performed for this thesis were restricted to one degree of freedom. For multiple degrees of freedom, the interaction of one joint with another needs to be considered, making it a significantly more complex issue.

- The variable impedance actuator prototype that was implemented for this thesis is too big and too heavy for it to be used in a human-sized robotic arm. Therefore, its use is restricted to stationary test benches and experimental research.

- Experiment 3 was performed with a simulated VIA as the tool device with some idealizations. The hysteresis observed in the Dyrac prototype and any influence of the load on the motor positions were neglected. This could mean that experiments with a physical variable impedance actuator could yield slightly different results.

- For Experiment 3, only one configuration of the self-adapting impedance variation has been used. No parameter sweep was performed, and no general law was developed to find the parameters for a specific task. For other tasks on other actuators or with different loads, the algorithm's parameters would need to be re-tuned to obtain good results.

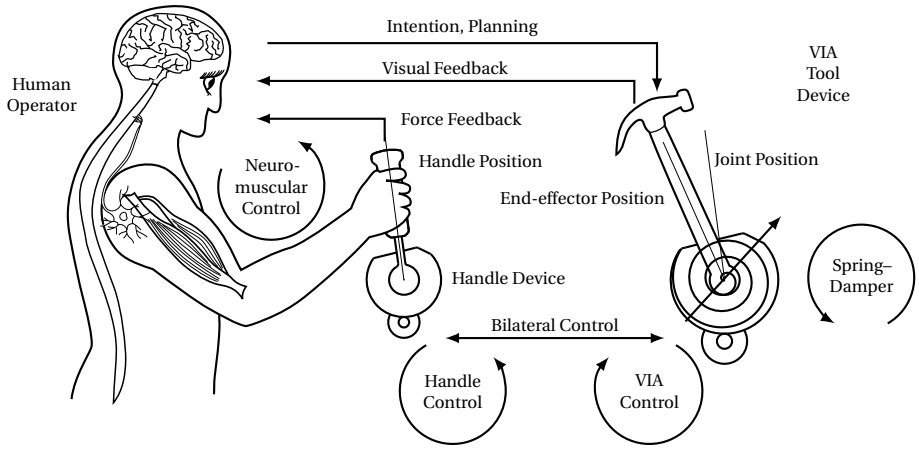

Figure 5.5: Control loops in a teleoperation system with a VIA tool device. The human operator defines the desired trajectory of the end-effector and assesses the result through visual and force feedback. For this, multiple controllers have to work together: neuromuscular control of the operator's arm, bilateral control between handle device and tool device with device controllers on each side, and the spring-damper link between the tool device joint and the end-effector, which can be considered as a mechanical PD-controller.

- No mental load assessment was performed during the human user studies (*e.g.*, NASA-TLX), making it difficult to compare the benefits of tool elasticity to explosive movement tasks with increased operator effort.

5.5. Open Questions

1. Task performance and teleoperation accuracy: Should the handle device position be mapped to the joint position of a VIA tool device or to its end-effector position?

   In a teleoperation system with a VIA tool device, several coupled controllers influence the end-effector trajectory (cf. figure 5.5). At the highest level, the intention and planning of a motion emanates from the human operator, and is verified by him or her through visual and force feedback. The human motion planning is translated into muscular actions in the arm through the operator's neuromuscular control system. As the operator is holding the handle, he or she interacts with the bilateral controller of the teleoperation system, which mirrors the motions between the handle device and the tool device. The VIA control consists of a controller for the joint motor and the impedance variation mechanism. The VIA's spring-damper system can be considered another (mechanical) PD-controller for position between the VIA joint and the end-effector, with the spring stiffness as P-gain and the damping as D-gain.[7]

   The teleoperation system's desired behavior depends on the type of task: *e.g.*, small

[7] The analogy refers to the fact that a position PD-controller will react to an error relative to the setpoint with a correcting force proportional by the P-gain to the position error and proportional by the D-gain to the velocity error. Similarly, the spring force is proportional by the spring stiffness to a deflection, and the damper force is proportional by the viscous damping coefficient to a velocity difference.

overshoot, small acceptable steady-state error, and fast settling for precision tasks, but larger overshoot, larger acceptable steady-state error, and slower settling for dynamic tasks. So the question of whether the handle device position should be mapped to the VIA joint or end-effector position is closely related to the question of how accurate the velocity tracking [48] needs to be at the end-effector. This is a highly task-dependent question that was not addressed in the scope of this thesis. The author's opinion is that "the human knows it best" for an unguided telemanipulation system, as he or she is the only one that knows about the intended trajectory, speed, acceptable errors, etc. Therefore, he or she defines the instantaneously acceptable tracking error. The human operator does not assess the tracking error according to the definition of a teleoperation system, *i.e.*, as error between the handle device and the tool device. Rather, he or she compares the achieved effect of the end-effector interacting with the environment with his or her intention through the visual and haptic feedback provided and adapts his or her actions accordingly. Moreover, mapping the handle device position to the end-effector position potentially leads to a more complex or unstable controller than mapping it to the joint position because of the elasticity between joint and end-effector introducing phase lag.

Therefore, the author's intuition is that a system intended for unguided telemanipulation should be designed for good transparency between the handle device and the VIA joint, leaving the end-effector control to the human operator. The considerations might again be different for teleoperation with shared control in the manner of the framework proposed by Smisek [126]. These can be interesting questions for future research.

2. Dynamic range coverage: How can the range of dynamic motions be covered best and with a homogeneous transition from slow and precise to fast and energetic?

   We hypothesized that this could be achieved by a unified control system that can detect the required stiffness at every moment in time based on the velocity of the handle device and tested it for two extreme types of tasks: positioning and hammering. Further research is required to extend the palette of tasks and find an "all-round solution." The author's opinion is that the self-adapting impedance variation can most likely yield good results on slow tasks requiring soft contacts, *e.g.*, for peg-in-hole insertion if the transparency of the teleoperation system is good. Then, while the VIA impedance is set to high due to the low velocity, the operator has good control over the applied force and can consciously keep the contact forces low.

   The problematic tasks with the self-adapting approach are more likely to be the ones that are not at one extreme of the velocity spectrum as the velocity is the decisive parameter for the impedance variation. No experiments were performed with intermediary velocities within the scope of this thesis, so it remains unclear how the self-adapting approach would perform for such tasks. In any case, the system's efficiency will most likely be the lowest-weighted factor, with stability, usability and wear weighted much higher. For these factors, the "slow and stiff/fast and soft" approach, together with variable physical damping, is a promising starting

point for further research in variable impedance teleoperation.

3. Limitations and performance improvements of the human operator: Can the performance of the human operator for explosive movement tasks be improved in a sensible way, *e.g.*, through shared control?

   Garabini *et al.* have shown that an additional velocity increase of 30 % can be achieved by varying the stiffness of a VSA during an explosive motion [43]. Although this was not exploited in Experiment 3, it could be intriguing for future research to test how optimal control and teleoperation could be combined in shared control for highly dynamic tasks in teleoperation.

4. Stability: How can the stability of the VIA be maintained while performing highly dynamic tasks?

   The important role of a variable damping capability has already been mentioned, but how should the variable damping be regulated? For example, a passivity observer [127] could monitor stability, or the force feedback could be reduced to dissipate energy present in the system. For example, some ideas have been presented by Kronander *et al.* [128]

5.6. Prospects

This thesis shows that it can be expected that human operators can do hammering through a teleoperation system with an elastic tool device, even under less than perfect conditions in terms of transparency and operator skills. A VIA with self-adapting impedance variation further gives the operator the flexibility to perform positioning tasks or hammering tasks without explicit mode change, thereby taking some cognitive load off the operator to anticipate the next movement and to reconfigure the teleoperation system. These are encouraging results for the use of VIAs in future dynamic teleoperation systems, as similar tasks, such as shaking, jolting, and throwing, could also benefit from VIA tool devices.

In the last decade, autonomous robots with impressive dynamic range have been developed, *e.g.*, the Boston Dynamics Atlas or the DLR David [129]. This thesis tries to contribute to making this dynamic range also accessible to teleoperation, such that robot robustness can be optimally combined with human experience, adaptability, and creativity. Future teleoperation could eventually become as intuitive and efficient for operators as direct manipulation.

Four recommendations emerge from this thesis for the design of teleoperation systems with VIA tool device actuators:

1. Considering that the quality of the force feedback in teleoperation is less critical for high-speed tasks than for slow dexterous manipulation, the force fed back to the operator could be scaled down for faster tasks without performance penalties, thereby reducing the power delivered by the handle device. This can be used in passivity observer and controller approaches to increase the stability of teleoperation systems without introducing high damping in the handle device, such as described by Rebelo *et al.* [52].

2. As the precise matching of excitation frequency and the resonance frequency seems not to be critical to obtain a velocity gain, the elastic hammer's stiffness can be driven by design requirements other than the resulting resonance frequency. Even for elastic hammers, it is often desirable that the stiffness is sufficiently high to avoid excessive deflection. The results of Experiment 1 show that the elastic hammer could be designed with a resonance frequency 40 % higher than reachable by a human operator and still achieve a velocity gain of more than 200 %. Consequently, if a higher tool stiffness is desired while still allowing human operators to achieve a good velocity gain, stiffnesses resulting in resonance frequencies up to about 11 Hz could be chosen.

3. Variable physical damping was identified as an important requirement for a teleoperated VIA to control the energy stored in the elastic element without compromising the dynamic bandwidth of the actuator. If a choice has to be made between variable physical damping and mechanically variable stiffness to keep the actuator simple and achieve high power density, it seems better from this thesis to choose a design with constant series elastic stiffness and variable physical damping for highly dynamic tasks.

4. For many tasks such as positioning tasks and dexterous tasks, oscillations of the tool device should be avoided. Therefore, the teleoperation system should not be specialized in dynamic tasks, but cover dynamic tasks and precision tasks alike, *e.g.*, through self-adapting impedance variation, similar to the algorithm presented in this thesis.

References

[1] G. Niemeyer, C. Preusche, S. Stramigioli, and D. Lee, *Telerobotics,* in *Springer Handbook of Robotics*, edited by B. Siciliano and O. Khatib (Springer International Publishing, Cham, 2016) pp. 1085–1108.

[2] S. Kawatsuma, M. Fukushima, and T. Okada, *Emergency response by robots to Fukushima-Daiichi accident: summary and lessons learned,* Industrial Robot: An International Journal **39**, 428 (2012).

[3] S. Huh, U. Lee, H. Shim, J. Park, and J. Noh, *Development of an unmanned coal mining robot and a tele-operation system,* in *2011 11th International Conference on Control, Automation and Systems* (2011) pp. 31–35.

[4] K. D. Katyal, C. Y. Brown, S. A. Hechtman, M. P. Para, T. G. McGee, K. C. Wolfe, R. J. Murphy, M. D. M. Kutzer, E. W. Tunstel, M. P. McLoughlin, and M. S. Johannes, *Approaches to robotic teleoperation in a disaster scenario: From supervised autonomy to direct control,* in *2014 IEEE/RSJ International Conference on Intelligent Robots and Systems* (2014) pp. 1874–1881.

[5] G. Bruzzone, R. Bono, G. Bruzzone, M. Caccia, P. Coletta, E. Spirandelli, and G. Veruggio, *Internet-Based Teleoperation of Underwater Vehicles,* IFAC Proceedings Volumes **36**, 193 (2003).

[6] T. Fong, C. Provencher, M. Micire, M. Diftler, R. Berka, B. Bluethmann, and D. Mittman, *The Human Exploration Telerobotics project: Objectives, approach, and testing,* in *2012 IEEE Aerospace Conference* (IEEE, 2012) pp. 1–9.

[7] J. Marescaux and F. Rubino, *Telesurgery, telementoring, virtual surgery, and telerobotics,* Current Urology Reports **4**, 109 (2003).

[8] S. Laniel, D. Létourneau, M. Labbé, F. Grondin, J. Polgar, and F. Michaud, *Adding navigation, artificial audition and vital sign monitoring capabilities to a telepresence mobile robot for remote home care applications,* in *2017 International Conference on Rehabilitation Robotics (ICORR)* (2017) pp. 809–811.

[9] A. J. Islam, S. S. Alam, K. T. Ahammad, F. K. Nadim, and B. Barua, *Design, kinematic and performance evaluation of a dual arm bomb disposal robot,* in *2017 3rd International Conference on Electrical Information and Communication Technology (EICT)* (IEEE, 2017) pp. 1–6.

[10] O. Khatib, *Human-centered robotics and haptic interaction: from assistance to surgery, the emerging applications,* in *Proceedings of the Third International Workshop on Robot Motion and Control, 2002. RoMoCo '02.* (Poznan Univ. Technol, 2002) pp. 137–139.

[11] D. A. Lawrence, *Stability and Transparency in Bilateral Teleoperation,* IEEE Transactions on Robotics and Automation **9**, 624 (1993).

[12] C. Preusche and G. Hirzinger, *Haptics in telerobotics,* The Visual Computer **23**, 273 (2007).

[13] R. Featherstone and D. E. Orin, *Dynamics,* in *Springer Handbook of Robotics*, edited by B. Siciliano and O. Khatib (Springer International Publishing, Cham, 2016) pp. 37–66.

[14] W. K. Chung, L.-C. Fu, and T. Kröger, *Motion Control,* in *Springer Handbook of Robotics*, edited by B. Siciliano and O. Khatib (Springer International Publishing, Cham, 2016) pp. 163–194.

[15] G. A. Pratt, M. M. Williamson, P. Dillworth, J. Pratt, and A. Wright, *Stiffness isn't everything,* in *Experimental Robotics IV*, edited by O. Khatib and J. K. Salisbury (Springer-Verlag, London, 1997) pp. 253–262.

[16] S. M. McGill, J. D. Chaimberg, D. M. Frost, and C. M. J. Fenwick, *Evidence of a Double Peak in Muscle Activation to Enhance Strike Speed and Force: An Example With Elite Mixed Martial Arts Fighters,* Journal of Strength and Conditioning Research **24**, 348 (2010).

[17] S. Lenetsky, R. J. Nates, M. Brughelli, and N. K. Harris, *Is effective mass in combat sports punching above its weight?* Human Movement Science **40**, 89 (2015).

[18] K. Kubo, *Active muscle stiffness in the human medial gastrocnemius muscle in vivo,* Journal of Applied Physiology **117**, 1020 (2014).

[19] A. Schouten, E. de Vlugt, J. van Hilten, and F. van der Helm, *Quantifying Proprioceptive Reflexes During Position Control of the Human Arm,* IEEE Transactions on Biomedical Engineering **55**, 311 (2008).

[20] S. Terryn, G. Mathijssen, J. Brancart, G. V. Assche, B. Vanderborght, and D. Lefeber, *Investigation of self-healing compliant actuators for robotics,* in *2015 IEEE International Conference on Robotics and Automation (ICRA)* (2015) pp. 258–263.

[21] S. Eppinger and W. Seering, *Understanding bandwidth limitations in robot force control,* in *Proceedings. 1987 IEEE International Conference on Robotics and Automation*, Vol. 4 (1987) pp. 904–909.

[22] S. Yang, H. Li, Y. Guo, L. Shi, and M. Xiong, *Design and simulation of an adaptable and compact impact pile driver,* Automation in Construction **112**, 103104 (2020).

[23] S. S. Pang and W. Goldsmith, *Momentum and energy processes during jackhammer operation,* Rock Mechanics and Rock Engineering **22**, 205 (1989).

[24] T. Bruchmueller, N. Huegel, S. Wacker, and S. Matthiesen, *Modelling of Tool Workpiece Interactions–Coefficient of Restitution for Hammer Drilling of Concrete,* Forschung im Ingenieurwesen **83**, 21 (2019).

[25] G. A. Pratt and M. M. Williamson, *Series Elastic Actuators,* Intelligent Robots and Systems 95. 'Human Robot Interaction and Cooperative Robots', Proceedings. 1995 IEEE/RSJ International Conference on **1**, 399 (1995).

[26] S. Wolf, G. Grioli, O. Eiberger, W. Friedl, M. Grebenstein, H. Hoppner, E. Burdet, D. G. Caldwell, R. Carloni, M. G. Catalano, D. Lefeber, S. Stramigioli, N. Tsagarakis, M. Van Damme, R. Van Ham, B. Vanderborght, L. C. Visser, A. Bicchi, and A. Albu-Schäffer, *Variable Stiffness Actuators: Review on Design and Components,* IEEE/ASME Transactions on Mechatronics **21**, 2418 (2016).

[27] B. Vanderborght, A. Albu-Schäffer, A. Bicchi, E. Burdet, D. G. Caldwell, R. Carloni, M. Catalano, O. Eiberger, W. Friedl, G. Ganesh, M. Garabini, M. Grebenstein, G. Grioli, S. Haddadin, H. Hoppner, A. Jafari, M. Laffranchi, D. Lefeber, F. Petit, S. Stramigioli, N. Tsagarakis, M. Van Damme, R. Van Ham, L. C. Visser, and S. Wolf, *Variable impedance actuators: A review,* Robotics and Autonomous Systems **61**, 1601 (2013).

[28] S. Haddadin, F. Huber, K. Krieger, R. Weitschat, A. Albu-Schäffer, S. Wolf, W. Friedl, M. Grebenstein, F. Petit, J. Reinecke, and R. Lampariello, *Intrinsically elastic robots: The key to human like performance,* in *Intelligent Robots and Systems (IROS), 2012 IEEE/RSJ International Conference on* (2012) pp. 4270–4271.

[29] A. Jafari, N. G. Tsagarakis, and D. G. Caldwell, *AwAS-II: A new Actuator with Adjustable Stiffness based on the novel principle of adaptable pivot point and variable lever ratio,* in *Robotics and Automation (ICRA), 2011 IEEE International Conference on* (2011) pp. 4638–4643.

[30] A. Radulescu, M. Howard, D. J. Braun, and S. Vijayakumar, *Exploiting variable physical damping in rapid movement tasks,* in *2012 IEEE/ASME International Conference on Advanced Intelligent Mechatronics (AIM)* (IEEE, 2012) pp. 141–148.

[31] A. Bicchi and G. Tonietti, *Fast and "Soft-Arm" Tactics,* IEEE Robotics & Automation Magazine **11**, 22 (2004).

[32] T. Wimböck and C. Ott, *Dual-Arm Manipulation,* in *Towards Service Robots for Everyday Environments*, edited by E. Prassler, M. Zöllner, R. Bischoff, W. Burgard, R. Haschke, M. Hägele, G. Lawitzky, B. Nebel, P. Plöger, and U. Reiser (Springer Berlin Heidelberg, Berlin, Heidelberg, 2012) pp. 353–366.

[33] R. Haschke, M. Schöpfer, and H. Ritter, *Grasping Objects of Unknown Geometry with Tactile Feedback,* in *Towards Service Robots for Everyday Environments*, edited by E. Prassler, M. Zöllner, R. Bischoff, W. Burgard, R. Haschke, M. Hägele, G. Lawitzky,

B. Nebel, P. Plöger, and U. Reiser (Springer Berlin Heidelberg, Berlin, Heidelberg, 2012) pp. 431–440.

[34] C. C. Kemp, P. Fitzpatrick, H. Hirukawa, K. Yokoi, K. Harada, and Y. Matsumoto, *Humanoids,* in *Springer Handbook of Robotics*, edited by B. Siciliano and O. Khatib (Springer Berlin Heidelberg, Berlin, Heidelberg, 2008) pp. 1307–1333.

[35] C. Breazeal, A. Takanishi, and T. Kobayashi, *Social Robots that Interact with People,* in *Springer Handbook of Robotics*, edited by B. Siciliano and O. Khatib (Springer Berlin Heidelberg, Berlin, Heidelberg, 2008) pp. 1349–1369.

[36] Y. Liu and M. Y. Wang, *Optimal Design of Remote Center Compliance Devices of Rotational Symmetry,* in *Precision Assembly Technologies and Systems*, edited by S. Ratchev (Springer, Berlin, Heidelberg, 2014) pp. 161–169.

[37] A. Albu-Schäffer, O. Eiberger, M. Grebenstein, S. Haddadin, C. Ott, T. Wimbock, S. Wolf, G. Hirzinger, T. W. Ock, and S. Wolf, *Soft robotics,* Robotics & Automation Magazine, IEEE **15**, 20 (2008).

[38] S. Mejri, V. Gagnol, T.-P. Le, L. Sabourin, P. Ray, and P. Paultre, *Dynamic characterization of machining robot and stability analysis,* The International Journal of Advanced Manufacturing Technology **82**, 351 (2016).

[39] G. Tonietti, R. Schiavi, and A. Bicchi, *Optimal Mechanical/Control Design for Safe and Fast Robotics,* in *Springer Tracts in Advanced Robotics*, edited by A. M.H. and K. O. (Springer, Berlin, Heidelberg, 2006) pp. 311–320.

[40] M. C. Özparpucu and S. Haddadin, *Optimal control for maximizing link velocity of visco-elastic joints,* in *2013 IEEE/RSJ International Conference on Intelligent Robots and Systems* (IEEE, 2013) pp. 3035–3042.

[41] S. Haddadin, T. Laue, U. Frese, S. Wolf, A. Albu-Schäffer, and G. Hirzinger, *Kick it with elasticity: Safety and performance in humanrobot soccer,* Robotics and Autonomous Systems **57**, 761 (2009).

[42] S. Wolf and G. Hirzinger, *A new variable stiffness design: Matching requirements of the next robot generation,* in *Robotics and Automation, 2008. ICRA 2008. IEEE International Conference on* (2008) pp. 1741–1746.

[43] M. Garabini, A. Passaglia, F. Belo, P. Salaris, and A. Bicchi, *Optimality principles in variable stiffness control: The VSA hammer,* in *Intelligent Robots and Systems (IROS), 2011 IEEE/RSJ International Conference on* (2011) pp. 3770–3775.

[44] K. Hashtrudi-Zaad and S. E. Salcudean, *Transparency in time-delayed systems and the effect of local force feedback for transparent teleoperation,* IEEE Transactions on Robotics and Automation **18**, 108 (2002).

[45] J. Trevelyan, W. R. Hamel, and S.-C. Kang, *Robotics in Hazardous Applications,* in *Springer Handbook of Robotics* (Springer International Publishing, Cham, 2016) pp. 1521–1548.

[46] H. Boessenkool, J. Thomas, J. G. Wildenbeest, C. J. Heemskerk, M. R. de Baar, M. Steinbuch, and D. A. Abbink, *Where to improve in human-in-the-loop teleoperated maintenance? A phased task analysis based on video data of maintenance at JET,* Fusion Engineering and Design (2017), 10.1016/J.FUSENGDES.2017.09.007.

[47] B. Milne, X. Chen, C. Hann, R. Parker, and P. Milliken, *Design and Development of Teleoperation for Forest Machines,* in *Engineering Creative Design in Robotics and Mechatronics*, edited by M. K. Habib and J. P. Davim (IGI Global, 2013) pp. 186–207.

[48] G. A. V. Christiansson, *Hard Master, Soft Slave Haptic Teleoperation*, Ph.D. thesis, Delft University of Technology (2007).

[49] D. Braun, M. Howard, and S. Vijayakumar, *Optimal variable stiffness control: formulation and application to explosive movement tasks,* Autonomous Robots **33**, 237 (2012).

[50] S. Haddadin, M. Weis, S. Wolf, and A. Albu-Schäffer, *Optimal control for maximizing link velocity of robotic variable stiffness joints,* in *IFAC World Congress* (2011) pp. 6863–6871.

[51] M. Aiple and A. Schiele, *Towards teleoperation with human-like dynamics: Human use of elastic tools,* in *2017 IEEE World Haptics Conference (WHC)* (IEEE, 2017) pp. 171–176.

[52] J. Rebelo and A. Schiele, *Time Domain Passivity Controller for 4-Channel Time-Delay Bilateral Teleoperation,* IEEE Transactions on Haptics **8**, 79 (2015).

[53] M. Friedman, *The Use of Ranks to Avoid the Assumption of Normality Implicit in the Analysis of Variance,* Journal of the American Statistical Association **32**, 675 (1937).

[54] F. Wilcoxon, *Individual Comparisons by Ranking Methods,* Biometrics Bulletin **1**, 80 (1945).

[55] K. R. Murphy, B. Myors, and A. Wolach, *Statistical Power Analysis*, 4th ed. (Routledge, New York, N.Y. :, 2014) p. 212.

[56] R. R. Wilcox, *Fundamentals of Modern Statistical Methods* (Springer New York, New York, NY, 2010) p. 258.

[57] S. L. R. Ellison, T. J. Farrant, V. Barwick, and Royal Society of Chemistry (Great Britain), *Practical statistics for the analytical scientist : a bench guide.* (RSC Publishing, 2009) p. 268.

[58] M. Aiple, *Human hammering with an elastic hammer restricted to 1-DOF with different stiffnesses,* (2018).

[59] *Global Ping Statistics - WonderNetwork,* (2018).

[60] M. Aiple, *Instructional video to the teleoperated flexible hammering experiment,* (2017).

[61] K. Hashtrudi-Zaad and S. E. Salcudean, *Analysis of Control Architectures for Teleoperation Systems with Impedance/Admittance Master and Slave Manipulators,* The International Journal of Robotics Research **20**, 419 (2001).

[62] M. Aiple, *Human hammering with an elastic hammer through a 1-DOF teleoperator with different feedback types,* (2018).

[63] B. W. Verdaasdonk, H. F. J. M. Koopman, and F. C. T. Van Der Helm, *Resonance tuning in a neuro-musculo-skeletal model of the forearm,* Biological Cybernetics **96**, 165 (2007).

[64] N. G. Hatsopoulos and W. H. Warren Jr, *Resonance Tuning in Rhythmic Arm Movements,* Journal of Motor Behavior **28**, 3 (1996).

[65] E. Kunesch, F. Binkofski, and H.-J. Freund, *Invariant temporal characteristics of manipulative hand movements,* Experimental Brain Research **78**, 539 (1989).

[66] T. B. Sheridan, *Telerobotics, automation, and human supervisory control* (MIT press, 1992).

[67] P. Richard, G. Birebent, P. Coiffet, G. Burdea, D. Gomez, and N. Langrana, *Effect of Frame Rate and Force Feedback on Virtual Object Manipulation,* Presence: Teleoperators and Virtual Environments **5**, 95 (1996).

[68] J. G. W. Wildenbeest, D. A. Abbink, C. J. M. Heemskerk, F. C. T. Van Der Helm, and H. Boessenkool, *The impact of haptic feedback quality on the performance of teleoperated assembly tasks,* IEEE Transactions on Haptics **6**, 242 (2013).

[69] A. M. Smith, *Does the cerebellum learn strategies for the optimal time-varying control of joint stiffness?* Behavioral and Brain Sciences **19**, 399 (1996).

[70] B. Vanderborght, A. Bicchi, E. Burdet, D. Caldwell, R. Carloni, M. Catalano, G. Ganesh, M. Garabini, M. Grebenstein, G. Grioli, S. Haddadin, A. Jafari, M. Laffranchi, D. Lefeber, F. Petit, S. Stramigioli, N. Tsagarakis, M. V. Damme, R. V. Ham, L. C. Visser, S. Wolf, and A. Albu-Schäffer, *Variable impedance actuators: Moving the robots of tomorrow,* in *Intelligent Robots and Systems (IROS), 2012 IEEE/RSJ International Conference on* (2012) pp. 5454–5455.

[71] M. Aiple, J. Smisek, and A. Schiele, *Increasing Impact by Mechanical Resonance for Teleoperated Hammering,* IEEE Transactions on Haptics , 1 (2018).

[72] M. Zinn, O. Khatib, B. Roth, and J. K. Salisbury, *Playing it safe [human-friendly robots],* Robotics & Automation Magazine, IEEE **11**, 12 (2004).

[73] J. W. Hurst, J. E. Chestnutt, and A. A. Rizzi, *The Actuator With Mechanically Adjustable Series Compliance,* Robotics, IEEE Transactions on **26**, 597 (2010).

[74] P. M. Wensing, A. Wang, S. Seok, D. Otten, J. Lang, and S. Kim, *Proprioceptive Actuator Design in the MIT Cheetah: Impact Mitigation and High-Bandwidth Physical Interaction for Dynamic Legged Robots,* IEEE Transactions on Robotics **33**, 509 (2017).

[75] S. Haddadin, T. Laue, U. Frese, S. Wolf, A. Albu-Schäffer, and G. Hirzinger, *Kick it with elasticity: Safety and performance in humanrobot soccer,* Robotics and Autonomous Systems **57**, 761 (2009).

[76] S. Haddadin, K. Krieger, and A. Albu-Schäffer, *Exploiting elastic energy storage for cyclic manipulation: Modeling, stability, and observations for dribbling,* in *Decision and Control and European Control Conference (CDC-ECC), 2011 50th IEEE Conference on* (2011) pp. 690–697.

[77] F. Petit, M. Chalon, W. Friedl, M. Grebenstein, and A. Albu-Schäffer, *Bidirectional Antagonistic Variable Stiffness Actuation : Analysis , Design & Implementation,* Proceedings of the 2010 IEEE International Conference on Robotics and Automation , 4189 (2010).

[78] S. Wolf, O. Eiberger, and G. Hirzinger, *The DLR FSJ: Energy based design of a variable stiffness joint,* in *Robotics and Automation (ICRA), 2011 IEEE International Conference on* (2011) pp. 5082–5089.

[79] S. S. Groothuis, G. Rusticelli, A. Zucchelli, S. Stramigioli, and R. Carloni, *The variable stiffness actuator vsaUT-II: Mechanical design, modeling, and identification,* IEEE/ASME Transactions on Mechatronics **19** (2014), 10.1109/TMECH.2013.2251894, arXiv:1706.00339 .

[80] M. Laffranchi, N. G. Tsagarakis, D. G. Caldwell, and W. B. Sheffield, *A Variable Physical Damping Actuator (VPDA) for Compliant Robotic Joints,* in *Robotics and Automation (ICRA), 2010 IEEE International Conference on* (IEEE, 2010) pp. 1668–1674.

[81] A. H. C. Gosline, V. Hayward, S. Member, and V. Hayward, *Eddy Current Brakes for Haptic Interfaces: Design, Identification, and Control,* Mechatronics, IEEE/ASME Transactions on **13**, 669 (2008).

[82] A. Milecki, *Investigation and control of magnetorheological fluid dampers,* International Journal of Machine Tools and Manufacture **41**, 379 (2001).

[83] R. Van Ham, B. Vanderborght, M. Van Damme, B. Verrelst, and D. Lefeber, *MACCEPA, the mechanically adjustable compliance and controllable equilibrium position actuator: Design and implementation in a biped robot,* Robotics and Autonomous Systems **55**, 761 (2007).

[84] M. G. Catalano, G. Grioli, M. Garabini, F. Bonomo, M. Mancini, N. Tsagarakis, A. Bicchi, M. Mancinit, N. Tsagarakis, and A. Bicchi, *VSA-CubeBot: A modular variable stiffness platform for multiple degrees of freedom robots,* in *Robotics and Automation (ICRA), 2011 IEEE International Conference on* (2011) pp. 5090–5095.

[85] M. Catalano, G. Grioli, M. Garabini, F. W. Belo, A. Basco, N. Tsagarakis, A. Bicchi, A. di Basco, N. Tsagarakis, and A. Bicchi, *A Variable Damping Module for Variable Impedance Actuation,* in *Robotics and Automation (ICRA), 2012 IEEE International Conference on* (2012) pp. 2666–2672.

[86] M. Laffranchi, N. Tsagarakis, and D. G. Caldwell, *A compact compliant actuator (CompAct) with variable physical damping,* in *Robotics and Automation (ICRA), 2011 IEEE International Conference on* (2011) pp. 4644–4650.

[87] W. Friedl, M. Chalon, J. Reinecke, and M. Grebenstein, *FAS A flexible antagonistic spring element for a high performance over,* in *2011 IEEE/RSJ International Conference on Intelligent Robots and Systems* (IEEE, 2011) pp. 1366–1372.

[88] M. Zinn, O. Khatib, and B. Roth, *A new actuation approach for human friendly robot design,* in *Robotics and Automation, 2004. Proceedings. ICRA '04. 2004 IEEE International Conference on*, Vol. 1 (2004) pp. 249–254 Vol.1.

[89] M. Aiple and W. Gregoor, *Solidworks model and system identification data of the Dynamic Robotic Actuator (Dyrac),* (2019).

[90] F. A. Mussa-Ivaldi, N. Hogan, and E. Bizzi, *Neural, mechanical, and geometric factors subserving arm posture in humans,* The Journal of Neuroscience **5**, 2732 (1985).

[91] M. Aiple, A. Schiele, and F. C. T. van der Helm, *Self-Adapting Variable Impedance Actuator Control for Precision and Dynamic Tasks,* IEEE Transactions on Haptics (submitted for publication) (2020), arXiv:2009.10444 .

[92] N. Hogan, *Adaptive control of mechanical impedance by coactivation of antagonist muscles,* IEEE Transactions on Automatic Control **29**, 681 (1984).

[93] M. Aiple, W. Gregoor, and A. Schiele, *A Dynamic Robotic Actuator with Variable Physical Stiffness and Damping,* Mechanism and Machine Theory (submitted for publication) (2020), arXiv:1906.07669 .

[94] C. Semini, V. Barasuol, T. Boaventura, M. Frigerio, M. Focchi, D. G. Caldwell, and J. Buchli, *Towards versatile legged robots through active impedance control,* The International Journal of Robotics Research **34**, 1003 (2015).

[95] J. Buchli, E. Theodorou, F. Stulp, and S. Schaal, *Variable impedance control a reinforcement learning approach,* Robotics: Science and Systems VI , 153 (2011).

[96] A. A. Blank, A. M. Okamura, and L. L. Whitcomb, *Task-dependent impedance and implications for upper-limb prosthesis control,* The International Journal of Robotics Research **33**, 827 (2014).

[97] K. Van Teeffelen, D. Dresscher, W. Van Dijk, and S. Stramigioli, *Intuitive Impedance Modulation in Haptic Control Using Electromyography,* in *2018 7th IEEE International Conference on Biomedical Robotics and Biomechatronics (Biorob)* (IEEE, 2018) pp. 1211–1217.

[98] M. D. Hill and G. Niemeyer, *Real-time estimation of human impedance for haptic interfaces,* in *EuroHaptics conference, 2009 and Symposium on Haptic Interfaces for Virtual Environment and Teleoperator Systems. World Haptics 2009. Third Joint* (2009) pp. 440–445.

[99] D. S. Walker, R. P. Wilson, and G. Niemeyer, *User-controlled variable impedance teleoperation,* in *Robotics and Automation (ICRA), 2010 IEEE International Conference on* (2010) pp. 5352–5357.

[100] R. V. Dubey, C. Tan Fung, S. E. Everett, T. F. Chan, S. E. Everett, C. Tan Fung, and S. E. Everett, *Variable damping impedance control of a bilateral telerobotic system,* Control Systems, IEEE **17**, 37 (1997).

[101] J. Park, R. Cortesão, and O. Khatib, *Robust and adaptive teleoperation for compliant motion tasks,* in *In Proceedings of the International Conference on Advanced Robotics* (2003) pp. 513–519.

[102] M. Aiple, *Instructional video to the self-adapting variable impedance actuator experiment,* (2019).

[103] D. E. Seborg, T. F. Edgar, D. A. Mellichamp, and F. J. Doyle III, *Process Dynamics and Control*, 4th ed. (Wiley, 2016) p. 512.

[104] D. S. Kerby, *The Simple Difference Formula: An Approach to Teaching Nonparametric Correlation,* Comprehensive Psychology **3**, 11.IT.3.1 (2014).

[105] H. B. Mann and D. R. Whitney, *On a Test of Whether one of Two Random Variables is Stochastically Larger than the Other,* The Annals of Mathematical Statistics **18**, 50 (1947).

[106] H. W. Wendt, *Dealing with a common problem in Social science: A simplified rank-biserial coefficient of correlation based on the U statistic,* European Journal of Social Psychology **2**, 463 (1972).

[107] M. Aiple, *Human performing precision and dynamic tasks through a 1-DOF teleoperator with self-adapting variable impedance actuator,* (2020).

[108] J.-H. Ryu, D.-S. Kwon, and B. Hannaford, *Stability Guaranteed Control: Time Domain Passivity Approach,* IEEE Transactions on Control Systems Technology **12**, 860 (2004).

[109] A. Banerjee, *Automated Broad and Narrow Band Impedance Matching for RF and Microwave Circuits* (Springer International Publishing, Cham, 2019).

[110] R. C. H. Li, *RF Circuit Design*, 2nd ed., Information and communication technology series ; 102 (John Wiley & Sons, Inc., Hoboken, NJ, USA, 2012).

[111] Y. Mori, *Mechanical Vibrations* (John Wiley & Sons, Inc., Hoboken, NJ, USA, 2017).

[112] Y. Tanaka, T. Tsuji, and M. Kaneko, *Task readiness impedance in human arm movements for virtual ball-catching task,* in *IECON'03. 29th Annual Conference of the IEEE Industrial Electronics Society (IEEE Cat. No.03CH37468)*, Vol. 1 (IEEE, 2003) pp. 478–483.

[113] M. C. Özparpucu and S. Haddadin, *Optimal control of elastic joints with variable damping,* in *2014 European Control Conference (ECC)* (IEEE, 2014) pp. 2526–2533.

[114] O. Baser and M. A. Demiray, *Selection and implementation of optimal magnetorheological brake design for a variable impedance exoskeleton robot joint,* Proceedings of the Institution of Mechanical Engineers, Part C: Journal of Mechanical Engineering Science **231**, 941 (2017).

[115] F. Petit and A. Albu-Schäffer, *State feedback damping control for a multi DOF variable stiffness robot arm,* in *Robotics and Automation (ICRA), 2011 IEEE International Conference on* (2011) pp. 5561–5567.

[116] T. Hulin, C. Preusche, and G. Hirzinger, *Stability Boundary for Haptic Rendering: Influence of Physical Damping,* in *2006 IEEE/RSJ International Conference on Intelligent Robots and Systems* (IEEE, 2006) pp. 1570–1575.

[117] I. Sarakoglou, N. G. Tsagarakis, and D. G. Caldwell, *Development of a hybrid actuator with controllable mechanical damping,* in *Robotics and Automation (ICRA), 2014 IEEE International Conference on* (2014) pp. 1078–1083.

[118] R. D. Howard, *Joint and actuator design for enhanced stability in robotic force control*, Ph.D. thesis, Massachusetts Institute of Technology (1990).

[119] J. F. Veneman, R. Ekkelenkamp, R. Kruidhof, F. C. van der Helm, and H. van der Kooij, *A Series Elastic- and Bowden-Cable-Based Actuation System for Use as Torque Actuator in Exoskeleton-Type Robots,* The International Journal of Robotics Research **25**, 261 (2006).

[120] D. P. Losey, A. Erwin, C. G. McDonald, F. Sergi, and M. K. O'Malley, *A Time-Domain Approach to Control of Series Elastic Actuators: Adaptive Torque and Passivity-Based Impedance Control,* IEEE/ASME Transactions on Mechatronics **21**, 2085 (2016).

[121] W. M. dos Santos and A. A. Siqueira, *Impedance Control of a Rotary Series Elastic Actuator for Knee Rehabilitation,* IFAC Proceedings Volumes **47**, 4801 (2014).

[122] M. Zinn, O. Khatib, B. Roth, and J. K. Salisbury, *Large Workspace Haptic Devices - A New Actuation Approach,* in *Haptic interfaces for virtual environment and teleoperator systems, 2008. haptics 2008. symposium on* (2008) pp. 185–192.

[123] J. P. Whitney, M. F. Glisson, E. L. Brockmeyer, and J. K. Hodgins, *A low-friction passive fluid transmission and fluid-tendon soft actuator,* in *2014 IEEE/RSJ International Conference on Intelligent Robots and Systems* (IEEE, 2014) pp. 2801–2808.

[124] R. B. Stein, *What muscle variable(s) does the nervous system control in limb movements?* Behavioral and Brain Sciences **5**, 535 (1982).

[125] E. Burdet, R. Osu, D. W. Franklin, T. E. Milner, and M. Kawato, *The central nervous system stabilizes unstable dynamics by learning optimal impedance,* Nature **414**, 446 (2001).

[126] J. Smisek, *Systematic Framework for Teleoperation with Haptic Shared Control*, Ph.D. thesis, Delft University of Technology (2017).

[127] J.-H. Ryu, J. Artigas, and C. Preusche, *A passive bilateral control scheme for a teleoperator with time-varying communication delay,* Mechatronics **20**, 812 (2010).

[128] K. Kronander and A. Billard, *Stability Considerations for Variable Impedance Control,* IEEE Transactions on Robotics **32**, 1298 (2016).

[129] M. Grebenstein, A. Albu-Schäffer, T. Bahls, M. Chalon, O. Eiberger, W. Friedl, R. Gruber, S. Haddadin, U. Hagn, R. Haslinger, H. Hoppner, S. Jorg, M. Nickl, A. Nothhelfer, F. Petit, J. Reill, N. Seitz, T. Wimbock, S. Wolf, T. Wusthoff, and G. Hirzinger, *The DLR hand arm system,* in *Robotics and Automation (ICRA), 2011 IEEE International Conference on* (2011) pp. 3175–3182.

[130] M. J. Panik, *Statistical Inference* (John Wiley & Sons, Inc., Hoboken, NJ, USA, 2012).

Glossary

accurate precise and close to the true value 113

agonist and antagonist muscles muscles pulling in opposing directions on a human articulation to move and position a limb in one direction or another 4

compliant quality of an actuator to have relatively low stiffness, typically in the order of magnitude that humans can achieve in their limbs, and well defined behavior under external loads 7

confidence interval range obtained from a sample indicating an interval which contains a statistical population parameter (*e.g.*, median) with a certain probability (often 95%) [130] 22, 26, 33, 84, 86–90, 92–95, 97, 101

efficient requiring little energy for a large effect (*e.g.*, for explosive motions) 8, 104

handle device local device of the teleoperation system with a haptic interface for the operator to interact with 6, 7

head injury criterion (HIC) measure for the severity of an impact on a human head 116

intuitive usable to operators without training 8, 104

percentile figure indicating that a certain percentage of values of a sample lies below the given figure, *e.g.*, the 50^{th} percentile corresponds to the median, the 25^{th} percentile to the first quartile 82, 84, 88–90, 94–96, 98, 100

proprioceptive reflexes low-level control loop of the central nervous system (CNS) to achieve certain motoric behavior 4

remote center of compliance device slightly elastic component placed at the tip of a robot end-effector to allow for small deformations in order to compensate for misalignments during placement tasks 7

series elastic actuator (SEA) robotic actuator with an elastic element making the end effector compliant and that can store potential energy to be released as kinetic energy viii, 5, 7, 11–13, 17, 34–36, 40, 66, 67, 98, 100, 110–115

stiffness metric for the force of a material resisting deformation calculated as force per deformation 2

teleoperation mode of operation where a human operator interacting with a handle device controls a robotic tool device in real-time, ideally able to manipulate objects in the operating environment as if he or she was interacting with the objects with his or her own hands 6, 9

teleoperation system system for teleoperation, consisting of the handle device, the tool device and a communication link connecting the two 5–8, 104

tool device remote device of the teleoperation system that interacts with the environment 6, 7

transparent quality of a teleoperation system to make tool and handle device appear with equal force and position to their environment and the human operator at any time 6

variable impedance actuator (VIA) robotic actuator whose effective mechanical impedance (stiffness and damping) can be changed dynamically 9, 39–41, 43, 63–67, 69, 74–77, 98, 102, 110–112, 114–116, 118–122

variable stiffness actuator (VSA) robotic actuator whose effective mechanical stiffness can be changed dynamically 7, 17, 111–114, 121

versatile suited for different applications (*e.g.*, precision tasks and dynamic tasks) 8, 104

virtual stiffness stiffness that is rendered by a control loop through a mechanically stiff robot 4

Symbols

a velocity scaling factor of the self-adapting impedance variation algorithm 75, 76

a length of excentered disc axis to sliding pivot axis (design parameter of Dyrac actuator) 46, 48, 49, 54, 55

α deflection angle of Dyrac actuator output axis to position motor axis 46, 48, 49, 61, 73

α significance level 22, 83, 86–89, 92–97

b viscous damping coefficient 13–15, 31, 42, 54, 58, 75, 76, 110, 111

β angle between pivot force F_P and pivot of Dyrac actuator 46, 48, 49

b_{set} viscous damping coefficient set point for Dyrac actuator controller 54, 61, 73

b_{wall} virtual wall damping coefficient 74

C_4 velocity gain tool to handle device of four-channel teleoperation controller 29, 30, 74–76

χ^2 chi-square value of Friedman's test 25, 27, 31

$\mathbf{CI}_{95\%}$ 95% confidence interval 25, 27, 86–89, 92–95, 97–101, 108, 109

c length between spring axis and pivot axis of Dyrac actuator 46, 48, 49

C_m handle device feedback gain of four-channel teleoperation controller 29, 30, 74–76

C_1 velocity gain handle to tool device of four-channel teleoperation controller 29, 30, 74–76

C_s tool device feedback gain of four-channel teleoperation controller 29, 30

C_3 force gain handle to tool device of four-channel teleoperation controller 29, 30, 74

C_2 force gain tool to handle device of four-channel teleoperation controller 29, 30, 74–76

C_{Z_s} tool device impedance adaptation function 74–76

DA dynamic task adaptive condition of Experiment 3 77–80

DC dynamic task counter-reference condition of Experiment 3 (high impedance) 77, 80

δ angle between excentered disc position and disc force direction of Dyrac actuator 46, 48

DL delayed condition of Experiment 2 28, 29, 34

D_{max} maximum damping ratio parameter of the self-adapting impedance variation algorithm 76

D_{min} minimum damping ratio parameter of the self-adapting impedance variation algorithm 76

DR dynamic task reference condition of Experiment 3 (low impedance) 76, 80

dt infinitesimal time step 81

$\hat{E}_{flx}$ peak energy of flexible hammer 15

$\hat{E}_{rig}$ peak energy of rigid hammer 15

E_k kinetic energy 16, 117

ϵ angle between motor 1 position and force F_D direction of Dyrac actuator 46, 48, 49

E_p potential energy of spring 16, 111

η_{act} measured output axis position of

Dyrac actuator controller 54, 59, 61, 73

η output axis position of Dyrac actuator 46

$\dot{\eta}_{act}$ measured output axis velocity of Dyrac actuator controller 54, 61, 73

$\dot{\eta}$ output axis velocity of Dyrac actuator 54, 59, 61

FA familiarization phase of Experiment 3 with adaptive impedance 77–79

F_D force transmitted through excentered disc of Dyrac actuator 46, 49, 62, 63

f_e force on the hammer as result of its impedance 75

$f_{\tilde{e}}$ external forces on the hammer 30, 74, 75

FF full feedback condition of Experiment 2 27, 29

F force 5, 15, 42, 110, 111, 113

f frequency 14–16, 21, 22, 25–27, 31, 33

FH familiarization phase of Experiment 3 with high impedance 77–79

f_h force exerted by the human operator on the handle device as result of the arm impedance and force consciously exerted by the operator 75

$f_{\tilde{h}}$ force intentionally exerted by the human operator on the handle device 30, 75

FL familiarization phase of Experiment 3 with low impedance 77–79

f_{mc} force commanded by the controller to the handle device 30, 75

F_P force generated at point P by the spring torque of Dyrac actuator 46, 49, 62, 63

f_0 resonance frequency 14–16, 23, 106

f_{sc} force commanded by the controller to the tool device 30

F_{T_1} force generated at point P by motor 1 torque of Dyrac actuator 46, 49, 62, 63

F_{T_2} force generated at point B by motor 2 torque of Dyrac actuator 46, 49

γ angle between motor 2 torque generated force F_{T_2} and force F_D 46, 48, 49

G gain 15, 21, 22, 25–27, 29, 31, 33

$H_{elastic}$ elastic hammer transfer function 106

$H_{flexible}$ flexible hammer transfer function 14, 15

H_{max} peak transfer function magnitude 15, 106

H_{rigid} rigid hammer transfer function 13, 14

H transfer function 23

ITAE integral of time-weighted absolute error $\int_0^T t\,|x - x_0|\,dt$ 80–82, 84, 87, 89, 90, 100

j imaginary unit $j^2 = -1$ 14

$k_{e,set}$ kesetstiffness 54

k_e effective stiffness of the Dyrac actuator 49, 50, 55

k_{max} maximum stiffness parameter of the self-adapting impedance variation algorithm 75, 76

k_{min} minimum stiffness parameter of the self-adapting impedance variation algorithm 75, 76

K fitting factor for environment impedance fitting of Experiment 2 31

k stiffness 14–16, 31, 48–50, 75, 76, 110, 111

K Kvar 31

k_{wall} virtual wall stiffness 74

k_0 material stiffness of an elastic element 111, 113

l length between spring axis and center axis of Dyrac actuator 46, 48–50

MAD median absolute deviation function 22

m mass of a body 13–16, 31, 76, 113

NF no force-feedback condition of Experiment 2 27–29, 34

n sample size 25, 27, 31, 86–89, 92–97

NV no visual-feedback condition of Experiment 2 27–29, 34

PA position task adaptive condition of Experiment 3 76, 78–80
PC position task counter-reference condition of Experiment 3 (low impedance) 76, 80
φ_{act} measured neutral position of Dyrac actuator controller 54, 60, 61, 72, 73
$\dot{\varphi}_{act}$ measured neutral position velocity of Dyrac actuator controller 54, 61, 73
φ neutral position of Dyrac actuator 45, 46, 55
$\varphi_{d,act}$ measured angle between motor 1 and motor 2 of Dyrac actuator controller 54, 60, 72
φ_d angle between motor 1 and motor 2 of Dyrac actuator 45, 46, 48, 54, 55, 63
$\dot{\varphi}$ neutral position velocity of Dyrac actuator 54, 59, 61
$\varphi_{d,set}$ commanded angle between motor 1 and motor 2 of Dyrac actuator controller 60, 72
φ_1 motor 1 position of Dyrac actuator 55
$\varphi_{1,set}$ motor 1 position set point of Dyrac actuator controller 54
φ_{set} neutral position set point of Dyrac actuator controller 54, 60, 61, 72, 73
$\varphi_{2,act}$ measured motor 2 position of Dyrac actuator controller 54
φ_2 motor 2 position of Dyrac actuator 55
$\varphi_{2,set}$ motor 2 position set point of Dyrac actuator controller 54
p probability 25, 27, 31, 86–89, 92–95, 97, 99
PR position task reference condition of Experiment 3 (high impedance) 76, 80

r_{act} measured pivot radius of Dyrac actuator controller 61, 73
r correlation coefficient 82, 83, 86–89, 92–95, 97, 99, 100
r_D length of excentered disc axis to center axis (design parameter of Dyrac actuator) 46, 48, 49, 54, 55
r pivot radius of Dyrac actuator 45, 46, 48–50, 54, 55, 57, 58, 70, 71
r_{set} pivot radius set point of Dyrac actuator controller 59, 61, 73
r^2 linear fit coefficient of determination 98

$\overline{\sigma}$ estimated sample standard deviation 22, 25, 27, 31
s Laplace variable $s = j\omega$ 13–15, 23, 29–31, 76, 106

T_A torque generated by spring deflection of Dyrac actuator 46, 49
T_d time delay 29, 30
T duration 81
TF_{motor} tool device motor velocity transfer function 74, 75
θ deflection angle of Dyrac actuator spring 46, 48, 49
$\dot{\theta}_e$ end-effector angular velocity 23
$\dot{\theta}_h$ hammer angular velocity 23
T_1 motor 1 torque of Dyrac actuator 48, 49, 60
T^* period of optimal excitation 16
T_O output torque of Dyrac actuator 46, 48, 49
T oscillation period 21
T_0 period of resonance excitation 15, 16
$T_{3,act}$ measured motor 3 torque of Dyrac actuator controller 54, 61, 73
$T_{3,set}$ motor 3 torque set point of Dyrac actuator controller 54, 61
T_3 motor 3 torque of Dyrac actuator 54, 60, 72
t time 14, 61, 81, 110, 111, 113
T_2 motor 2 torque of Dyrac actuator 48, 49, 60

V_{flx} velocity of the flexible hammer (Laplace domain) 14
v_{flx} velocity of the flexible hammer 14–16

$\hat{v}$ peak velocity 15, 21, 22, 25, 26, 31, 33
$\hat{v}_{flx}$ peak velocity of flexible hammer 15
$\hat{v}_{in}$ peak input velocity 15, 21
$\hat{v}_{rig}$ peak velocity of rigid hammer 15
V_{in} input velocity (Laplace domain) 14
v_{in} input velocity 14, 15, 21
$\dot{x}_m$ handle device velocity 30, 74–76
$\dot{x}_{m,max}$ maximum handle device velocity 75, 76
$\dot{x}_{m,min}$ minimum handle device velocity 75, 76
V_{rig} velocity of the rigid hammer (Laplace domain) 14
v_{rig} velocity of the rigid hammer 14–16
$\dot{x}_s$ tool device velocity 30, 75
v velocity 5, 16, 21, 42

ω angular velocity 14
ω_0 resonance angular velocity 23, 113

x actual/end-effector position 81, 110, 111, 113
Δx spring deflection 16
$\dot{x}$ end-effector velocity 110, 111
$\dot{x}_0$ virtual joint velocity 110
x_1 mechanical joint position 111, 113
x_0 target position 81
x_0 neutral/joint position 110

Z_e environment impedance 29–32
ζ damping ratio 23
Z_h human impedance 30, 75
Z impedance, linking force F and velocity v such that $F = Z\,v$ 5
Z_m handle device impedance 30
Z_s tool device impedance 30, 74, 75
z_{sc} impedance setting command of the self-adapting impedance variation algorithm 74, 75
Z_{to} transmitted impedance 29, 31, 32

Acknowledgements

I would like to thank all persons involved directly or indirectly in my PhD project for helping me to get this far:

André and Frans for giving me the opportunity to do this thesis and all the support, guidance and expertise along the way.

All members of the Telerobotics and Haptics Lab for their support, and especially Jan, João, Stefan and Thomas for sharing their scientific expertise with me.

Jules, Michael, Stef, Michiel, and Teun from the Science Center for their help and the office, lab and workshop space to work and perform my experiments.

Wouter en Frank from DEMO for helping me with the Dyrac design and manufacturing.

All volunteers that contributed by participating in my experiments.

The members of the Delft Haptics Lab and the H-Haptics project for helpful input and feedback in discussions.

The secretaries of BME, for the help in organizational matters.

Wim of the 3me workshop for the help with the manufacturing of parts for my experiments.

Klaas Visser to volunteer as mentor for me as PhD student.

Last but not least, I would like to thank my friends and family for their moral support, distraction and patience over the years.

Curriculum Vitæ

Manuel Aiple

Manuel Aiple was born on 26 June 1985 in Breisach am Rhein, Germany, where he also lived until finishing his *Abitur* at the local Martin-Schongauer-Gymnasium in 2004. He then followed the *Classes Préparatoires aux Grandes Écoles* at the Centre International de Valbonne in Sophia-Antipolis, France.

In 2006, he was admitted after competitive exams (*Concours*) to Arts et Métiers ParisTech (formerly *École nationale supérieure d'arts et métiers*) for a double-diploma program of the Franco-German University with the mechanical engineering curriculum of the Karlsruhe Institute of Technology (formerly University of Karlsruhe), which he followed in parts in Karlsruhe, Germany, and Bordeaux and Paris, France. In 2010, he finished the program, earning the master's degree diploma as engineer of Arts et Métiers ParisTech and the master's degree in general mechanical engineering of the Karlsruhe Institute of Technology (*Diplom-Ingenieur*).

He was subsequently admitted to the German Trainee Program of the German Aerospace Center (DLR) which he followed from 2010 to 2011 at the European Space Operations Centre (ESOC) in Darmstadt, Germany, and from 2011 to 2012 at the Telerobotics and Haptics Lab in the European Space Research and Technology Centre (ESTEC) in Noordwijk, Netherlands. From 2012 to 2015, he worked at the Telerobotics and Haptics Lab as engineer, developing electronics and software for the Haptics-1 experiment conducted in July 2014 onboard the International Space Station (ISS) and contributing to the follow-up Haptics-2 and Interact experiments.

Since 2015, he is a PhD student at the BioMechanical Engineering Department in the Faculty of Mechanical, Maritime and Materials Engineering (3me) at the Delft University of Technology in Delft, Netherlands. Since 2018, he also works part-time as engineer at the X Innovation Laboratory of Delta Labs B.V. in Rotterdam, Netherlands.

List of Publications

1. **M. Aiple**, A. Schiele, *Pushing the limits of the CyberGrasp for haptic rendering*, IEEE International Conference on Robotics and Automation, 2013.

2. A. Schiele, **M. Aiple**, T. Krueger, F. Van Der Hulst, S. Kimmer, J. Smisek, E. Den Exter, *Haptics-1: Preliminary results from the first stiffness JND identification experiment in space*, International Conference on Haptics: Perception, Devices, Control, and Applications, EuroHaptics, 2016.

3. A. Schiele, T. Krueger, S. Kimmer, **M. Aiple**, J. Rebelo, J. Smisek, E. Den Exter, E. Mattheson, A. Hernandez, F. Van Der Hulst, *Haptics-2 - A system for bilateral control experiments from space to ground via geosynchronous satellites*, IEEE International Conference on Systems, Man, and Cybernetics (SMC), 2016.

4. **M. Aiple**, A. Schiele, *Towards teleoperation with human-like dynamics: Human use of elastic tools*, IEEE World Haptics Conference, 2017.

5. **M. Aiple**, A. Schiele, *Increasing Impact by Mechanical Resonance for Teleoperated Hammering*, IEEE Transactions on Haptics, 2019.

Data Publications

1. M. Aiple, *Instructional video to the teleoperated flexible hammering experiment*,
DOI: 10.4121/UUID:32CB858B-C37F-4E25-BE0D-B0EA6C5C2B86, 2017.

2. M. Aiple, *Human hammering with an elastic hammer restricted to 1-DOF with different stiffnesses*,
DOI: 10.4121/UUID:D485CF76-0137-4600-A6CC-753FF3ACC5D6, 2018.

3. M. Aiple, *Human hammering with an elastic hammer through a 1-DOF teleoperator with different feedback types*,
DOI: 10.4121/UUID:85CA44C4-A4EC-4D64-BB97-B225914ED6FA, 2018.

4. M. Aiple, W. Gregoor, *Solidworks model and system identification data of the Dynamic Robotic Actuator (Dyrac)*,
DOI: 10.4121/10.4121/13625951, 2018.

5. M. Aiple, *Instructional video to the self-adapting variable impedance actuator experiment*,
DOI: 10.4121/UUID:D3309B3B-DCE7-4F1A-BFD7-0113646152C3, 2020.

6. M. Aiple, *Human performing precision and dynamic tasks through a 1-DOF teleoperator with self-adapting variable impedance actuator*,
DOI: 10.4121/13625411, 2020.